DEVELOPMENT AND VALIDATION OF A KINEMATICALLY-DRIVEN COMPUTATIONAL MODEL OF THE PATELLOFEMORAL JOINT

by

Jonathan Adam Gustafson

BS in Biomedical Engineering, New Jersey Institute of Technology, 2012

Submitted to the Graduate Faculty of

Swanson School of Engineering in partial fulfillment

of the requirements for the degree of

Doctor of Philosophy

University of Pittsburgh

2017

UNIVERSITY OF PITTSBURGH

SWANSON SCHOOL OF ENGINEERING

This dissertation was presented

by

Jonathan Adam Gustafson

It was defended on

March 30, 2017

and approved by

John J. Elias, PhD, Senior Research Scientist, Department of Research, Cleveland Clinic Akron General

Mark C. Miller, PhD, Associate Research Professor, Department of Mechanical Engineering and Materials Science and Bioengineering

Scott Tashman, PhD, Professor, Department of Orthopaedic Surgery, University of Texas Health Science Center

Dissertation Co-Director: Shawn Farrokhi, PT, PhD, DPT, Senior Scientist, DOD/VA Extremity Trauma and Amputation Center, Naval Medical Center San Diego

Dissertation Co-Director: Richard E. Debski, PhD, Associate Professor, Departments of Bioengineering and Orthopaedic Surgery

DEVELOPMENT AND VALIDATION OF A KINEMATICALLY-DRIVEN COMPUTATIONAL MODEL OF THE PATELLOFEMORAL JOINT

Jonathan Adam Gustafson, PhD

University of Pittsburgh, 2017

The patellofemoral joint represents one of the most challenging musculoskeletal systems to understand and manage. Disruption in the normal tracking of the patellofemoral joint can lead to elevated stress and microtrauma to the articular cartilage, cascading to the development of osteoarthritis. To develop effective treatment therapies, relationships between altered patellar motion and subsequent changes in articular cartilage loading must be measured. Computational modeling provides joint-specific changes in contact mechanics, but current techniques are limited by force-based assumptions and lack validation. The objective of this work was to develop a subject-specific modeling framework driven by highly accurate knee joint kinematics as a tool to estimate knee joint contact stress in vivo. First, a repeatable knee joint testing system for simultaneous measurement of patellofemoral joint kinematics and joint contact pressures was established. Measurements of patellofemoral and tibiofemoral translations and rotations were highly repeatable with intraclass correlation coefficients greater than 0.98/0.90 and 0.80/0.97, respectively. Measurements of joint contact pressure were repeatable within 5.3% - 6.8%. Second, a unique patellofemoral modeling framework employing the discrete element method combined with accurate knee joint kinematics was developed using two cadaveric knee joint specimens. Model-generated stresses were validated using experimentally measured pressures. The model predicted the experimental data well, with percent error (%) differences in contact

stress distribution being less than 13%, validating the model's ability to predict the experimental changes in joint contact. Lastly, this validated model was implemented in a group of individuals with patellofemoral osteoarthritis (n=5) and a control group (n=6) during a downhill walking task. The model predicted unique patellofemoral joint stress patterns between the two groups such that individuals with patellofemoral osteoarthritis experienced greater (58%) lateral facet joint contact stress early within the loading phase of the gait cycle compared to the control group (38%). This dissertation has validated and implemented a novel modeling technique driven by highly accurate, subject-specific kinematics to estimate patellofemoral joint contact stress during a downhill walking task. Future use of these models can provide quantitative evidence of the effectiveness of current patellofemoral treatment solutions and allow for the development of improved rehabilitation strategies.

TABLE OF CONTENTS

LIST OF TABLES

LIST OF FIGURES

PREFACE

It is hard to believe the immense growth I have gone through over the past five years, as a person and as a scientist. This is most certainly due to the help contribution to all of those listed below, as well as many others. First and foremost, I must thank my PhD advisor, Dr. Shawn Farrokhi. I still remember the first day meeting you at a summer lab meeting within the first month of moving to Pittsburgh from New Jersey. Little did I know was that the conversation we had then would truly shape who I have become over the past 5 years: a passionate, hard-working scientist with a true appreciation to both the science behind research and, perhaps more importantly, the clinical impact we can make. Shawn, you have truly been an excellent mentor, demonstrating the patience and wisdom to always push me to be better. I am truly grateful for the relationship we have made since that fateful day at the end of the summer of 2012. You have taught me much about research, but more importantly, the "big picture" and why it is we are carrying out the work we do. You taught me a great deal about work-life balance and you have been a true role-model for me to strive for as a scientist.

I must also give a special thank you to Dr. Richard Debski, who has been a great co-advisor since I came to Pitt. The one thing I truly appreciate out of every meeting we would have is the amount of positivity you could place into almost any situation. Your happy-go-lucky attitude and cheerful tone have made many days much easier when I did not always feel the most confident as a scientist: "Life is good!"…these are words to live by, something that I will never

forget to keep the big picture in view. "Life is good." Thank you as well to your wonderful wife Mandy for always having such a great sense of humor and being able to brighten any room.

I would like to thank all of the members of my dissertation committee for their abundance of knowledge and support throughout the years: Dr. John Elias, Dr. Mark Miller and Dr. Scott Tashman. You all have provided invaluable feedback to my project when I would likely reach a barrier and was not sure where to turn. Dr. Miller, thank you for providing all of your much needed input in regards to both the pressure measuring techniques I have used, as well as an understanding of the basic biomechanics behind the calculations I was performing. Many times you provided excellent feedback as to where I could look at my data for some form of "sanity check" when it came to results. Dr. John Elias, thank you for your immense knowledge in the discrete element method. When I had proposed my dissertation, I remember feeling a little nervous about the potential prospect of creating my own unique modeling framework within MATLAB. Your input and feedback over the years have truly made me appreciate the power and tools available to us as engineers. Your sincerity and time when I would hit a rough patch in building my code helped so much more than words can express. Dr. Tashman, I must give a great thank you to you as well. Thank you for always challenging me and asking the difficult questions. I have been with you nearly since I started, working on the pilot knee joint biomechanics study in older adults as a young graduate student. I remember the first time I had a conversation with you was because I was trying to understand the kinematic output files and coordinate system reference from the BDL tracking system. You spent almost 2 hours working through the pipeline of the files with me. I was truly amazed at how patient you were with me, a first year graduate student you had just met, and how passionate you are with the science.

I must thank all of my friends and colleagues here at Pitt who have provided some great memories that will carry with me through the years. Working with many of you at outreach events (Deepthi, Danielle, Mitali, and Sam) has been some of the greatest highlights of my time. What better fun than to share our passion for bioengineering with young minds! Dan, thanks for the great breaks to talk beach volley or head over to Schenley for some disc golf. You have been an incredible friend over the past 4 years. Special thank you to the members of the ORL and HMRL for their support. Kyle, you have been here at Pitt since the beginning with me, but as an undergrad. I truly am proud of the work we accomplished all those years ago, when we felt at times were working with the "cursed project." Late night testing and dinners at the Cheesecake Factory were nice breaks from the 30-some hour test protocol we originally sought to carry out! Will, not only did you provide some great technical help in the lab, but you always came in with a smile. Masa, I appreciate your help with many of the dissections that I needed to do as well as provide the clinical expertise I did not have. Your insight was truly a gift. Gerald and Matt, I always enjoyed our lunch session playing "boss monster" or going over to Fat Heads from some sammies and a beer. You all helped me to learn so much about myself as a person and researcher.

I also would like to thank some of the important folks at the University of Pittsburgh who made my time here as a graduate so much easier. In particular, a special thank you to Nick Mance for always helping when I had no idea how to register for classes or where to get the forms I needed for certain credits. A thank you to Glenn Peterson for always stopping by to share a nice conversation and see how I was doing, especially when I first started. I would like to thank Dr. Shroff for his infinite wisdom and mentorship. You have made me feel like an "ambassador for the sciences" and I am truly blessed to have gotten to know you over the years. I must also

give a special thank you to the support I received from the Department of Physical Therapy and the Department of Bioengineering throughout my time here at Pitt.

I would like to thank my family for all of their support. Mom, thank you for always being my role-model, teaching me to always value education and that everything in life is possible if we work hard to get there. You have truly provided support that words cannot describe. I know that Papa would be very proud of the work that I have been able to achieve, and you have been the rock to get all four of us kids to where we are. To my big sister, Dr. Lena, thank you for always providing the breaks I needed to simply talk to you about life and some of my worries with school. You always provided great advice in times of need. To my brothers, Miguel and Jose, thank you both for providing some great support from such a distance, whether it would be late nights playing "smash" or surprise trips to Pittsburgh to hang out for the weekend. All of you have been truly amazing in supporting my decision to move to Pittsburgh for so many years.

Last, but not least, to my fiancé Rachel, who, closing in on the better part of a decade, have been there through some of the greatest challenges of our relationship. After 4 years of long distance in college, you made the decision to support me and be an incredible partner by moving to Pittsburgh with me. I am so blessed to have such an incredible woman in my life and I can only hope to be a great soon-to-be husband. I look forward to June 17th and cannot wait to say "I do." Your support through the many late nights, especially these past 4 months, has been incredible. I look forward to the many adventures ahead of us and sharing it with you. I love you.

1.0 INTRODUCTION AND BACKGROUND

Osteoarthritis (OA) is a joint disease that is marked by degeneration of the articular cartilage and subchondral bone. OA impacts approximately 27 million adults in the United States alone, with the knee being one of the most commonly affected joints with a 50% lifetime risk of developing symptoms [1, 2]. OA is one of the leading causes of mobility limitation and chronic disability in the elderly [3] and has incurred close to $185 billion over the past decade in aggregate annual medical care expenditures [4]. Currently, there is no cure for OA and most non-operative treatment options involve symptomatic management [5]. In the most severe instances of late-stage OA, the only primary solution is joint replacement surgery. In the US alone knee replacements tally to over 400,000 procedures per year with an estimated cost of $10 billion [6]. These costs are expected to increase dramatically with the increase in the aging population due to the "baby boomer" population [7] as well as the increased national obesity rate [8], which are both well known risk factors associated with OA [9-11].

OA is marked by degenerative changes at the bone, commonly in the form of osteophytes, and cartilage surfaces, primarily consisting of focal defects, fractures or softening of the cartilage [12-14]. It should be noted that the causes of primary OA are distinguishably different from secondary OA, which is commonly caused by traumatic injury or metabolic diseases. The causes of the degenerative changes to the articular cartilage observed in primary OA are multifactorial, involving biological [15-17], mechanical [18-20], and structural [21, 22]

mechanisms. These different pathways are interrelated and, as such, make it challenging to understand the primary drivers for the onset of the disease. A conceptual framework for the onset and progression of OA has been discussed [23] with empirical data indicating that a disruption in the mechanical environment of the joint is directly related to its health and function. Thus, changes at the in vivo system in terms of mechanical loading certainly appear to be a major contributor to the pathogenesis of OA. It stands to reason that a better understanding of joint loading and changes in joint loading as a result of altered motion or disease state may elucidate this complex problem.

While OA at the knee predominantly occurs in the tibiofemoral joint [24-27], OA of the patellofemoral joint has gained recent attention as it has been shown to occur independent of tibiofemoral joint OA [28-31] and may be as common, if not more common, than tibiofemoral OA [32, 33]. OA of the patellofemoral joint affects about 25% of the population [34], and yet despite its high prevalence, the etiology of patellofemoral OA remains poorly understood. Patellofemoral pain (PFP) at a young age is recognized as an early indicator for the development of OA [35, 36]. While the specific mechanism of PFP development may vary, it has been proposed that increased contact stress at the cartilage surfaces and subchondral bone resulting from maltracking of the patella is responsible for pain development during daily activities [37-39]. Understanding the mechanical factors contributing to articular stress induced by joint motion would allow for early intervention in the hopes of mitigating the risk of early-onset OA development.

1.1 MOTIVATION

Despite a seemingly simple design, the patellofemoral joint represents one of the most challenging musculoskeletal systems to understand and manage. As an integral part of the knee complex, the patellofemoral joint is often subjected to the greatest biomechanical forces in the body [40-42]. If there is a disruption in the normal tracking of the patellofemoral joint, a cascade of elevated stress and microtrauma to the articular cartilage can begin to occur, potentially leading to OA development and symptoms [23]. While there has been much work in understanding the pathology and causes of tibiofemoral OA [30, 43-46], research looking into the prevalence of patellofemoral OA is only recent [47-49]. To this end, a magnetic resonance imaging assessment of 970 knees determined that evidence of patellofemoral joint damage was deemed to be as common, if not more frequent, than damage to the tibiofemoral joint [33]. Additionally, research has shown that patellofemoral OA affects more than one third of individuals greater than 60 years of age, inducing disability and loss of independence [50, 51]. The pain and disability that are accompanied with patellofemoral OA can have devastating effects for the patient's quality of life and emphasizes the importance of understanding the underlying joint mechanics behind patellofemoral OA development.

1.2 ANATOMY AND FUNCTION OF THE PATELLOFEMORAL JOINT

The patella is one of the largest sesamoid bones in the human body. The patella is imbedded proximally within the quadriceps femoris tendon and provides several services to the knee joint: 1) protection to integral parts of the knee joint structures, 2) reduction in frictional forces at the

tendon, 3) guides the forces of the extensor mechanism to the patellar tendon, and 4) ultimately provides stability to the knee joint [39, 52, 53]. In general, the patella is ovoid in shape with the anterior portion consisting of two distinct regions: 1) the proximal base where the broad fibers of the quadriceps femoris and vasti intermedius tendons can attach, and 2) the distal apex, which is enveloped by the patellar tendon, attaching down to the tibial tuberosity. Both of these insertions consist of a fibrocartilaginous interface, which aids in minimizing local stresses and transmission of these stresses to the articular cartilage during ambulation [52].

1.2.1 Cartilage composition

Cartilage tissue is unique in that it is avascular and aneural. It is important to note that cartilage has a limited capacity for healing, due to the nature of its avascularity, therefore leaving it at high risk for injury. The primary makeup of cartilage is type II collagen and proteoglycans, as well as chondrocytes, and water, all of which contribute to its function to withstand compressive loads. During application of articular contact forces, rapid flow of the water content within the cartilage causes local increases in pressure within the joint. As the pressure causes fluid to flow out of the cartilage, the extracellular matrix lined with the collagen fibers and proteoglycans resists this flow through negative electrostatic repulsion forces [54]. This interaction of solid and fluid phases contribute to the mechanical function of cartilage.

1.2.2 Patellar cartilage

The posterior surface of the patella is comprised of cartilage (hyaline) divided into asymmetrical facet zones separated by a distinct midline ridge that runs vertically. This median ridge coincides

with the trochlear groove of the anterio-distal surface of the femur and provides the articulation between the two bone surfaces. The patellar cartilage roughly encompasses ~75% of the posterior surface of the patella [55]. The patella is the site of the thickest articulating cartilage in the body, which is evident by its function (to be discussed further in section 1.3), reaching up to ~4 to ~5 mm of thickness [52, 55, 56].

The articular cartilage of the patella can be divided into medial and lateral facets, defined by the median ridge, which is vital to the function of the patella. It has been well documented that the anatomy of these facets can vary significantly [57, 58]; the most frequent morphology observed (65% of cases) consisted of a concave lateral facet with a rather flat medial facet, often considerably smaller than the lateral facet [59]. The anatomy of these facets is vital to the function of the patella throughout knee flexion (discussed further in section 1.3).

1.3 PATELLOFEMORAL TRACKING AND JOINT CONTACT MECHANICS

At the surface, the patellofemoral joint can be viewed as a simple mechanical lever, designed to improve the function of the knee extensor muscle group (i.e. quadriceps). The complex interaction of the different structures at the patellofemoral joint is vital to its role in joint motion. When tracking normally, the patella acts as a mechanical lever for the quadriceps muscles while maintaining a consistent articulation with the underlying trochlea throughout knee flexion. Due to the large forces required by the knee extensors for functional activities, the patella is subject to some of the greatest biomechanical forces in the body [40-42], some measured as high as 8 times bodyweight [60, 61]. Interestingly, the patella is also the site of greatest articular cartilage thickness in the body, potentially as a result of the high loads transmitted by the knee extensors

[61]. Any disruption in the normal tracking of the patellofemoral joint can lead to elevated stress and potential microtrauma to the articular cartilage, potentially leading to OA development and symptoms [23].

Three-dimensional (3D) kinematic measurements of the patella are important to understanding its function, thus requiring highly accurate tracking systems, as changes between normal and abnormal patellar kinematics can be small. Typical camera-based tracking systems as seen in many gait research labs using markers attached to the skin seen are not sensitive enough to discern changes in patellofemoral motion, in large part due to significant soft tissue motion that can introduce errors. To this end, several research groups have utilized wide ranging kinematic measurement techniques, both contact and non-contact, including the use of electromagnetic sensors [62] and imaging methods, ranging from magnetic resonance imaging (MRI) techniques [63-67], dual-orthogonal fluoroscopic systems [68-70], and even dynamic ultrasound systems [71, 72]. Many of these systems are capable of measuring patellar motions within sub-degree and sub-millimeter accuracy in terms of patellar rotations and translations.

1.3.1 Patellofemoral tracking

When describing the motion of the patella, it is important to have a clear definition and understanding of the coordinate system being utilized to describe the motions. A review article by Katchburian and colleagues [73] discusses some of the challenges in tracking the patella. There is a large disparity in terms of the coordinate systems used to describe patellar motion, as well as the choice of reference. Some classical studies chose to define the patellar motion relative to the tibia [74, 75], which is not clinically relevant, as the motion of interest is the patella relative to its opposing bone with which it articulates: the femur. In describing the motion of the

patella relative to the femur, there have been numerous studies with wide ranging definitions of their coordinate systems [76-81]. In general, body fixed coordinate systems can be used to define relative motion of the patella and femur, or the relationship of the two bones can be performed around a floating axis (i.e. Grood and Suntay [82]), which is one of the most commonly used methods. The greatest benefit of utilizing this floating axis coordinate system is that rotations are sequence independent when describing patellar motion, unlike other rigid body description methods like Euler angles. The resulting patellar motions can be seen in Figure 1.1.

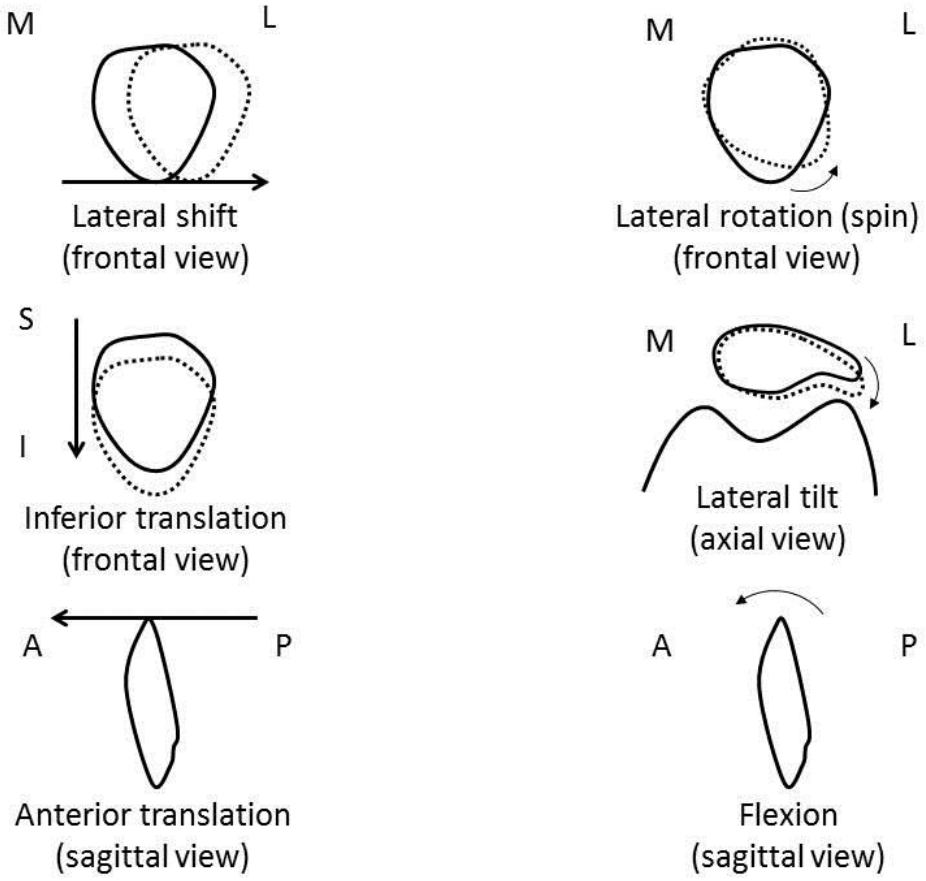

Figure 1.1. Patellar motion for a right knee (adapted from Katchburian et al., 2003[73])

Patellar tracking can be influenced significantly by several factors: 1) knee joint alignment, 2) muscle forces, and 3) passive stabilizing forces. It has been theorized that maltracking of the patella as a result of disruption of one of these factors can lead to significant disorders, such as patellar instability, dislocation, and pain due to increased contact stress.

1.3.2 Alignment and patellar tracking

Lower limb alignment can have significant bearing on patellar tracking by changing the relative position of the femoral trochlea or increasing the tension in the soft tissue restraints. The effect of altered tibial and femoral rotations on joint contact stress in the patellofemoral joint has been explored extensively. Experimental studies have shown the effect of increased internal femoral rotation or external tibial rotation on increased lateral patellofemoral joint contact pressure [83, 84]. The natural anatomical alignment of the femur – patella – tibia bones can be used to measure the quadriceps angle (Q-angle) to visualize the direction of pull of the quadriceps tendon. The Q-angle is drawn by measuring a line from the superior iliac spine down to the center of the patella, and then adding a line from the center of the patella to the attachment of the patellar tendon to the tibial tuberosity. These two lines represent the force vectors applied at the patella by the quadriceps and patellar tendons and the intersection of these lines is the Q-angle (Figure 1.2). The Q-angle is a commonly used clinical measure in assessing the magnitude of lateral directed forces acting on the patella from the resultant summation of the two force vectors of the quadriceps and patellar tendons. This resulting lateral force is commonly termed the “law of valgus” and has a significant effect on the tracking of the patella such that the lateral patellar facet receives 60% more force than the medial facet [85]. It has also been proposed that tibial abduction, or valgus, can also lead to increased lateral patellofemoral facet loading due to an

increasing Q-angle [86]. Increases in the Q-angle have been found to correspond with increasing joint contact pressure in the lateral facet [87, 88], which may place the patellofemoral joint at risk for degeneration over time. In support of this, varus-valgus alignment has been shown to correlate with compartment specific patellofemoral OA [89]. While lower limb alignment is an important consideration to understanding patellofemoral joint loading, it should be noted that static alignment does not necessarily imply poor dynamic loading, as it is possible for individuals to dynamically correct "poor" alignment through the use of altered muscular contraction strategies.

Figure 1.2. Direction of quadriceps force vector ($F_{quadriceps}$) and patellar tendon force vector ($F_{patellar\_tendon}$) result in anatomically-directed lateral force ($F_{resultant}$)

1.3.3 Active muscle forces on patellofemoral alignment

The quadriceps mechanism can have a significant effect on patellar tracking. The role of the quadriceps during gait (or other weight-bearing activities) is the effective shock absorption of the loads transmitted through the tibiofemoral joint from heel contact. The patellofemoral joint is not engaged within the trochlear groove until ~20° of flexion, and therefore can be affected significantly by the direction and magnitude of the quadriceps muscles. In particular, the vastus medialis obliqus (VMO) has been shown in cadaveric studies to be an important stabilizer for the patella, providing medial restraint throughout motion [90, 91]. Understanding the effect of muscle loads on altered patellar motion and alignment becomes more confounding when considering a disease state such as OA, as quadriceps weakness is a common observation in individuals with knee OA [92, 93]. At the present, there is a need for improved understanding of the effect of altered muscle loads and resulting changes in patellofemoral joint stress during functional tasks.

1.3.4 Passive stabilizers and patellar tracking

The retinacular fibers of the patellofemoral joint provide a large portion of the passive stability throughout the range of knee motion. The soft tissue contributions from structures such as the distal attachment site of the iliotibial band [94], as well as the joint capsule and ligaments all contribute to patellar stability [95]. One of the most studied passive tissues is the medial patellofemoral ligament (MPFL), as it is believed to play a major role in normal tracking [96-98]. The MPFL has been shown to account for approximately 50-60% of the medial stabilization forces during knee flexion, centralizing the patella as it engages with the trochlear groove [97].

Injury to this structure can lead to increased lateral patellofemoral tilting and potential increased stresses. Boney and articular geometry at the patella and distal femur also play a significant role in patellar stability and tracking [99]. Prior studies have shown differing patterns in patellar motion dependent on whether the tracking was relative to the femur [67] or femoral groove [100].

1.3.5 Patellofemoral contact mechanics

Patellofemoral contact pressure is a result of the compressive forces applied by the "pulley-like" mechanism from the quadriceps and patellar tendon and the contact area between the patella and distal trochlea of the femur. The patellar cartilage is subject to contact forces spanning from the inferior, middle, and superior regions of the articular surface (in order) with increased knee flexion. Contact between the distal patella and proximal femoral trochlea takes place at full extension. This contact changes significantly at approximately 30 degrees of tibiofemoral flexion, where the patella should be fully engaged within the trochlear groove [52]. Additionally, there is an increased lateral translation of the patella once engaged with the femoral trochlea. While the compressive joint contact forces are significantly increased in deeper flexion angles, the congruency between the patellar cartilage and femoral trochlea increase contact area, which leads to only marginal increases in stress. The ratio of these forces and area directly affect the changes in pressure.

In weight bearing from full extension to 90 degrees of flexion, there is an increase in both the contact area and patellofemoral joint reaction force, with the force increasing significantly in deeper flexion due to the increased tension in the quadriceps to support these flexions [101]. There has been mixed evidence as to the pattern of the contact pressure with increasing flexion

during weight bearing, but the general consensus is that contact pressure increases significantly in earlier flexion (0 - 30 degrees) and then increases minimally in later flexion (30 – 90 degrees) as the patella becomes fully engaged with the trochlea and contact area has been maximized [85, 87]. Perhaps more relevant are the stress distributions occurring at lower knee flexion angles, particularly as these joint positions place the patella at greater risk for maltracking due to the increased impact of active, passive, and anatomical components discussed above on patellar motion.

1.4 RELATIONSHIP BETWEEN MALTRACKING, ELEVATED CONTACT STRESS, AND OA

Altered tracking of the patellofemoral joint can have potential detrimental effects streamlined to the articular cartilage, leading to lesions and potential degeneration. The effect of altered kinematics on long-term articular joint degeneration has been examined in the anterior cruciate ligament (ACL) deficient knee of both animal models [102-104] as well as in the human knee joint [105-110]. Results from these studies have shown that ACL tears are a significant risk factor for OA development [105, 111-113], which underscores the importance of altered motion on articular cartilage health. Herzog and colleagues [104] explored the in-situ changes in the patellofemoral joint after transection of the ACL in a cat model. Comparisons between the ACL-deficient joint and intact joint in terms of cartilage properties (i.e. thickness and stiffness) and joint contact pressures measured using pressure sensitive film were made after 16 weeks of ACL transection. The authors found osteophyte formation and significant increases in cartilage thickness of the ACL-transected joint, with no changes in the cartilage material properties. These

changes in thickness were directly related to a decrease in stiffness and peak contact stress, potentially indicative of altered movement strategies to off load the injured knee. The results of these studies and others demonstrate a complex interplay between altered movements and loading, which has important implications when considering the mechanical loading environment at the cartilage level.

A classic review by Andriacchi and colleagues [23] emphasizes a framework for the relationship of the multifaceted and interrelated pathways that can cause degeneration of the articular cartilage (i.e. biological, mechanical and structural). Focusing on the mechanical aspect, articular cartilage exhibits a unique response to loading. Prior studies found that articular cartilage has an adaptive response to repetitive loading, such that the cartilage in load bearing regions was found to have increased thickness compared to regions not exposed to loading [114, 115]. However, initiation of the OA process may be related to altered mechanical loading at the cartilage interface to regions of cartilage unaccustomed to loading [23], which is commonly observed in ACL-deficient patients (see above). With continued alterations in loading, the articular cartilage will begin to undergo microtrauma, after which catabolic breakdown of the cartilage matrix proteins takes place [116]. With aging, the articular cartilage is unable to adapt to these changes appropriately and the OA process will continue. It is vital to understand these key aspects of the OA process so that appropriate interventions can be made to either slow or avert this progression.

An important note must be made in regard to the relationship between early development of patellofemoral pain (PFP) and patellofemoral OA development later in life. Patellofemoral pain at a young age is recognized as an early indicator for the development of OA [35]. While the specific mechanism of PFP development may vary, it has been proposed that increased

contact stress at the cartilage surfaces and subchondral bone resulting from maltracking of the patella is responsible for pain development during daily activities [37, 117]. Over the lifetime of the knee joint, these alterations in patellar tracking are hypothesized to lead to cartilage and subchondral degradation in the form of OA.

It is essential to gain an understanding of the contact mechanics at the patellofemoral joint to develop appropriate treatment for individuals with patellofemoral dysfunction. Numerous studies have quantified patellofemoral contact mechanics using one of two contact measuring techniques: direct and indirect methods. Direct methods for assessing articular joint contact involve the use of either pressure measurement sensors inserted into the joint capsule or through the use of instrumented joint-sensors (i.e. total knee replacement) [84, 87, 118-122]. Many of these classic studies in knee joint biomechanics have shaped our understanding of joint contact and answered some of the theoretical concepts and models with regards to changes in joint contact mechanics due to altered motion. While these studies have truly expanded our understanding of some of the underlying mechanics at the knee joint, these techniques are not feasible in human-subject studies due to their invasive nature.

Indirect methods for evaluating joint contact commonly involve the use of imaging techniques. The most commonly used imaging technique for measuring articular contact is magnetic resonance imaging (MRI). Improvements in the technology and imaging sequences for MRI have made it a valuable resource for both clinicians and researchers in understanding patellofemoral joint pathology. In an effort to understand the joint contact mechanics of the patella and cartilage during in vivo joint loading, several studies have explored the natural motions of the patella during various tasks using MRI [64, 65, 123, 124] and taken a step further to assess the effect of different rehabilitative treatments on patellar tracking and joint contact

[125]. Despite the technological improvements over the years in the use of indirect imaging methods for patellar tracking in vivo, there still exists a gap in understanding the association between patellar motions and resulting joint contact stress during dynamic tasks.

1.5 PATELLOFEMORAL OA AND MANAGEMENT

Despite the prevalence of patellofemoral OA, the effect of conservative treatments on the outcomes of patellofemoral OA has been unanswered [126]. Interventions for individuals with patellofemoral OA are wide ranging, with the main goal aimed at restoring normative joint motion and joint contact while decreasing stress. However, no current tool exists to be able to quantify the effect of treatment strategies in restoring joint motion and subsequently decreasing knee joint stress. Numerous treatment strategies for individuals with patellofemoral OA have been researched with some low-to-moderate evidence to support their uses, which include: patella taping [127, 128], patella bracing [129, 130], implementation of foot orthotics [131], the use of anti-inflammatory agents, and lower extremity stretching and neuromuscular training aimed at strengthening the hips and quadriceps [132-134]. Success of these different treatments is typically measured using patient-reported outcomes and different clinical tests, such as knee range of motion and strength. However, the relationship between improvements in these outcome measures and direct changes in knee joint stress is unknown.

1.6 COMPUTATIONAL MODELING

Computational modeling is an attractive solution for studying the effect of different treatments on joint mechanics. Specifically, the use of subject-specific geometry and knee joint kinematics as inputs to drive models would allow for researchers and clinicians to better understand joint contact mechanics during functional tasks and provide a novel tool for prescribing and evaluating subject-specific rehabilitative treatment solutions. The primary goal of this dissertation was to develop a computational framework utilizing subject-specific knee joint geometry and knee joint kinematics to estimate changes in the mechanical environment of the patellofemoral joint (i.e. joint contact stress) in response to altered kinematics. This dissertation will discuss the computational framework involved and the development and validation of a unique computational modeling technique which incorporates subject-specific geometry and joint kinematics to estimate resulting joint-specific contact stress throughout functional joint positions.

1.6.1 Finite element analysis

The finite element (FE) analysis approach is one computational modeling framework, which allows for estimation of patellofemoral joint cartilage stress in-vivo [135]. FEA begins by discretizing a two-dimensional (2D) or three-dimensional (3D) geometry into small, simple, geometrical shapes, termed elements. This process of discretizing geometry into these subdivided elements is called meshing. Each of these discretized elements can be assigned certain material properties which determine how they will behave in response to loading, which is applied by boundary conditions (i.e. forces or displacements). These forces are applied to each

element and the FE solver can then assemble the resulting partial differential equations in order to determine force equilibrium at all of the "connectors" of each element (nodal interface) [136]. This process of dividing complex geometries into smaller and smaller elements allows for numerical approximations to problems with no hope of attaining analytical solutions.

The greatest challenge in utilizing FEA is in handling contact problems between multiple bodies. Modeling contact is such a challenge due to the nonlinearity associated with predicting and understanding deformation between two contacting bodies [137]. Numerical convergence problems are a common obstacle, which are exacerbated when dealing with highly non-linear geometries, leading to increased computational resources and time. To resolve some of convergence challenges associated with modeling contact, significant meshing and time is required to eliminate any potential irregularities in the geometry that may cause focal or sharp contact within the model. Thus, many studies employing FE models are limited in the number of analyses that can be performed. This presents a challenge, as often parametric analyses exploring the effect of certain aspects of the model are often desired when making clinical suggestions.

Despite the challenges associated with employing FEA-based modeling techniques to biomechanical problems, FE models have been useful for understanding stress distributions throughout complex biological structures [138, 139]. For instance, FE models have been used previously to calculate the stresses throughout the patellofemoral joint at different knee flexion angles [140, 141] and with various degrees of femoral rotation [142]. Despite some of the dramatic improvements technologically in terms of improved computing power, FE methods are still a time intensive problem that may not be clinically useful for addressing questions related to larger, clinical-based research studies.

1.6.2 Discrete element analysis

Discrete element analysis (DEA) is an alternative modeling method that utilizes linear elastic theory to simplify joint contact problems [122, 143]. Contact at the joint is broken down into a "bed of springs" analysis, where linear elastic, compression-only springs are spread out between the surfaces of two rigid bodies, thus representing the cartilage layer. Any load or displacement implemented within the system will cause the springs to deform, thus allowing for a simple calculation of force engendered through each spring using Hook's Law. While DEA methods are significantly more efficient than FEA due to the simplification of the contact problem, DEA is only capable of estimating the joint contact forces and stresses between two rigid bodies, as opposed to FEA, which can generate stress profiles throughout the body. A small comparison of the two techniques is presented in Table 1.1.

Table 1.1. Comparison of finite element and discrete element methods

Model Choice	Pros	Cons
FEA	• Tissue level information • 3D stresses and strains	• Costly (time) • Process not clinically feasible
DEA	• Time-efficient solution • Provide clinical information relative to contact stress	• Only provides surface stress analysis

The implementation of discrete element modeling in articular joints has been described by Blankevoort et al. [144], which discusses the major assumptions associated with utilizing these models: 1) the contacting surfaces are assumed to behave as a linear, elastic, isotropic,

homogeneous material, 2) the size of the contact area over the surface is significantly greater than the thickness through the cartilage, and 3) the subchondral bone is considered a rigid body. Any spring deformations can be related to the stresses occurring at the rigid body. Typically, these deformations are assessed via a penetration analysis, where any overlapping areas of cartilage upon being loaded or displaced are indicative of the surface deformation [145]. This method is commonly used in other proximity-based measures of contact between two surfaces, typically included in rigid-body dynamics software [146]. Interestingly, the properties of the springs can be changed to account for small and large strain problems, as well as surface strain and shear to tailor the problem to any joint of interest.

DEA modeling techniques have been implemented in numerous joints, such as the hip [147-149], the ankle [150], and the knee joint, both tibiofemoral [151-153] and patellofemoral [154-156]. Many of these studies primarily employed DEA methods to assess the effect of different surgical reconstruction techniques on changes in joint contact stress. However, the effect of different non-operative treatment regimens has not been explored with these modeling techniques, particularly at the patellofemoral joint.

1.6.3 DEA implementation to the patellofemoral joint

There has been limited application of discrete element modeling at the patellofemoral joint. Studies using DEA techniques in the patellofemoral joint have been performed by Elias et al. [154, 155, 157-161] with the intent of understanding the effect of altered forces (i.e. Q-angle load, hamstring loads, etc.) on patellofemoral joint contact stress. Many early DEA models incorporated force-based methods in order to minimize the potential energy stored within each spring [144, 145], while other more recent models have incorporated the use of imaging systems

(dynamic computed tomography (CT)) to better understand the effect of surgical techniques on patellar instability [162]. A related modeling technique to DEA is rigid-body modeling, which has been used by several authors in conjunction with musculoskeletal models to explore the effect of total knee replacements on joint contact stress [146, 163] and develop improved knee replacements. These models utilize iterative optimization algorithms to balance the forces and moments across the multiple soft tissue structures included in each model (muscles, passive fibers, tendons). These techniques can be valuable when looking to investigate the role of graft fixations on altered motion or how altered motion can potentially change forces within a graft. However, if the goal is to examine the effect of altered motion on joint cartilage stress and develop methods to examine how to mitigate stress, then force-driven models may not be the most optimal solution.

The choice to employ finite element and discrete element modeling techniques is dependent on the research question and desired outcomes from the model to address these questions. Finite element-based models provide in-depth analyses into the complex deformation and stresses (compressive and shear) of the cartilage resulting from varying loading conditions, which is important to understanding cartilage degradation at a material level. Discrete-based methods provide surface contact stress changes due to altering loading conditions, which is important in understanding how different rehabilitations or surgical techniques will alter the contact stress distribution. Current models employing both FEA and DEA techniques rely on estimations and assumptions of the magnitude and direction of passive (i.e. ligament, soft-tissue) and active (i.e. muscle) forces and their contribution to joint contact and cartilage stress. By utilizing highly accurate knee joint kinematics as input to DEA models, it is possible to bypass the numerous assumptions associated with force-based models and provide estimates of joint

contact stress in direct response to the subject-specific changes in joint motion. However, accurate measures of joint motions are required as input for these displacement-driven models, which also have not been validated. To this end, this dissertation will discuss the development of a modeling framework to employ displacement-driven DEA models to estimate resulting patellofemoral cartilage stress.

1.7 MODELING VALIDATION

Model validation is a vital step to ensure that model predictions are robust and representative of what is occurring physically. It is important any experimental design built for validation purposes replicate the state of the tissue with which the model will be applied. At the patellofemoral joint, there have only been a handful of studies assessing validation. Elias et al. [155] performed validation of their patellofemoral model using the lateral facet force percentage, which was the percentage of the total force applied to the cartilage on the lateral facet. The model was well correlated to the experimental data and able to predict the experimental force changes due to alterations in the Q-angle of the knee models. Other studies employing finite element techniques commonly utilize resulting model kinematics as a form of validation [164]. However, these forms of validation do not directly validate the resulting joint contact stress. A summary of validation metrics in biomechanics has been discussed [165] and can range from deterministic, graphical comparisons, to correlations, to experimental uncertainty metrics, such as bias and precision. This dissertation will take a combination of all of these approaches, as it is important to fully understand the differences and error associated with both experimental measurements of stress in the knee joint and errors associated with the modeling framework.

2.0 SUMMARY OF THE PROBLEM

There have been many studies attempting to understand the role that mechanical loading plays on cartilage health and whether changes in mechanical loading precede joint deterioration that is accompanied with OA or whether the joint contact mechanics are compromised due to the disease process [23, 114, 166]. Regardless of the mechanism, presence of OA at the patellofemoral and tibiofemoral joints has been shown to be associated with excessive pain, stiffness and functional limitations [31, 167]. The goal of current treatment methods for these individuals is aimed at restoring "normal" motion while limiting pain and increasing function. However, the primary outcome of these treatments is self-reported pain and function improvements without any quantitative measure evaluating the ability of these treatments to reduce joint contact stress. Development of new and effective, patient-specific treatments is dependent on understanding the joint-specific contact stress distributions in these individuals during functional activities, which is currently not practical.

Computational modeling is an excellent tool that can be used for estimating patellofemoral joint contact stresses in vivo to better understand the relationship between joint contact mechanics and different knee states. Specifically, creating computational models driven by experimental knee kinematics would provide a better understanding of the physiologic loads at the knee joint during functional tasks. However, it is necessary to validate these models prior to implementation in vivo. This will be addressed in vitro by developing a reliable methodology

for the collection of joint surface contact pressures (specific aim 1) at different knee positions. Simultaneously, knee joint kinematic data will be collected to act as input for the models being developed (specific aim 2), driving the contact observed as part of specific aim 1. Validation of these models will be performed by comparing the differences between experimental and computational results in terms of joint contact stress distribution (hypotheses 2). Once properly validated, these subject-specific models will be utilized in vivo to compare differences in knee joint contact mechanics between patients with and without knee OA throughout a downhill walking task (specific aim 3). Overall, this study will provide a methodology and proof of concept for the development and use of subject-specific knee models driven by accurate knee joint kinematics in vivo with the ultimate goal of assessing the effect of rehabilitation treatments for patients with patellofemoral dysfunction.

2.1 SPECIFIC AIMS AND HYPOTHESES

In order to meet the objectives of this study, the following specific aims were implemented:

2.1.1 Aim 1

Establish a highly repeatable methodology for simultaneously measuring patellofemoral kinematics and joint contact stress.

Hypothesis 1a: Data collection methodology will be repeatable based on an intraclass correlation coefficient of greater than 0.8.

Hypothesis 1b: Measures of knee joint contact pressure in terms of mean and peak pressure will be within 10% of the average measures across multiple, repeated tests.

2.1.2 Aim 2

Develop a discrete element model driven by experimental kinematics and validate patellofemoral joint contact stress predicted by the model.

Hypothesis 2: Discrete element model results of contact stress distributions will show minimal bias (average difference) relative to experimental results based on Bland-Altman analysis and will be significantly correlated ($p<0.05$).

2.1.3 Aim 3

Evaluate a discrete element model in comparing in vivo joint contact distributions and contact stress difference in individuals with patellofemoral OA and healthy controls during gait.

Hypothesis 3a: Patients with patellofemoral OA will exhibit increased joint contact stress compared to healthy controls.

Hypothesis 3b: Significant differences in joint stress loading profile will be determined throughout the loading response phase of gait.

3.0 AIM 1: IN VITRO ASSESSMENT OF PATELLOFEMORAL KINEMATICS ON JOINT STRESS

The complex interplay of the passive and active soft tissue components of the knee as well as underling boney geometry and articulating surfaces of the femur and patella contribute significantly to normal motion and loading at the articular surface. Any disruption in this force-couple system can alter loading mechanics at the articular cartilage interface and potentially lead to a mechanistic breakdown of the articular cartilage prevalent in patellofemoral osteoarthritis (OA) [23, 168]. Understanding the relationship between patellofemoral tracking and joint contact mechanics is crucial in developing proper treatment solutions for individuals with patellofemoral OA. In order to investigate this relationship, a reliable testing system for simultaneously measuring patellofemoral joint kinematics and contact mechanics in physiologic, functional loading states must be established. The first aim of this dissertation was to develop a sophisticated system for repeated measurement of patellofemoral kinematics and joint contact stress in vitro when simulating physiologic, in vivo motions.

3.1 DEVELOPING A REPEATABLE SYSTEM FOR SIMULTANEOUSLY MEASURING PATELLOFEMORAL JOINT KINEMATICS AND CONTACT STRESS

3.1.1 Introduction

Patellofemoral joint mechanics are complex and depend on not only the ratio of forces applied by the quadriceps extensor group, but also depend on the anatomical alignment of both the femur and tibial attachment sites. In order to maintain normal function of the patella mechanism, it is vital for both the active (i.e. muscle) and passive (i.e. bony surfaces, retinacular fibers, and tendons) stabilizers to maintain a proper balance throughout functional tasks. The patella is a vital component of force transmission from the quadriceps muscles to the patellar tendon. These forces can exceed several times body weight and have been investigated extensively [101, 169-171]. Although the patella is commonly modelled as a frictionless, pulley-based system, studies have shown that the force ratios from the quadriceps tendon to the patellar tendon are not 1:1 [101, 171, 172]. It is important to understand the interaction of these forces in order to replicate the complexities of the patellofemoral joint when designing in vitro testing systems [118].

The distribution of forces across the patella can lead to significant joint contact stress within the articular cartilage. The articular cartilage at the patellar and femoral trochlea surfaces act to withstand the high forces transmitted across the joint and as an unsurprising result is also the site of greatest cartilage thickness within the body [41, 173, 174]. Significant and abnormal increases in the patellofemoral joint stress, or a shift in the location of the stress, has been

theorized to be a precursor for development of joint degradation and patellofemoral osteoarthritis (OA) [23, 168]. In lieu of this, the development of anterior knee pain (chondromalacia) has been correlated to the development of patellofemoral OA [35], indicating the need to understand the effect of altered loading on the contact stress within the knee joint. To this end, several studies have attempted to explore the effects of altered loading on patellofemoral joint contact mechanics [84, 120, 121, 175]. While these studies have contributed significantly to our understanding of changes in patellofemoral mechanics in response to co-contraction loads [121] and tibial rotations [84], application of large, non-physiologic loads and excessive tibial and femoral rotations makes extrapolation of this knowledge to the in-vivo loading condition challenging.

As has been discussed, prior studies have explored the change in patellofemoral joint contact mechanics through a broad range of motion and loading applications, but limited work has been performed on motion and loading consistent with daily activity. Particularly, limited data exists in quantification of patellofemoral contact stress at low flexion angles (less than 20°) or with varying femoral rotation. Investigating the patellofemoral mechanics at these positions is important as activities like walking impart high loads and stresses at the knee joint in these lower flexion positions [38, 168, 176]. These joint positions place the patella at higher risk for increased stresses as there is limited contact area prior to 20° of tibiofemoral flexion when the patella engages with the femoral trochlea, which is an important consideration when developing a framework for investigating patellofemoral joint mechanics, measuring joint kinematics, and, ultimately, in developing computational models for estimating joint stress.

The objective of this study was to develop a sophisticated testing system for simultaneously measuring patellofemoral kinematics and joint contact mechanics under complex

patellofemoral and tibiofemoral loading conditions and evaluate the repeatability of collecting these measurements with repeated testing. The motivation to develop this system was to establish a repeatable testing environment for the development of subject-specific patellofemoral computational models driven by highly accurate knee joint kinematics collected experimentally. We hypothesized that the repeatability for knee joint kinematics (average of standard deviation across several, repeated joint positions) would be at a submillimeter and sub-degree level and the joint contact pressures would be within the repeatability of the pressure measurement system (10% repeatability across joint contact outcome measures).

3.1.2 Methods

Two fresh-frozen cadaveric knees (ages in years: specimen #1 = 52; specimen #2 = 46) were utilized in the development of the in vitro system for simultaneously measuring patellofemoral kinematics and joint contact mechanics. The system utilized in this study, along with the methodology for testing each specimen, can be described in three parts: 1) specimen preparation; 2) pressure sensor preparation; and 3) patellofemoral testing. All cadaveric knee specimens underwent radiographic evaluation to ensure that all structures were intact. One of the two specimens tested showed signs of patellofemoral OA identified by an orthopaedic surgeon.

3.1.2.1 Specimen preparation

All skin and soft tissue was removed more than 10 cm proximal and distal to the joint line except for the quadriceps tendons (vasti medialis, lateralis, and intermedius/rectus femoris combined) and capsular ligaments of the patellofemoral and tibiofemoral joints. The proximal fibula was rigidly fixed to the tibia in its anatomical position using a screw. Both the distal tibia

and proximal femur end were potted in epoxy putty (Figure 3.1 A) to be mounted into the knee testing apparatus. Registration blocks (Figure 3.1 B) were securely fixed for kinematic tracking purposes to the medial tibia and femur near the joint line and on the center of the patella using cyanoacrylate and baking soda.

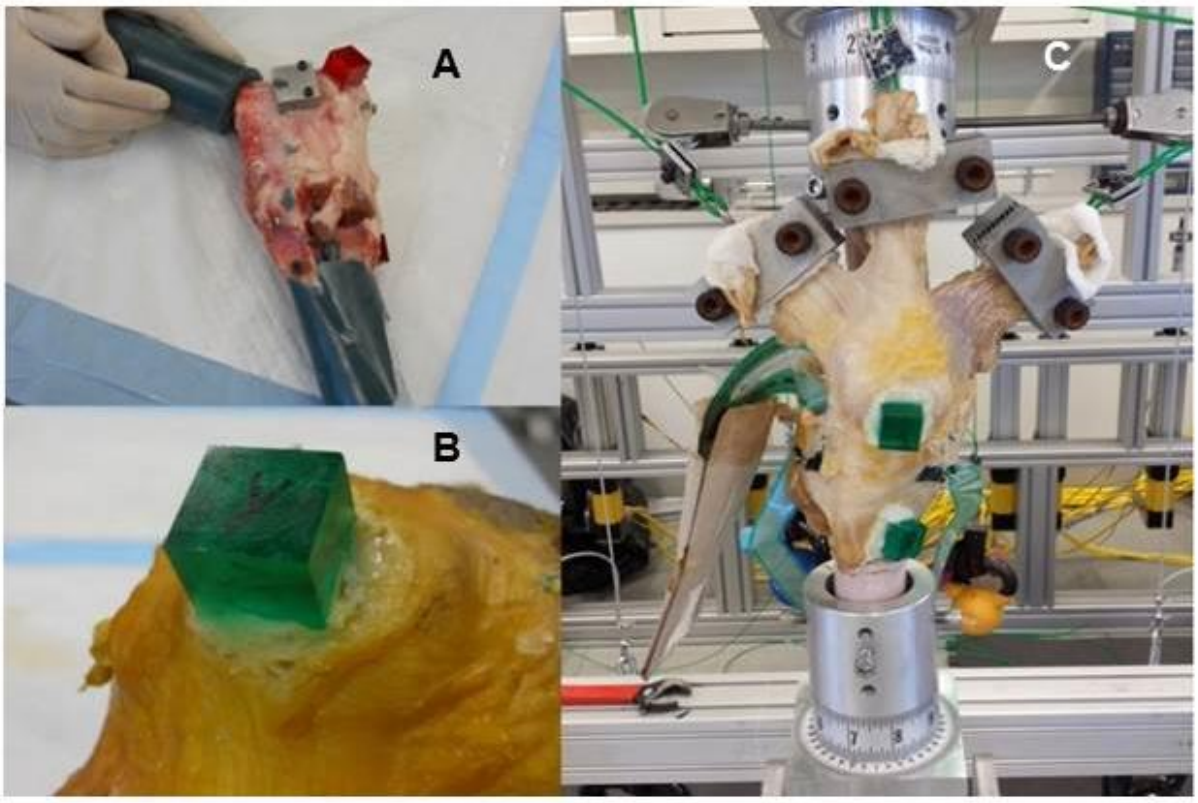

Figure 3.1. A) Femur and tibia in epoxy putty; B) Registration block rigidly attached to patella bone; C) In vitro experimental setup

3.1.2.2 Pressure sensor preparation

Patellofemoral joint contact pressures were measured using thin, flexible pressure sensors (K-scan Model 5051, 2.5K psi; Tekscan Inc., South Boston, MA). The sensors are 0.1-mm thick with 44 rows and columns of force-sensing elements (sensels) every 1.27 mm. Prior to testing, the sensors underwent a conditioning, equilibration, and calibration protocol. Conditioning is a

process of cyclically loading the sensors to minimize effects of drift and hysteresis of the sensel elements. Each sensor was conditioned using a materials testing machine (Model 4502; Instron Corp., Norwood, MA), where compressive loads of approximately 300 N was applied ten times at a rate of 10 mm/min. The 300 N compressive cyclic loading protocol was chosen based on manufacturer recommendation to condition the sensors by applying loads approximately 20% greater than the highest load expected experimentally.

Equilibration is a process of quality assurance for correct sensor operation that creates even sensitivity between all sensel elements. Equilibration is performed by applying uniform pressure distributions across the sensel elements and recording this information within the pressure sensor software to normalize each element and compensate for slight variations. Uniform pressure was applied to each sensor over the range of 200 KPa to 1,500 KPa using a hydraulic compressor (PB500C, Tekscan Inc., South Boston, MA).

Lastly, calibration is a vital step to quantify accurate pressure measurement data. Each sensor was calibrated on a materials testing machine (Model 4502; Instron Corp., Norwood, MA) using a two-point calibration with loads at approximately 20% and 80% of those anticipated during testing (50 to 200 N) [177]. Once preparation was completed, a lateral patellofemoral retinacular release was performed in each specimen to allow the pressure sensors to be inserted posterior to the patella and sutured to the proximal soft tissue and distal patellar tendon. Lateral release of the retinacular fibers has been shown to medialize patella translation and tilt by as much as 1.0 mm and 1.68°, respectively, while not significantly altering patellofemoral pressure [178]. Despite these observed changes, this study was focused on obtaining repeatable kinematic and contact pressure datsa across multiple tested positions as opposed to measuring the “true” or “natural” kinematics and contact mechanics of the patella.

3.1.2.3 Patellofemoral testing

Each specimen was mounted in a custom designed knee testing apparatus. The apparatus uses a counterweight system to assist with the weight of each specimen and allows for unconstrained, 6 degree of freedom (DOF) motion throughout knee flexion-extension while also allowing for application of tensile loads to the extensor tendons. The femur and tibia were rigidly fixed in the testing apparatus by inserting the bones into aluminum cylinders and clamped such that the long axes of the cylinders were representative of the mechanical axis/long axis of the bones. Each specimen was preconditioned through full flexion and extension range of motion ten times manually to reduce the effects of hysteresis and creep in the quadriceps tendons and patellar ligaments.

A mechanical digitizer (Faro Arm®, Lake Mary, FL) was used to quantify the positions of the patella with respect to the femur throughout the different testing states described below. The digitizer was mounted on a metal plate and screwed to the knee testing apparatus within arms distance on the medial side of the specimen. The digitizer was calibrated and used to record anatomical landmarks on the femur, tibia, and patella (Geomagic, Rock Hill, SC). Landmarks included the medial and lateral epicondyles and a point 10 cm away from the joint along the axis on both the femur and tibia. Patellar landmarks included the most proximal, distal, and medial points. These landmarks were used to generate anatomical coordinate systems for each bone according to the Grood and Suntay method [82].

In addition to the anatomical landmarks, the mechanical digitizer was used to measure the motion of the rigid bodies (femur, patella, and tibia bone) relative to one another throughout the testing conditions. This was done by manually digitizing points on the surface of three pre-defined faces of each registration block. These digitized points were imported into a custom

Matlab program (Mathworks, Natick, MA) in order to calculate orthonormal local coordinate systems for the femur, patella and tibia bones. These coordinate systems were calculated by fitting the data points on each face to a plane equation using a least-squares optimization technique. The optimization routine generated a local coordinate system for each block, with the origin located on the corner of the block and unit normal vectors from these planes being the coordinate axes [179]. The digitization and coordinate system process can be seen in Figure 3.2.

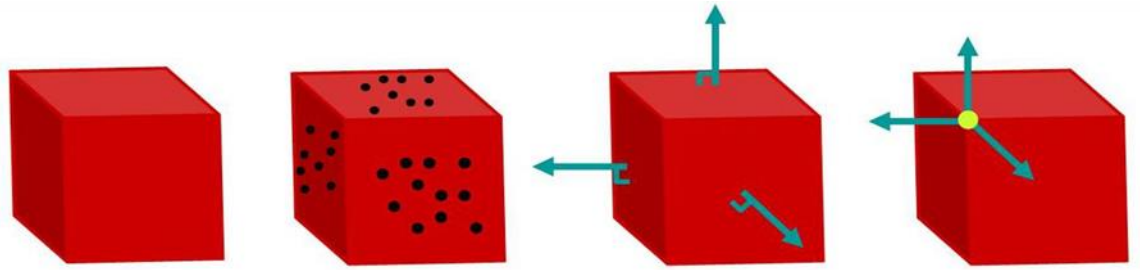

Figure 3.2. Local coordinate system development for tracking rigid bones

These local coordinate systems were used in conjunction with the anatomical coordinate systems of each bone to describe knee joint kinematics throughout the testing session. The following testing positions were applied to each knee: tibiofemoral flexion from 0° to 75° in 15° increments, with varying degrees of femoral rotation (5° internal and external femoral rotation) and varus/valgus alignment (5° varus and valgus positioning) at both the 0° and 15° flexion position. These joint positions are important as they simulate functional loading during a walking task [176, 180].

Each knee was initially pre-conditioned after insertion into the testing apparatus by moving the entire joint through the full range of flexion/extension ten times. A “neutral” alignment was determined upon completion of the pre-conditioning by positioning the knee at full extension with the femur and tibia free to rotate and settle into a “natural” state. Once this

state was established, the coronal and transverse planes of motion were locked. The knee was then moved to the desired flexion angle and then locked into place to provide rigidity during loading. Each quadriceps tendon was clamped and tensile loads simulating individual muscle forces were applied based on fiber direction and orientation. Briefly, tensile forces of 51 N, 87 N, and 77 N were applied to the vastus medialis, combined vastus intermedius and rectus femoris, and the vastus lateralis, respectively [181]. The loads for the vastus medialis and vastus lateralis were applied at a coronal plane angle of 47° and 19° from the mechanical axis of the femur, respectively [90, 182]. A compressive force of approximately 350 N was also added to the system at the proximal femur to simulate 50% of an individual's mean body weight to the tibiofemoral joint [177]. The final setup of the knee within the testing apparatus can be seen in Figure 3.1 C**.** The specimen was hydrated with saline solution regularly throughout the testing procedure.

Upon loading the knee at each testing position, patellofemoral contact pressure measurements were immediately recorded, followed by digitization of the registration blocks on the femur, patella and tibia bones. It was vital to capture the joint contact pressure data with minimal delay, as the pressure sensors are susceptible to drift with extended loading duration [183]. To assess the repeatability of the testing system and measurement techniques, knee joint kinematics and patellofemoral contact pressures (area, average and peak contact pressure) were collected on three separate occasions after complete removal and remounting of one knee specimen. To assess the sensitivity of these measurements at different joint positions, repeatability measures of joint kinematics and contact pressures were made at four different testing positions: 1) 15° of tibiofemoral flexion at neutral alignment; 2) 15° of tibiofemoral

flexion with 5° of internal femoral rotation; 3) 45°of tibiofemoral flexion; and 4) 75° of tibiofemoral flexion.

3.1.2.4 Pressure sensor processing

All pressure sensor data was processed in the I-Scan (Tekscan Inc., South Boston, MA) software. The pressure distribution map from each tested position was analyzed by dividing the pressure map into medial and lateral facet "boxed" regions. This division line was determined by taking measurements of the medial and lateral facet width using a digital caliper upon completing testing. These facet widths were measured from each lateral/medial edge of the patellar cartilage to the median ridge, respectively. A ratio of each facet to the total patellar width was calculated and this ratio was used to divide the pressure distribution in the I-scan software. Figure 3.3 shows the process of generating the pressure distribution plots and dividing them into medial and lateral facets. Once these facet regions were defined at each tested position, contact mechanics data in terms of contact area, average contact pressure, and peak contact pressure were calculated for each facet. A detailed protocol of the testing process, in addition to calibration procedures for the mechanical digitizer and pressure measurement system, can be found in Appendix A.

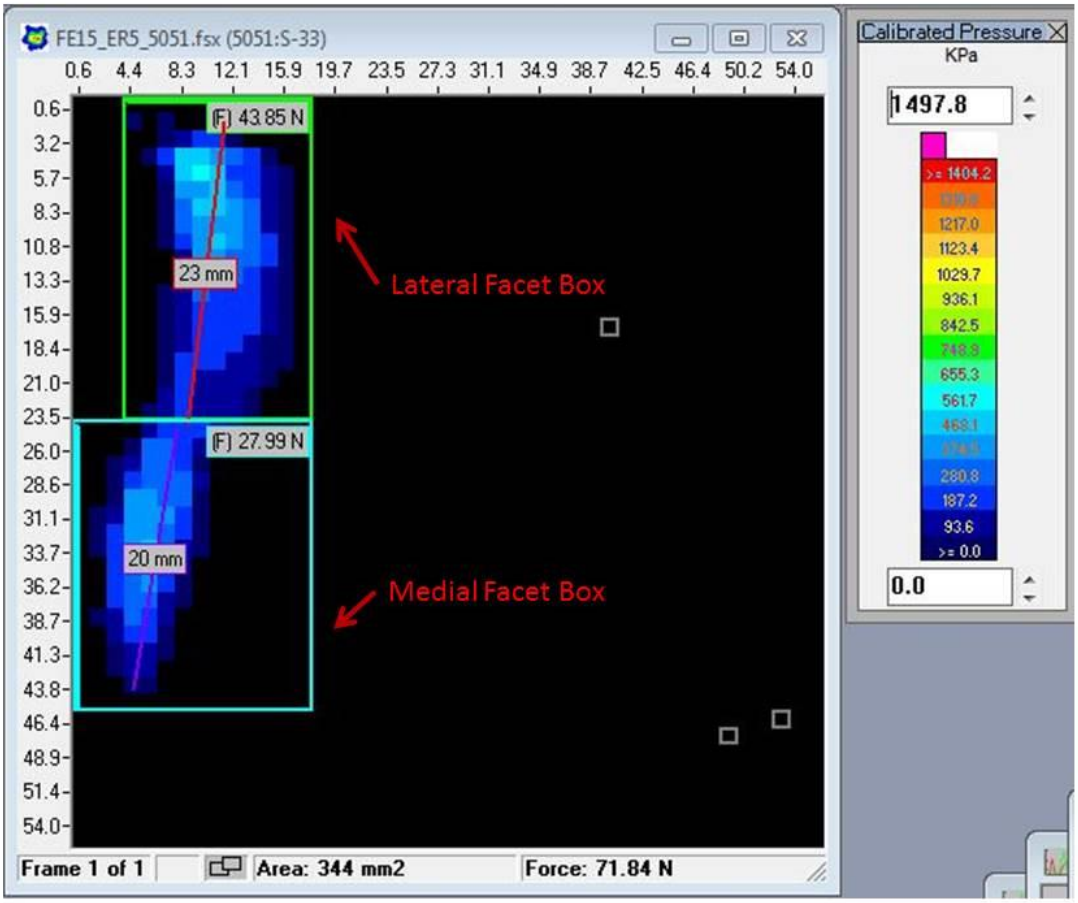

Figure 3.3. Division of medial and lateral patellar facet pressures in I-scan system

3.1.2.5 Data Analysis

A qualitative analysis of the contact pressure distribution outcome variables was performed and compared to prior literature. To assess the repeatability of the testing apparatus, the average of the standard deviation of the three, repeated measurements of knee joint kinematics and joint contact pressures across the four repeated testing positions was calculated. The mean of the standard deviation is a quantitative way for evaluating measurement uncertainty [184]. Intraclass correlation coefficients (ICC 1,1) were calculated for each outcome variable to assess test-retest repeatability. The system was deemed to be repeatable if the kinematic

measurements were able to be repeated within submillimeter and sub-degree precision in terms of translations and rotations of the patellofemoral and tibiofemoral kinematics. The joint contact pressure measurements were considered repeatable if the standard deviation of the pressure values relative to the mean (%) were within 10%.

3.1.3 Results

The contact pressure distributions across the flexion positions demonstrated increasing contact with increasing flexion. Additionally, there were increases on the lateral/medial patellar facet with increasing internal/external femoral rotation, respectively. Qualitatively, this can be seen in Figure 3.4, which shows increasing lateral facet contact area and contact pressure with increasing internal rotation (from 5° of external rotation to 5° of internal rotation). This trend was observed in both knee joints at the 15° flexion position as well as at full extension.

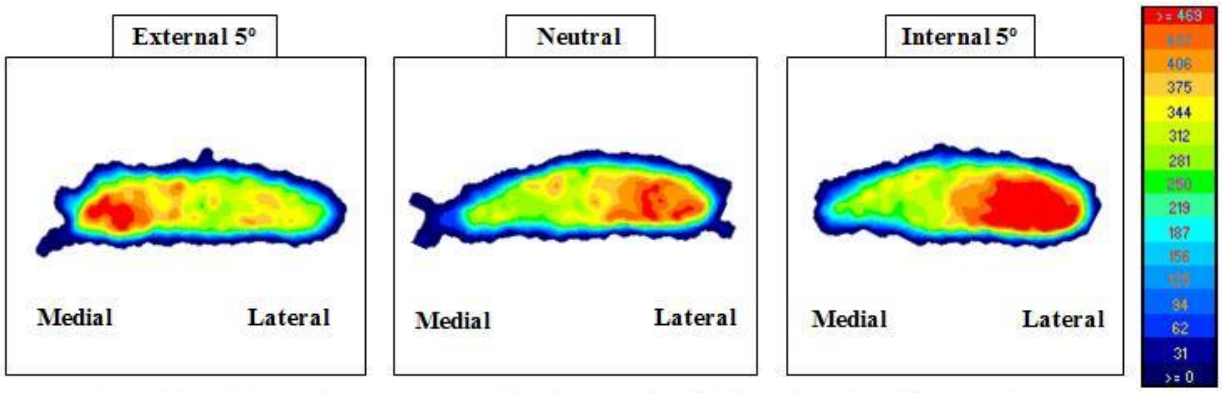

Figure 3.4. Sample pressure distribution plots at 15° of tibiofemoral flexion with varying femoral rotation

Quantitatively, there was a 2-fold increase in the lateral facet average and peak contact pressure when going from an externally rotated femoral alignment to an internally rotated alignment at full extension. This effect of increasing pressure on the lateral facet with internal

femoral rotation exhibited only 50% increases at 15° of tibiofemoral flexion. Conversely, the medial patellar facet exhibited decreases in average (up to 10% and 32%) and peak contact pressures (up to 17% and 41%) with increasing internal femoral rotation at both full extension and 15° of flexion, respectively. Regardless of facet, increasing knee flexion from a fully extended knee to 75° of tibiofemoral flexion led to approximately a 2.5 x increase in contact area; however, contact pressures (both average and peak) decreased with increasing flexion (Figure 3.5).

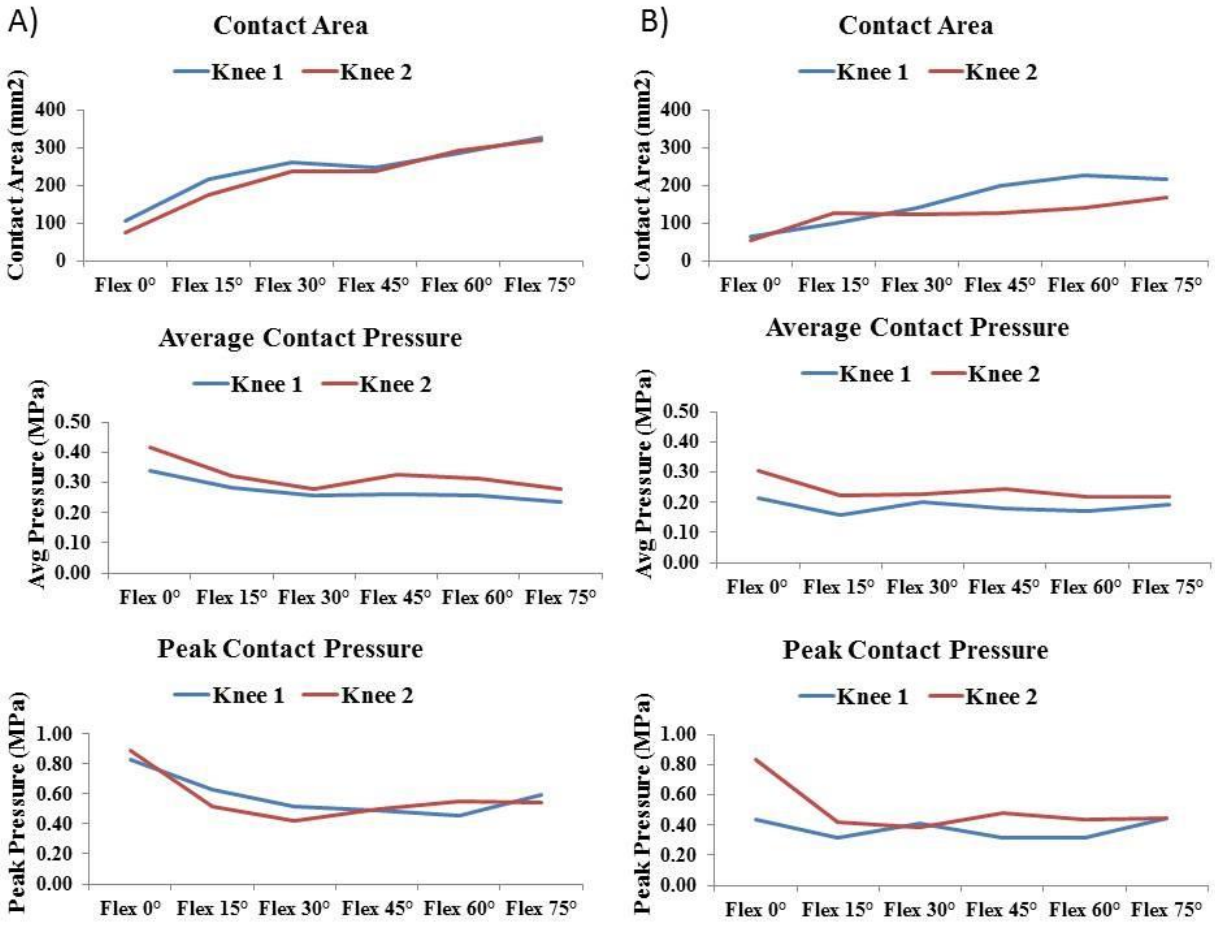

Figure 3.5. Sample Contact pressure results for A) lateral and B) medial patellar facets

The repeatability analysis from the one knee joint specimen tested demonstrated good measurement precision in terms of knee joint kinematics and patellofemoral contact mechanics.

Specifically, the average standard deviation (SD) of the translations across the three trials was at a sub-millimeter level for all variables (Table 3.1). The patellofemoral and tibiofemoral translations showed excellent test-retest repeatability across the planes of motion with an ICC of 0.98 and 0.83, respectively. The average standard deviation of the rotations across three trials at the repeated test positions was sub-degree for the frontal (abduction/adduction angle) and transverse (internal/external rotation) plane tibiofemoral kinematics (tibiofemoral: frontal plane SD = 0.33°, transverse plane SD = 0.50°). Similarly, the average standard deviation of the patellofemoral kinematics across the repeated test positions was sub-degree for the frontal (patellar spin) and transverse (patellar tilt) plane kinematics (patellofemoral: frontal plane SD = 0.26°, transverse plane SD = 0.49°). The patellofemoral and tibiofemoral rotations also showed excellent test-retest repeatability across the planes of motion with ICCs of 0.90 and 0.97, respectively. For both tibiofemoral and patellofemoral flexion, the average standard deviation across the repeated test positions ranged from 1.57° to 0.91°, respectively (Table 3.2).

Table 3.1. Measurement repeatability of kinematic translations (mm)

	Patellofemoral Joint			Tibiofemoral Joint		
Flexion angle (deg)	**LM**	**AP**	**SI**	**LM**	**AP**	**SI**
15, neutral	0.53	0.41	0.99	0.80	0.34	0.09
15, internal rotation 5°	0.22	0.34	1.18	0.42	0.51	0.05
45, neutral	0.08	0.09	0.17	0.58	0.03	0.34
75, neutral	0.17	0.07	0.13	0.23	0.69	0.11
Mean	**0.25**	**0.23**	**0.62**	**0.51**	**0.39**	**0.15**
Standard Deviation	**0.19**	**0.17**	**0.54**	**0.24**	**0.28**	**0.13**
LM = lateral/medial; AP = anterior/posterior; SI = superior/inferior						

Table 3.2. Measurement repeatability of kinematic rotations (degrees)

	Patellofemoral Joint			Tibiofemoral Joint		
Flexion angle (deg)	**Flexion**	**Spin**	**Tilt**	**Flexion**	**Varus/Valgus**	**Rotation**
15, neutral	1.8	0.3	0.5	2.8	0.5	0.5
15, internal rotation 5°	1.3	0.3	0.3	2.6	0.2	0.3
45, neutral	0.4	0.3	0.6	0.6	0.4	0.6
75, neutral	0.1	0.1	0.5	0.3	0.3	0.6
Mean	**0.9**	**0.3**	**0.5**	**1.6**	**0.3**	**0.5**
Standard Deviation	**0.8**	**0.1**	**0.1**	**1.3**	**0.1**	**0.1**

When assessing the repeatability of the pressure distribution in terms of contact area, average contact pressure, and peak contact pressure, the standard deviation relative to the mean (%) were all well within 10% (Table 3.3). The contact pressure measurements on the medial patellar facet were more variable than the lateral facet pressure measurements. Across both facets, the standard deviation relative to the mean of the repeated tests varied by 5.3% for contact area, 6.4% for average contact pressure, and 6.8% for peak contact pressure.

Table 3.3. Measurement repeatability of joint contact mechanics: standard deviation over three trials at each flexion, expressed as a percentage (%) of the mean value

	Lateral Facet			**Medial Facet**		
Flexion angle (deg)	**Area**	**Average Pressure**	**Peak Pressure**	**Area**	**Average Pressure**	**Peak Pressure**
15, neutral	4.0	4.1	8.1	5.0	4.8	1.3
15, internal rotation 5°	2.7	5.6	5.9	7.8	11.8	6.6
45, neutral	2.0	3.1	6.7	5.6	1.6	2.9
75, neutral	2.8	3.7	5.0	12.4	16.2	17.9
Mean	**2.9**	**4.1**	**6.4**	**7.7**	**8.6**	**7.2**
Standard Deviation	**0.8**	**1.1**	**1.3**	**3.4**	**6.6**	**7.5**

3.1.4 Discussion

This study evaluated a framework for simultaneously measuring patellofemoral joint kinematics and patellofemoral joint contact mechanics for the purpose of developing and validating computational models to predict knee joint contact stresses and test hypotheses relating to knee joint mechanics and cartilage degeneration. We assessed the repeatability of the system in measures of patellofemoral kinematics and pressure distribution in cadaver patellofemoral joints.

Repeatability of the measured motions and contact mechanics is vital as the intended use of this system is for validating computational models using the loading conditions and kinematics collected from this system. Many studies have been performed tracking the patellofemoral joint using various tracking techniques and various loading conditions [73, 74, 76-78, 80, 185]. Interestingly, most of these studies do not report the reproducibility of their system in tracking the motion of the patella under repeated loading conditions.

Two studies in particular [74, 78] reported the reproducibility of their tracking system under repeated loading conditions to be 0.15 – 0.3 mm for translations and 0.18° – 0.5° rotation rotations for both patellofemoral and tibiofemoral kinematics, respectively. The repeatability of the patellofemoral translations (SD range: 0.23 – 0.62 mm) and rotations (SD range: 0.3° - 0.5°) from the current study are on the same order of magnitude. However, the repeatability of the sagittal plane motions from our current system are much greater for both the patellofemoral (SD = 0.9°) and tibiofemoral (1.6°) flexions. This is most likely a result of the loading/unloading process for each repeated trial, where the knee was taken out and reloaded at each flexion angle using a goniometer. It has been shown that the intra-rater mean difference for measuring flexion and extension of the knee when using a goniometer is on the range of 2.7° - 2.2°, respectively [186]. The repeatability of achieving the same joint flexion position across three repeated trials in the current study is well within this measured difference.

Lastly, the highest error in our repeated measures was observed at 15° of tibiofemoral flexion, with an average SD of 0.9° and 1.3° across the planes of motion for the patellofemoral and tibiofemoral joint, respectively. One potential explanation is the positioning of the patella is not yet fully engaged within the trochlear groove and is in an unstable position relative to deeper knee flexion angles. As our kinematic measurement technique involves contacting the

registration blocks on the patella, it is possible that the patella can undergo small variations in motion due to digitizing the cube at more extended positions. Despite this limitation, we feel the repeatability of the kinematics is acceptable.

Our findings are also consistent with measurements from prior studies assessing the repeatability and accuracy of the Tekscan pressure measuring system when measuring the system on a flat surface as well as within a patellofemoral joint [187]. The primary outcome measure from this prior study was repeatability of force and force distribution, which was within 5% repeatability. The authors additionally reported repeatability values similar to the current study (range: 3% - 8%) in terms of contact area, mean pressure, and maximum pressure, although this was not divided into medial or lateral facet pressures, but rather total contact of the sensor. These findings, in conjunction with our results, provide confidence in the ability of the knee testing apparatus to repeatedly measure joint contact mechanics at the patellofemoral joint.

Special attention must be made as to the accuracy of this measuring system. The intended use of the current knee testing apparatus is to collect knee joint kinematics and contact mechanics to develop and validate computational models for estimating patellofemoral joint contact mechanics. Accuracy of a system in measuring the patellofemoral kinematics is vital when conducting experimental tests evaluating the difference between different knee states (i.e. ACL intact vs. ACL deficient) and making predictions and conclusions as to the effect of alterations in the knee state on measured kinematics. However, the kinematics of the current study will only be utilized as inputs to drive positioning of a computational model, which requires high precision. The measurement precision of the digitizer is 0.024 mm; however, this precision does not consider the kinematic tracking and calculations performed in the current study, as well as the precision of our testing system. As the goal of this testing system is to

develop knee joint models driven by knee joint kinematics and validate computational estimates of stress, it is important to evaluate the variability (lab equipment/user error) within a testing system, not just the individual measurement tool. The current testing system can reliably measure patellofemoral joint kinematics and contact mechanics.

Several limitations must be acknowledged for the current study. In terms of the contact mechanics, evaluating the accuracy of the pressure sensors has been undertaken by prior groups [187-189]. A limitation in these studies is accuracy was only assessed by either force or pressure measurements made using a materials testing machine under different loading scenarios [187, 188] or by comparing the Tekscan model sensors to prior pressure measuring techniques [189]. The Tekscan pressure system was shown to produce accurate measurements of contact area, average pressure and peak pressure within 10% of known, applied loads on a flat surface. Measuring the true contact pressures between two articulating surfaces, particularly at the patellofemoral joint, is a challenge due to the highly-curved geometry of the joint. Additionally, it is well understood that these pressure sensors are susceptible to variations in measurements based on the calibration method chosen [190]. Future work should be done to investigate optimal sensor choices, in terms of calibration and sensor design, when evaluating the contact mechanics at curved interfaces like the patellofemoral joint.

The goal of this study was to develop a repeatable system for simultaneously measuring patellofemoral joint kinematics and contact mechanics. The system used in this study was able to reproduce kinematic and contact mechanics across multiple tested positions within sub-degree and levels similar to the precision of the devices. Future studies will utilize this system to develop computational models of the patellofemoral joint driven by experimentally collected

kinematics and validate the contact stresses estimated from these models using contact pressure data collected experimentally.

4.0 AIM 2: FRAMEWORK FOR MODELING THE PATELLOFEMORAL JOINT

4.1 DEVELOPMENT AND VALIDATION OF A KINEMATICALLY-DRIVEN DISCRETE ELEMENT MODEL FOR ESTIMATING PATELLOFEMORAL JOINT CONTACT STRESS

As an integral part of the knee complex, the patellofemoral joint is often subjected to the greatest biomechanical forces in the body [40-42]. It has been reported that disorders of the patellofemoral joint affect as many as 22% of the general population, with higher incidence among women and those who are physically active [191-195]. Long term effects of patellofemoral disorders can lead to development of patellofemoral OA, with incidence rates as high as 33% and 36% in men and women over the age of 60 [196] and has been associated with significant functional limitations and pain [50, 167, 197]. Despite the high incidence of patellofemoral disease, the pathophysiology of this disorder remains unclear. Currently, the most accepted hypothesis as to the cause of patellofemoral pain, a well-documented precursor to patellofemoral OA [35], is related to abnormal patella alignment and/or tracking which elevates the patellofemoral joint stress environment and subsequently leads to the stimulation of highly concentrated nociceptors of the subchondral bone [41, 198-201].

In-vivo evaluation of patellofemoral joint stress is technically challenging, as many factors can influence stress, including the joint contact force, the geometry of the articulating

surfaces, material properties of the tissue, and thickness of the articular cartilage [135, 142]. Traditionally, quantification of patellofemoral joint stress has been made experimentally, using in-vitro cadaveric models [87, 120, 175, 202, 203]. Such studies have been valuable in providing information regarding the stress environment of the patellofemoral joint; however, the use of non-physiologic muscle loading has made extrapolation to the in-vivo condition questionable. More recently, advancements in numerical approximation techniques have allowed for development of more elaborate subject-specific computational models to investigate the internal stress environment of the patellofemoral joint.

The estimation of joint contact stresses can be achieved using a variety of methods, the most common of which implement finite element analysis (FEA). In general, FEA is a numerical technique for subdividing complicated domain problems into simpler finite element parts to solve a boundary value problem and approximate a solution for the large complex domain. This method has been implemented to assess stress in a variety of joints [37, 136, 138, 164, 204, 205]; however, the high logistical and computational cost of creating 3D contact FEA on a subject-specific basis makes FEA unattractive for stress analysis across large-scale studies and limits its clinical utility. A technical note by Anderson and colleagues [151] discusses the potential for utilizing discrete element modeling (DEA) techniques as a simple numerical framework for assessing articular contact. This method involves treating bones as rigid bodies and the cartilage across the joints as an array of compressive-only springs, significantly reducing computational cost [143, 144, 148, 206].

Current models of the patellofemoral joint incorporate the use of finite element techniques [37, 135, 142, 164, 207-209], discrete element methods [146, 155, 157, 158, 160, 210], or utilize a combination of subject-specific musculoskeletal computer models with accurate

in-vivo experimental data [140, 211, 212]. Most of these existing models require estimations of muscle and passive (i.e. ligament) forces along with load-based optimization techniques to drive the models and produce contact at the cartilage surfaces. Displacement control of models can bypass several of these passive and active force assumptions utilized with current force-control methods; however, highly accurate kinematics are essential for implementing displacement-driven models [213]. Theoretically, these displacement-driven models could be incorporated with highly accurate in vivo kinematic data collection techniques, such as biplane fluoroscopy, to estimate knee joint contact mechanics in patients with knee OA during functional tasks. With proper validation, models such as these offer the potential to understand the effect of altered patellofemoral motion associated with pathology on joint contact stress. In addition, these models would allow for improved prediction of the effect of conservative intervention strategies designed for treatment of patellofemoral dysfunction.

The primary objectives of this study were: 1) to develop a three-dimensional (3D), subject-specific modeling framework for estimating patellofemoral joint contact stress utilizing the discrete element method driven by highly accurate knee joint kinematics and 2) to validate the estimated contact stress distribution of the patellofemoral joint using this modeling framework in cadaveric knees. Model validation was carried out by comparing predicted patellofemoral joint contact stress distributions with those obtained from in vitro experiments. We hypothesized that the differences in the contact stress distribution, measured as the ratio of the lateral to medial patellofemoral facet contact stresses between the computational model and experiment, would be similar through Bland-Altman analysis [214, 215].

4.1.1 Methods

Two fresh-frozen cadaveric knees (age in years: specimen #1 = 52; specimen #2 = 46) were utilized for the development and validation of the modeling framework. Each knee specimen for this validation study was placed in a knee testing system discussed in Chapter 2. Briefly, both specimens were prepared for mounting in the knee testing system by dissection of soft tissues down to the capsule, with isolation of the quad tendons. The knee testing system allows for highly repeatable, unconstrained 6 degree of freedom (DOF) motion throughout knee flexion-extension while also allowing for application of tensile loads to the extensor tendons. Each knee specimen was positioned and loaded at several, discrete knee joint flexion angles to simulate the loading response phase of gait: 0° and 15° of tibiofemoral flexion with three femoral rotation positions (neutral alignment, 5° internal, and 5° external femoral rotation) and two varus/valgus positions (5° varus and valgus positioning). These joint positions were chosen for validation as they represent clinically relevant positions during the early portion of gait, when the patella is most susceptible to peak stresses [38, 169]. At each knee joint position, physiologic tensile loads were applied to the quadriceps tendons [181] and compressive loads applied to the proximal femur to simulate 50% of an individual's mean body weight (300 N) [177].

A mechanical digitizer (Faro Arm®, Lake Mary, FL) was used to quantify the positions of the patella with respect to the femur throughout the different testing states described above and in Chapter 3.1.2.3. Briefly, the digitizer was mounted on a metal plate and screwed to the knee testing system within arms distance of each registration block on the medial side of the specimen. The digitizer was calibrated and used to measure the motion of the rigid bodies (femur, patella, and tibia bone) relative to one another throughout the testing conditions. This was done by manually digitizing points on the surface of three pre-defined faces of each

registration block. These digitized points were imported into a custom Matlab program (Mathworks, Natick, MA) to calculate orthonormal local coordinate systems for the femur, patella and tibia bones [179].

Patellofemoral joint contact pressures serving as validation data for the model were collected at each testing position using calibrated, thin pressure sensors inserted into the joint space as described in Chapter 3.1.2.4. Briefly, patellofemoral joint contact pressures were measured using thin, flexible pressure sensors (K-scan Model 5051, 2.5K psi; Tekscan Inc., South Boston, MA). Prior to testing, the sensors underwent a conditioning, equilibration, and calibration protocol using a materials testing machine (Model 4502; Instron Corp., Norwood, MA). Once preparation was completed, a lateral patellofemoral retinacular release was performed in each specimen to allow the pressure sensors to be inserted posterior to the patella and sutured to the proximal soft tissue and distal patellar tendon. Lateral release of the retinacular fibers has been shown to medialize patella translation and tilt by as much as 1.0 mm and 1.68°, respectively, while not significantly altering patellofemoral pressure [178]. Despite these observed changes, this study was focused on validating joint contact pressures using a computational model driven by the patellofemoral kinematics. Thus, any change in kinematics due to the insertion process would be incorporated by the computational model in predicting the pressures measured at each position.

4.1.1.1 DEA modeling framework

The current DEA algorithm was implemented in MATLAB (2016a, The MathWorks, Natick, MA). The DEA methodology described required a preprocessing, model preparation step of the following: 1) subject-specific geometry segmentation from an imaging medical dataset; 2) mesh generation/refinement of the model; 3) cartilage thickness computation; and 4) alignment

of the model using subject-specific kinematics. Following these preparation steps, a contact algorithm was employed in order to calculate joint contact mechanics outcome variables (contact area and stress). A general outline of the model input and output can be seen in Figure 4.1.

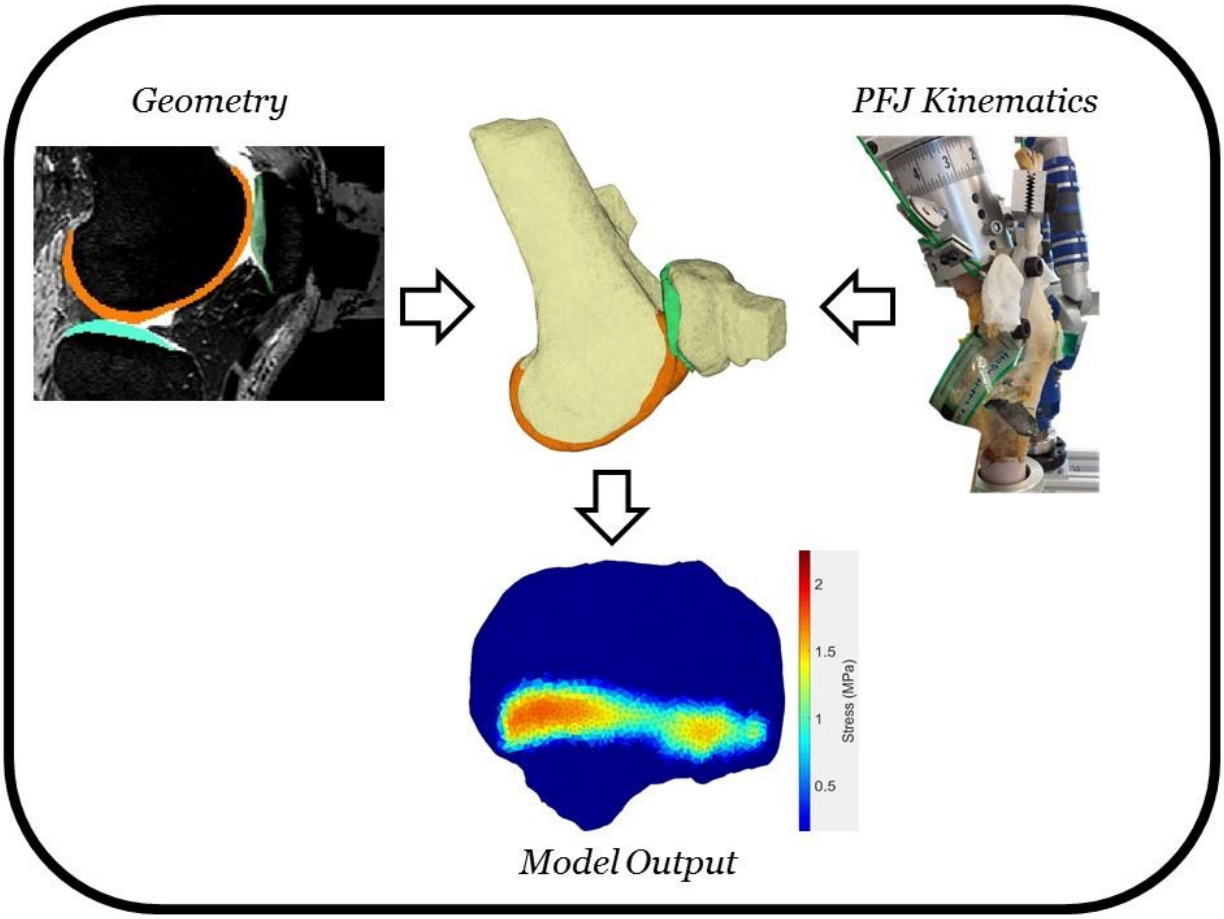

Figure 4.1. Discrete element modeling framework

4.1.1.2 Model preparation

Geometry preprocessing

Several steps were taken in order to generate specimen-specific bone and cartilage geometry, as well as developing the discretized mesh of the patellofemoral joint. First, rigid registration cubes were affixed to the femur and patella bone, which has been described in Chapter 3.1.2.1. Briefly, the rigid registration blocks were fixed to the medial femur near the joint line and on the center of the patella using cyanoacrylate and baking soda. These rigid

registration cubes were used in order to co-register the position of the bones in the computational model using experimental data, which will be discussed further in this chapter.

Second, high resolution, sagittal plane magnetic resonance images (MR) of each knee were acquired with a 3.0-T MR scanner (Siemens Medical Solutions, Malvern, PA, USA). All images were acquired using an eight-channel knee coil using a 3D, high-resolution, fat-suppressed, fast spoiled gradient recalled echo (SPGR) sequence (repetition time: 14.5 ms, echo time: 2.8 ms, flip angle: 10°, matrix: 320 x 320, field of view: 14 cm, slice thickness: 0.7 mm, pixel size: 0.44 mm, scan time of 8:58 min). This sequence has been shown to provide excellent images for distinguishing bone and articular cartilage for model development [37, 135]. Both knees were positioned supine in an extended position within the MR coil. In order to visualize the cubes within the MR scan, a petroleum jelly mixture was applied around the cubes.

The MR images were manually segmented (Mimics®, Materialise, Leuven, Belgium) by 1 observer with experience segmenting 5 different knee joint geometries. Briefly, separate masks were generated for the bones (femur and patella + respective registration blocks) and the articular cartilage (femoral and patellar cartilage). Once these masks were created, in-software Boolean operations were performed to ensure there were no overlapping voxels between the segmented bone and corresponding articular cartilage. Triangulated surfaces were then created for both bone and cartilage geometries from the segmented masks. An example of the segmentation process and 3D surface geometry generated from the segmentations can be seen in Figure 4.2.

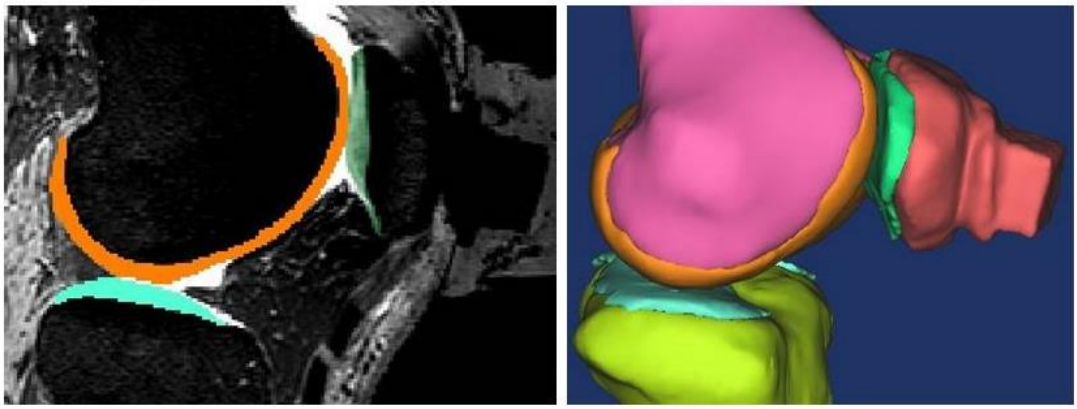

Figure 4.2. Sample image of segmented masks of geometry from MRI (left) and resulting 3D model (right)

Mesh generation and refinement

A mesh refinement was conducted on the surface geometry of the bones and articular cartilage using meshing software (Hypermesh, Altair Engineering Inc., Troy, MI). This meshing software allows for calculation of surface boundaries from triangulated surfaces in order to create a more uniform mesh based on the desired user preferences. Tetrahedral, shell elements were created for the bones and articular cartilage with an average element size of 1mm.

An important step in the development of a computational model is to assess the ability of the model to numerically calculate the outcome parameters repeatedly and to ensure all numerical approximations have been performed properly [216]. This process is known as a verification analysis and is typically performed by conducting a mesh convergence analysis in order to assess how sensitive the outcome variables are to changes in the average element length. A mesh sensitivity analysis was conducted for the tetrahedral elements at average side lengths of 4.0, 2.0, 1.0, 0.5 and 0.25 mm in order to assess convergence of the outcome parameters of mean and peak contact stress from the model (Figure 4.3). Results of the convergence study revealed that there were minimal changes in mean and peak contact stress between the 1 mm and 0.5 mm

case (average difference of 1.4%). Therefore, an average element size of 1 mm was deemed appropriate for all computational simulations.

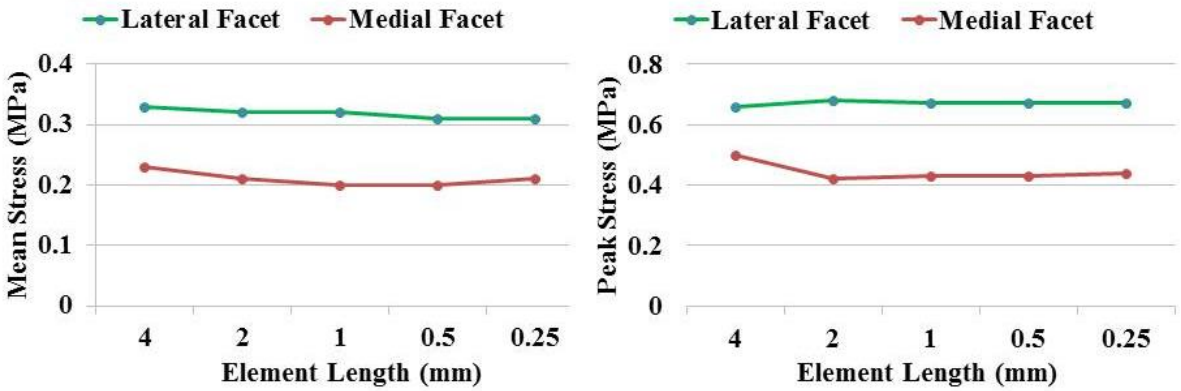

Figure 4.3. Results from the mesh convergence DEA analysis

Once each knee model was segmented and meshed, the individual bone and cartilage components were exported to a stereolithography (STL) file format, where each component of the model was stored as triangulated polygon surfaces consisting of a face-vertex mesh representation. This representation consists of a list of the faces of the individual elements, which contains set of the three vertex points making up each face, and a list of the vertices which contains the three-dimensional Cartesian coordinates of each vertex. These STL files were individually imported into MATLAB, where the DEA algorithm (described below) was applied in order to estimate knee joint contact stress at each joint position.

Cartilage thickness computation

The patellar and femoral cartilage thickness was calculated as a primary input to the DEA algorithm for estimating joint stress. This study utilized subject-specific cartilage segmented from the MRI in order to represent the detailed irregularities inherent in cartilage, which is

important when addressing joint contact in specific populations (i.e. knee OA). Cartilage thickness was computed by employing a nearest neighbor search on the entire collection of the articular cartilage surface faces to the underlying bone surface faces. This algorithm designated the articular cartilage surface for both the patella and femur as the "master" surface and the other subchondral bone surface designated as the secondary ("slave") surface. This designation ensured that each element on the patellar cartilage had a unique thickness value, which was calculated for each element by finding the Euclidian shortest distance to the subchondral bone using a nearest neighbor function (Equation 4.1).

Equation 4.1. Nearest neighbor search function

$$nn = \min_{ii=size(S)} (dist(q, P_{ii}))$$

An example of the nearest neighbor function can be visualized in Figure 4.4, where unique distances (i.e. thickness) for each element on the patellar cartilage were stored in the program for later use in the contact stress algorithm. Detailed information on this algorithm can be found in Appendix B.

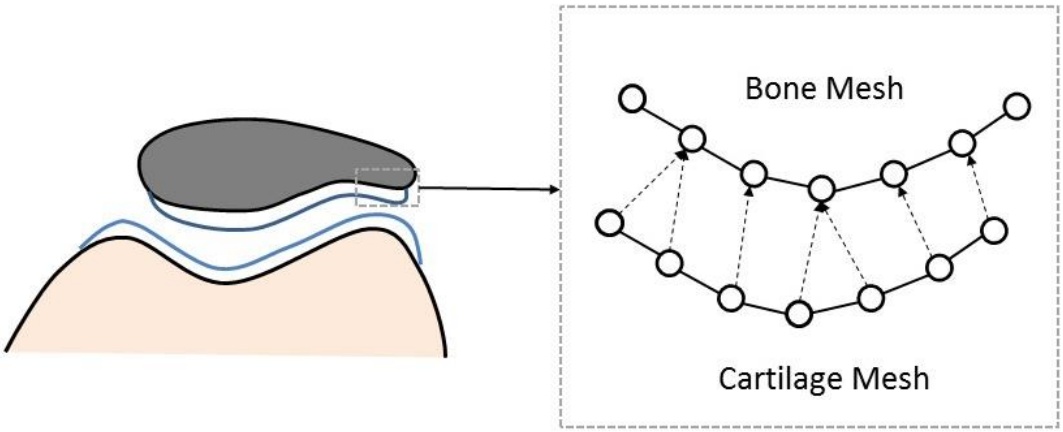

Figure 4.4. Cartilage thickness nearest neighbor algorithm

Model positioning using subject-specific kinematics

This dissertation employed a unique methodology for driving joint contact loading by deriving highly accurate kinematic transformation matrices collected during experimental testing. These transformation matrices were used to position the model-based geometry into the relative experimental loading condition, where the final, loaded apposition of the two contacting surfaces was used with the DEA analysis to calculate joint contact stress.

In order to position the computational model in the experimentally loaded conditions tested in Chapter 3, coordinate transformation matrices based on the registration blocks were calculated in order to navigate between the two primary coordinate systems in this study: 1) the experimental-based coordinate system measured from the mechanical digitizer and 2) the modeling-based coordinate system from the MR segmented images. This process of using local coordinate systems in a global reference frame to orient image-based geometry has been described in the past [179]. For this study, a multi-step process allowed for rigid transformation of coordinate points from the modeling coordinate system to the experimental coordinate system using transformation matrices for each rigid body (Equation 4.2).

Equation 4.2. Rigid body transformation matrix

$$T = \begin{bmatrix} 1 & 0 & 0 & 0 \\ LX & RXx & RXy & RXz \\ LY & RYx & RYy & RYz \\ LZ & RZx & RZy & RZz \end{bmatrix}$$

First, a local coordinate system was generated between the two reference frames. In this study, the two global reference frames being used were the magnetic resonance (MR) reference frame, in which the registration blocks were viewed in the medical image data set, and the experimental reference frame, in which the registration cubes were digitzed using the mechanical digitizer across the tested positions in Chapter 3.1.2.3. A general flow chart of the transformations used in this study to load the model in each experimental position can be seen in Figure 4.5.

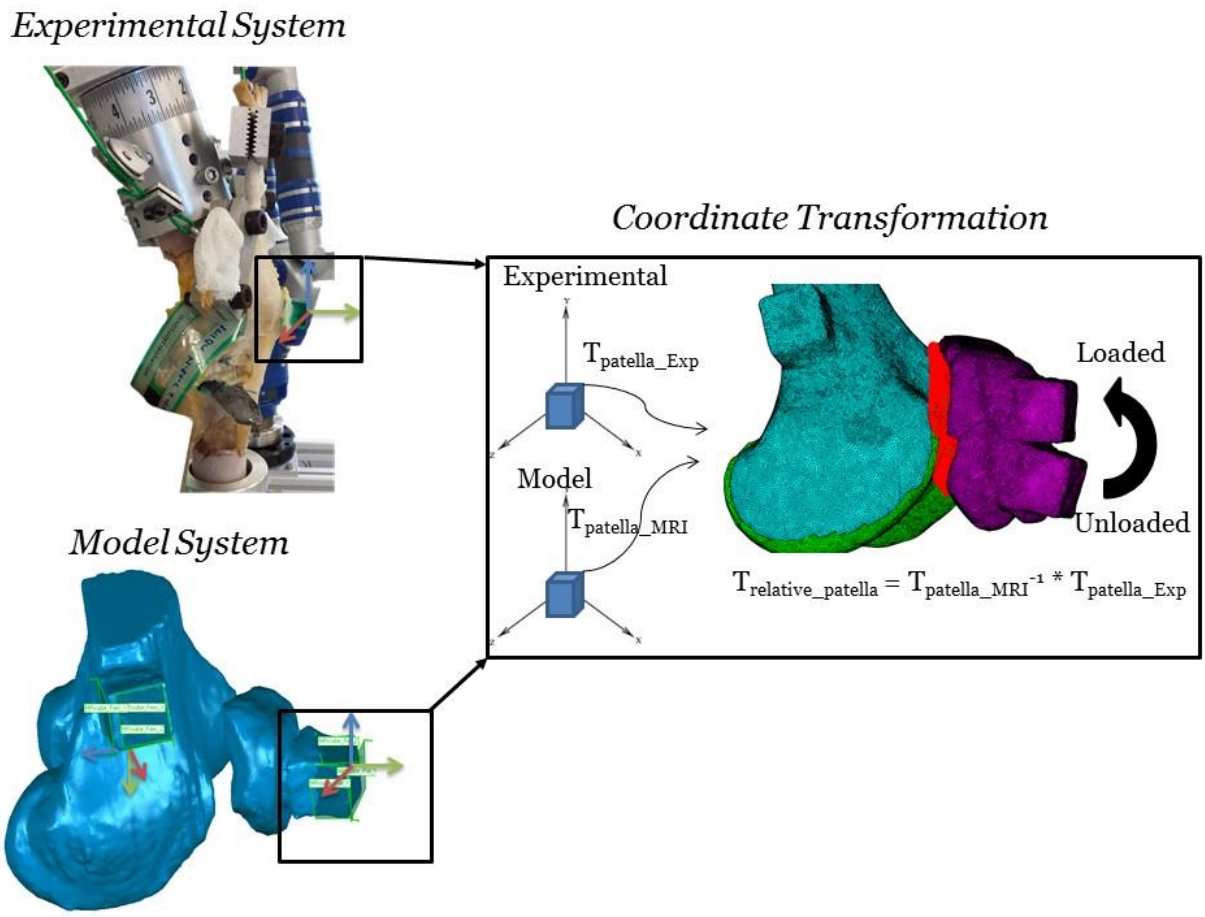

Figure 4.5. Flow chart of kinematic transformation from model-based patella (unloaded) to experimental position (loaded)

A local coordinate system was generated on the corner of the registration blocks by digitzing points on three, pre-defined faces of both the femur and patella blocks. A least-squares optimization technique was employed to fit the digitized points on each face of the block in either global reference frame (experimental/MRI) to the plane equation

Equation 4.3. Plane equation

$$Ax + By + Cz + D = 0$$

where the parameters A, B, and C represent the global X, Y, and Z components of a vector normal to the plane. These parameters are adjusted through a least squares optimization to minimize the distances, di, from each digitized point to the plane using the following equation:

Equation 4.4. Least square optimization method for creating best-fit plane

$$Min[\Phi\ (A,B,C,D)],\Phi = \sum_{i=1}^{N} di$$

$$di = \frac{|Ax_i + By_i + Cz_i - D|}{\sqrt{A^2 + B^2 + C^2}}$$

where x, y, and z correspond to the global coordinate (from MR or digitizer) of each digitized point. These three best-fit planes are used to define the orthonormal vector axes of each block, with the origin of the local coordinate system centered on the corner of the cube. This method resulted in an orthogonal, right-handed local coordinate system relative to the global reference frame (Figure 4.6).

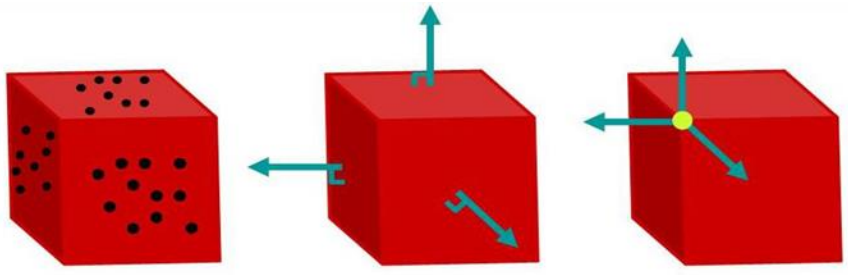

Figure 4.6. Creation of local coordinate system from digitized points

Once these local coordinate systems were generated for both the femur and patella registration blocks, affine transformation matrices were utilized to transform the position vector (points

defining the surface of each geometry) from the local coordinate system of the registration blocks in the MR model to the experimental registration cubes.

Equation 4.5. Transformation equation positioning the patella from the MR coordinate system to the experimental coordinate system

$$T_{loaded\_wrt\_global} = T_{Femur\_RB\_MRI} * T_{Patella\_wrt\_Femur\_MRI} * T_{Patella\_wrt\_Femur\_Exp}$$

These transformations were applied to the femur and patella, as well as their corresponding articular surfaces to position the model in the experimentally loaded states (Figure 4.5). This method has been shown to have an accuracy level of ±0.1 mm for translations and ±0.1° for rotations [179].

4.1.1.3 DEA simulation

Discrete element analysis: determining joint contact

The DEA method implemented in this dissertation consisted of the two, rigid femoral and patellar contact surfaces lined with a system of linear springs along the potential contact points. Springs were generated in the regions of apparent overlap detected between the contacting surfaces in response to the final, loaded apposition (displacement control) from application of the transformation matrices described above. The DEA method assumed apparent overlap as representative of the deformation within the tissue, thus defining the deformed length in each individual spring. These deformations in the springs relate to the engendered contact stress in each element of the contact surface. At each position, a single iteration of the DEA method was solved using the following steps: 1) efficient selection of nearest neighbor between the centroids

of the tetrahedral faces on the contacting surfaces, 2) generation of a spring system between the nearest neighbors, 3) determination of the engendered contact stress.

Efficient selection of nearest neighbors

To properly detect contact between the two articulating surfaces, distances between adjacent elements on the femoral and patellar cartilage was determined. This process is typically the most time-consuming aspect of any contact algorithm. The algorithm in the current study assumed that the surface can be represented by each of its individual element centroids and nearest neighbor distances between these centroids was found using a nearest neighbor algorithm Equation 4.1.

Multiple choices and criteria exist when performing a nearest neighbor search, all of which have their limitations and benefits [146]. The greatest consideration for selecting the nearest neighbor algorithm was the speed with which the algorithm was able to effectively select contact pairs. An example of a rudimentary method for selecting the nearest neighbor between two surfaces would be to calculate the distance between a point of interest (q) and every point (P) on a surface (S), such that the nearest neighbor pair is the minimum distance

Equation 4.6. Nearest neighbor search function

$$nn = \min_{ii=size(S)} (dist(q, P_{ii}))$$

While this simple algorithm allows one to obtain the nearest neighbor pairs, the computational time to find these pairs scales poorly with large data sets [217]. Therefore, this study employed a technique involving discretization of the searched surface into smaller “bins” using a space partitioning tree. In MATLAB, there are several space partitioning algorithms that can be employed. However, due to the geometric nature of the patellofemoral joint in terms of its

largely convex and concave surface structure, two algorithms were tested: 1) the inherent NearestNeighbor command in MATLAB, which uses the Triangulation MATLAB class to find the nearest triangle that contains the shortest Euclidian distance (Equation 4.7) between the vertex points of the triangle to the query point, and 2) the KD Tree Searcher, which breaks up the triangulated surface of interest into smaller sub regions and allows for faster distance measurements into each region as opposed to each individual point on the surface. Both algorithms were employed with the patellofemoral joint, and it was discovered that while the NearestNeighbor algorithm was significantly faster in computation time compared to the KD Tree Searcher (one order of magnitude), there were some important weaknesses to the Nearest Neighbor function that will be highlighted.

Equation 4.7. Three-dimensional coordinate Euclidian distance equation

$$distance(q,p) = \sqrt{(q_x - p_x)^2 + (q_y - p_y)^2 + (q_z - p_z)^2}$$

Due to the highly non-linear curvature of the patellofemoral joint, the NearestNeighbor algorithm would be unable to identify proper pairs from one surface to another. Specifically, this was problematic near the boundaries of contact pairs and particularly in the elements on the medial patellar facet, where the curvature in the patella can change quite rapidly. In these regions, a nearest neighbor would be identified as an element completely tangent to the primary direction of contact (anterior posterior), as opposed to an element along the surface normal of the expected deformation. To rectify this, a modified nearest neighbor function was employed for the current DEA method by using a KD Tree searcher to divide the femoral cartilage into smaller bins by using an expanding sphere searching technique from the centroid of the element of interest. This expanding sphere algorithm was used to identify all potential elements within a

certain radius (typically the thickness of the cartilage) of the patellar cartilage surface element. A search routine was additionally added to eliminate any elements within this "bounding sphere" that were not along the surface normal projection of the patellar cartilage surface face. Once the potential nearest neighbor candidates were narrowed using the sphere algorithm, the shortest Euclidean distance between the remaining pairs was calculated to find the correct match. Additional details on the use of this algorithm can be found in Appendix B.

Generating springs in contacting regions

Once the nearest neighbor pairs between the two surfaces were properly identified it was necessary to determine which pair of elements within the two surfaces to include in the DEA stress calculation. Springs were created between the surface pairs that had undergone apparent penetration. Penetration was determined by calculating the sign of the dot product of each element face's surface normal and the vector connecting the two surface faces paired in contact (Figure 4.7). If the patellar articular surface had undergone penetration with the femoral articular surface, F, the elements in overlap would have outward normal, n, in the opposite direction, i.e. anti-parallel (Equation 4.8).

Equation 4.8. Outward normal vector of overlapping surfaces are opposite in direction

$$n_{pcart} = -F \cdot n_{fcart}$$

Therefore, the sign of the dot product of overlapping areas would be negative, whereas areas that had not undergone penetration would have a positive value. Additional criteria were also added to eliminate potential pairs outside the area of contact, such as implementing a minimum distance threshold. This threshold was determined based on the amount of expected deformation and the thickness of the cartilage.

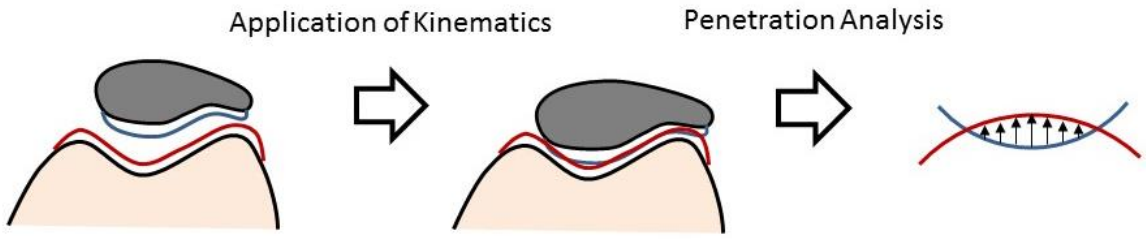

Figure 4.7. Articular cartilage penetration analysis

Once the springs were generated from the patella to the femur, the DEA contact stress was calculated. The current spring model assumed that the contact force in each spring was exclusively normal to the triangular face [144]. As the nearest neighbor pairs were computed from the centroid of each element in the surfaces, and accounting for the fact that multiple elements on the patellar contact surface were able to connect to a shared centroid element on the femoral contact surface, it was important to implement a correction to adjust the direction and length of the springs along the normal direction of each patellar surface element (Equation 4.9).

Equation 4.9. Spring normalization equation

$$S' = \mathrm{n} \cdot S$$

This correction was performed by calculating the dot product between the spring vector, S, and the unit normal vector, n, of each element to generate the new displacement of the contacting springs, S', thus projecting all of the springs in the normal direction of the contact surface.

Contact stress calculation

Once the system of springs was generated, contact stress was computed between the two surfaces. The following linear elastic spring model was employed to calculate the engendered contact stress (p):

Equation 4.10. Linear elastic spring model

$$P = \frac{(1 - v)E}{(1 + v)(1 - 2v)h} d$$

where v is Poisson's ratio, E is cartilage elastic modulus, h is the undeformed cartilage thickness and d is the spring deformation. The thickness, h, was computed as the combination of the cartilage thickness value assigned to each element associated with each spring. Spring deformation, d, was represented by the corrected distance between the nearest neighbor pairs of the contacting surfaces. The DEA-estimated joint contact stress was calculated at each joint position by creating compression-only springs (E=1MPa, ν=0.42 [144, 145]) at the centroid of each element of the segmented femoral and patellar cartilage surfaces [154]using Equation 4.10. This algorithm was implemented for every element on the patellar cartilage surface. Contact stress was then divided into medial and lateral patellar facet regions, defined by drawing a line through the inferior apex to the superior-most point on the base of the patella. More details on this calculation can be found in Appendix B. Outputs from the model in the current study included mean and peak contact stresses for each facet across the different flexion angles and rotation positions measured.

4.1.1.4 Validation analysis

The DEA model results were validated by using the data collected from experiments in specific Aim 1. Knee joint contact stress distribution, mean stress and peak stress were estimated

for each knee specimen at the different joint positions applied to the model. Qualitative comparisons of joint contact stress distributions between the experimental and computational results were performed as a first pass for each specimen. Quantitative comparisons of lateral facet and medial facet stresses as well as lateral to medial facet ratio of mean contact stress (Mean StressLatFacet / Mean StressMedFacet) and peak contact stress (Peak StressLatFacet / Peak StressMedFacet) of the patellofemoral joint were performed between the experimental and computational results. The ratio of the facet contact variables was used as the outcome measure to evaluate the ability of the model to predict the experimental contact pressures distributions from the pressure sensor results at the different flexion angles as well as with changes in rotations. Differences in the ratio of the lateral to medial patellofemoral facet contact stresses between the computational model and experiment were used to generate Bland-Altman plots to assess bias of the computational model and determine limits of agreement (LOA). Additionally, a Pearson product-moment correlation coefficient was computed to assess the relationship between the experimental and computational mean and peak stress. All statistical tests were performed in SPSS (IBM, Armonk, NY).

4.1.2 Results

In general, the computational model was able to predict the contact stress distributions from the experimental pressure sensors across the different joint positions. The following section will perform a case-by-case assessment of the model with each knee specimen, starting with a comparison of the stress distribution plots and discussing the quantitative results:

4.1.2.1 Specimen #1

Specimen #1 had a mean patellar articular cartilage thickness of 3.6 mm and mean femoral cartilage thickness of 2.6 mm. Cartilage regions were markedly thicker in the medial patellar cartilage and the medial trochlea of the femoral cartilage (Figure 4.8 & Figure 4.9).

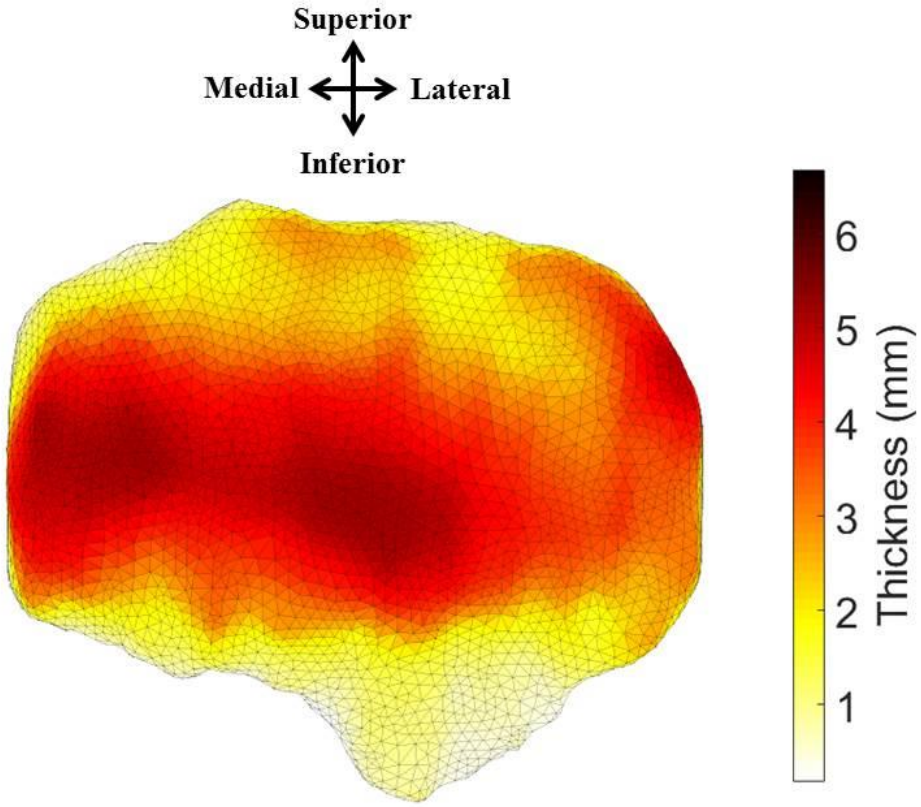

Figure 4.8. Patellar articular cartilage thickness map for specimen #1

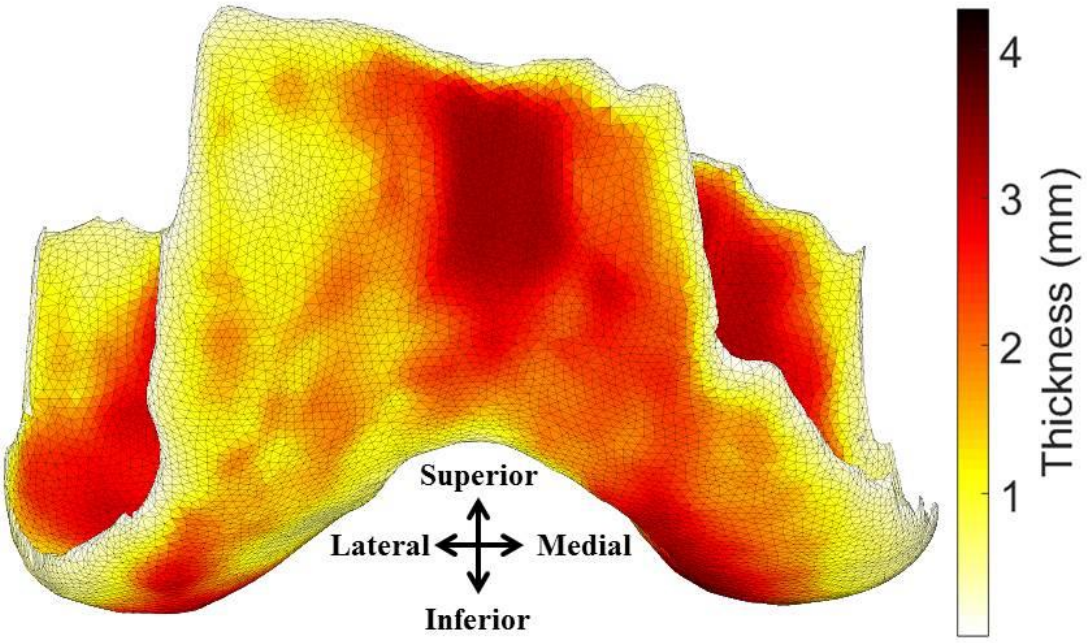

Figure 4.9. Femoral articular cartilage thickness map for specimen #1

Comparisons between the experimentally measured and DEA computed contact stress for Specimen #1 across the tested positions are shown in Table 4.1. Overall, locations of high contact stress were visually similar between the experimental and DEA contact stress distributions. At the full extension position, there is an appreciable change in the joint contact stress distribution when going from an external rotated femur to an internally rotated femur for both the experimental data and computational model (Figure 4.10). There is a more even distribution of stress between the medial and lateral facet at an externally rotated position (A). As the joint position moves into a more internally rotated position, the contact shifts from the medial facet to the lateral facet (B – C), with the greatest peak stresses observed on the lateral facet at an

internally rotate position (C). These trends were similar at 15° of tibiofemoral flexion as well (Figure 4.11) between the computational model and experimental stress plots.

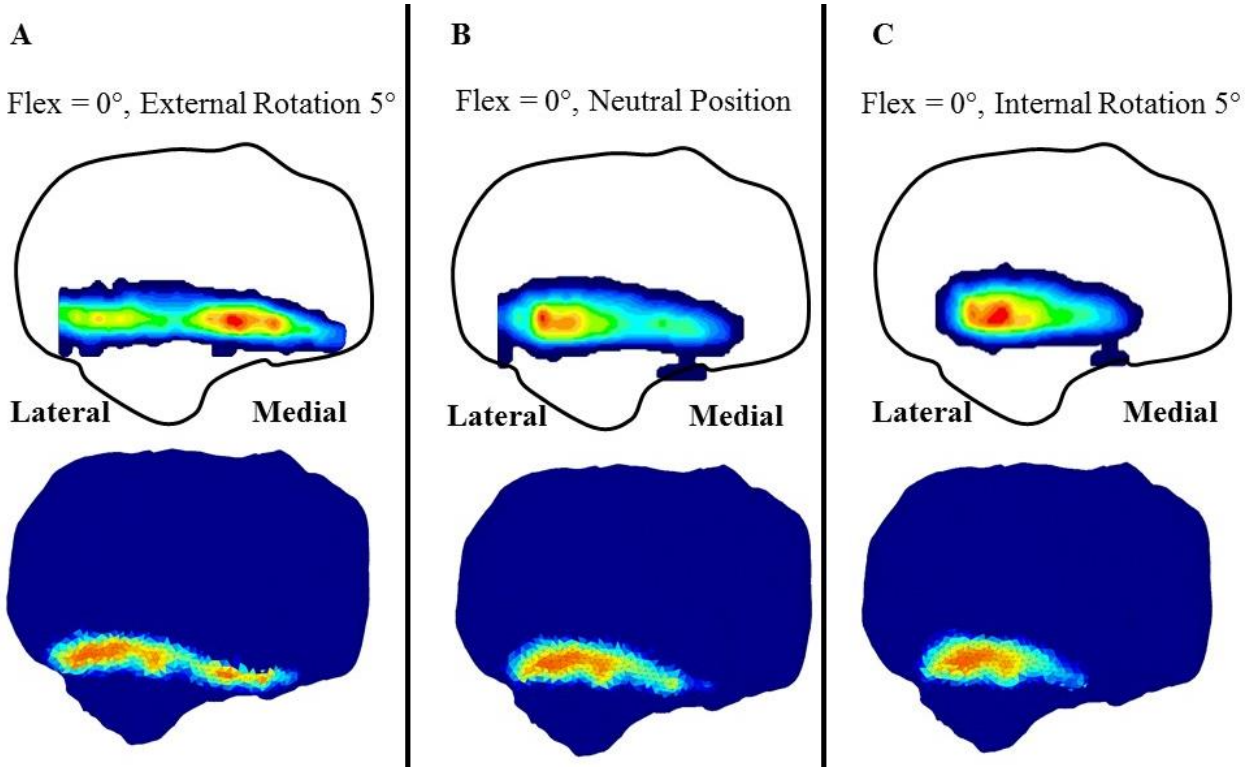

Figure 4.10. Experimental (top) and computational (bottom) patellofemoral contact stress distributions for specimen #1 at full extension with varying degrees of femoral rotation (A = 5° internal rotation; B = neutral femoral alignment; C = 5° of external rotation)

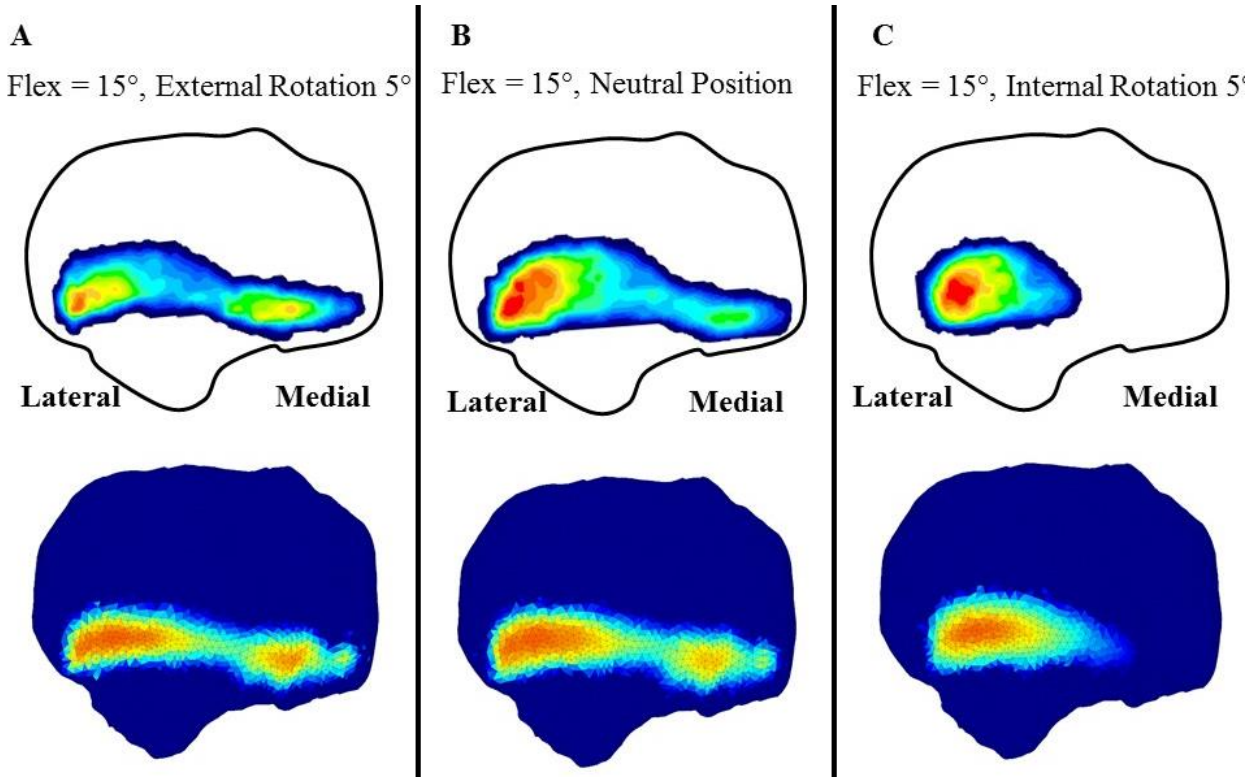

Figure 4.11. Experimental (top) and computational (bottom) patellofemoral stress distributions for specimen #1 at 15° knee flexion and varying degrees of femoral rotation (A = 5° internal rotation; B = neutral femoral alignment; C = 5° of external rotation)

Quantitatively, the computational model consistently overestimated the experimental stresses. The lateral facet mean contact stress ranged from 0.22 MPa – 0.40 MPa experimentally vs. 0.6 – 0.68 MPa computationally. The lateral facet peak contact stress ranged from 0.39 MPa – 0.93 MPa experimentally vs. 1.02 MPa – 1.19 MPa computationally. The medial facet mean contact stress ranged from 0.12 MPa – 0.25 MPa experimentally vs. 0.25 MPa – 0.6 MPa computationally. The medial facet peak contact stress ranged from 0.27 MPa – 0.57 MPa experimentally vs. 0.56 MPa – 0.99 MPa computationally. Overall, moderate, positive correlations were observed for lateral facet mean contact stress ($r = .40$, $p = 0.17$) and no correlation was observed for lateral facet peak contact stress ($r = 0.08$, $p = 0.80$) between the experimental and computational measure. When assessing the medial facet, no correlation was

found between the experimental and computational mean contact stress ($r = 0.23$, $p = 0.44$) and a weak to moderate, non-significant correlation was observed for peak contact stress ($r = 0.28$, $p = 0.11$).

Table 4.1. Contact stress results for specimen #1 across the knee joint positions tested

	Lateral Facet				**Medial Facet**			
	Mean Contact Stress (MPa)		Peak Contact Stress (MPa)		Mean Contact Stress (MPa)		Peak Contact Stress (MPa)	
Position (degrees)	Experimental	DEA	Experimental	DEA	Experimental	DEA	Experimental	DEA
0, external rotation 5	0.2	0.63	0.39	1.08	0.24	0.6	0.57	0.99
0, neutral	0.33	0.61	0.83	1.03	0.22	0.38	0.44	0.75
0, internal rotation 5	0.4	0.68	0.93	1.13	0.21	0.36	0.44	0.71
0, valgus 5	0.32	0.67	0.71	1.09	0.25	0.5	0.53	0.98
0, varus 5	0.29	0.6	0.71	1.02	0.23	0.48	0.53	0.91
15, external rotation 5	0.22	0.61	0.53	1.17	0.21	0.58	0.47	0.96
15, neutral	0.29	0.61	0.63	1.17	0.17	0.55	0.31	0.9
15, internal rotation 5	0.38	0.64	0.84	1.23	0.15	0.25	0.27	0.56
15, valgus 5	0.29	0.64	0.72	1.24	0.12	0.55	0.22	0.92
15, varus 5	0.3	0.63	0.66	1.19	0.14	0.51	0.27	0.84

Table 4.2. Contact stress results for specimen #2 across the knee joint positions tested

	Lateral Facet				**Medial Facet**			
	Mean Contact Stress (MPa)		Peak Contact Stress (MPa)		Mean Contact Stress (MPa)		Peak Contact Stress (MPa)	
Position (degrees)	Experimental	DEA	Experimental	DEA	Experimental	DEA	Experimental	DEA
0, external rotation 5	0.3	0.46	0.69	0.85	0.35	0.61	0.86	0.98
0, neutral	0.42	0.56	0.89	1.1	0.31	0.41	0.83	0.74
0, internal rotation 5	0.55	0.57	1.13	1.12	0.36	0.33	0.76	0.58
0, valgus 5	0.39	0.57	0.85	1.26	0.23	0.46	0.75	0.78
0, varus 5	0.38	0.52	0.86	1.03	0.24	0.36	0.73	0.69
15, external rotation 5	0.26	0.21	0.42	0.41	0.32	0.25	0.55	0.45
15, neutral	0.32	0.26	0.52	0.45	0.22	0.18	0.42	0.37
15, internal rotation 5	0.38	0.27	0.61	0.48	0.23	0.17	0.39	0.36
15, valgus 5	0.3	0.28	0.52	0.51	0.23	0.21	0.41	0.43
15, varus 5	0.33	0.3	0.57	0.55	0.23	0.21	0.41	0.42

4.1.2.2 Specimen #2

Specimen #2 had a mean patellar articular cartilage thickness of 2.8 mm and mean femoral cartilage thickness of 2.3 mm. Cartilage regions were markedly thicker in the medial patellar cartilage and the medial trochlea of the femoral cartilage, while signs of patellar cartilage thinning were observed on the superior-lateral aspect of the patellar cartilage (Figure 4.12 & Figure 4.13).

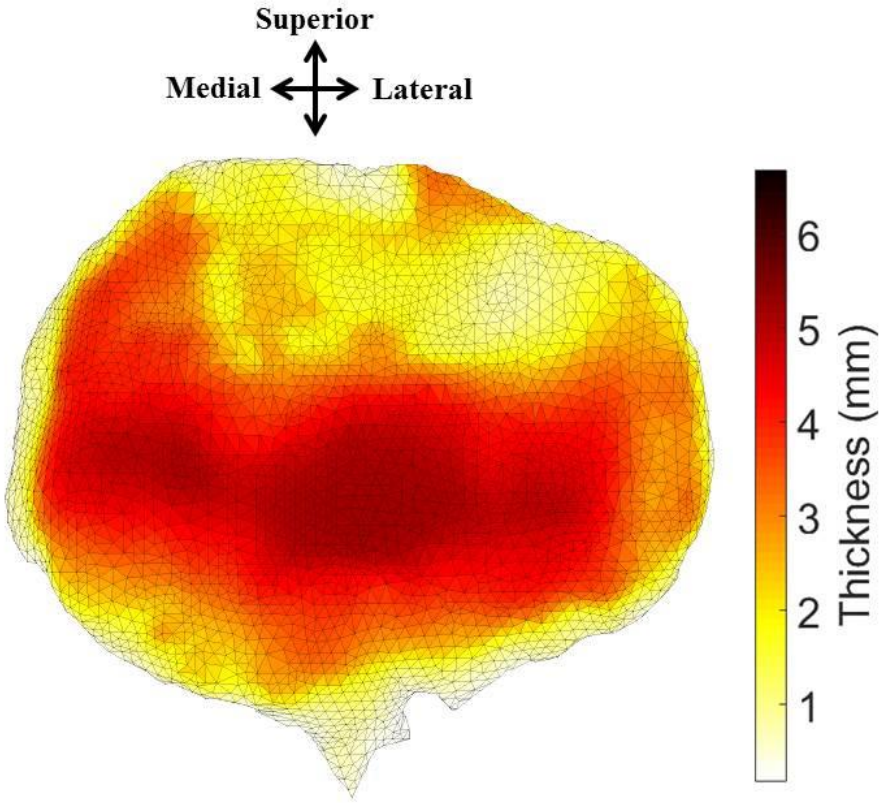

Figure 4.12. Patellar articular cartilage thickness map for specimen #2

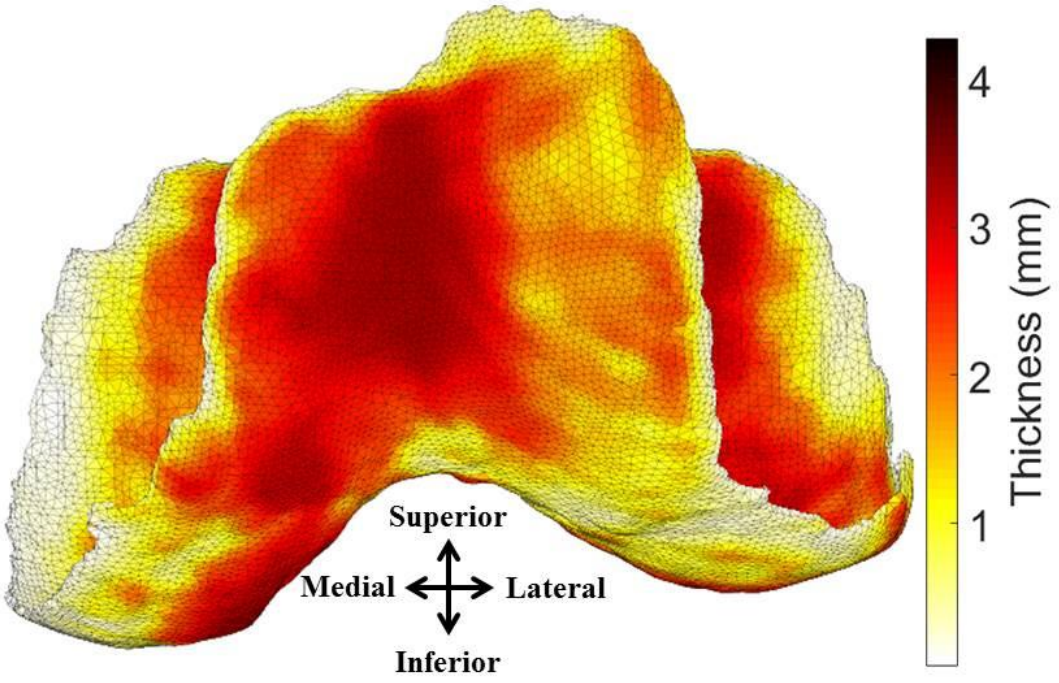

Figure 4.13. Femoral articular cartilage thickness map for specimen #2

Comparisons between the experimentally measured and DEA computed contact stress for Specimen #2 across the tested positions are shown in Table 4.2. Similar to specimen # 1, locations of high contact stress were visually similar between the experimental and DEA contact stress distributions. At both full extension and 15° of tibiofemoral flexion, there were appreciable increases in lateral facet contact stress when going from an externally rotated position to an internally rotated position (Figure 4.14 & Figure 4.15).

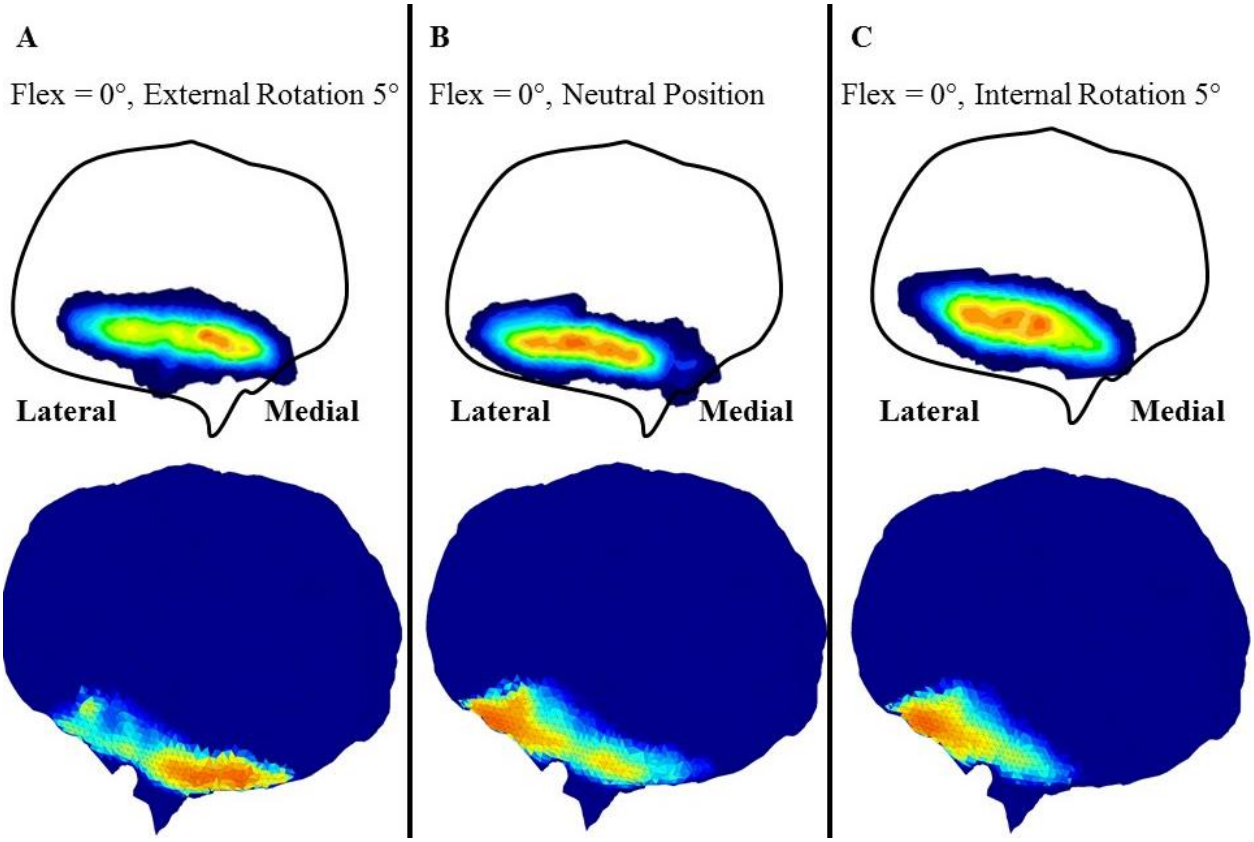

Figure 4.14. Experimental (top) and computational (bottom) patellofemoral stress distributions for specimen #2 at full extension with varying degrees of femoral rotation (A = 5° internal rotation; B = neutral femoral alignment; C = 5° of external rotation)

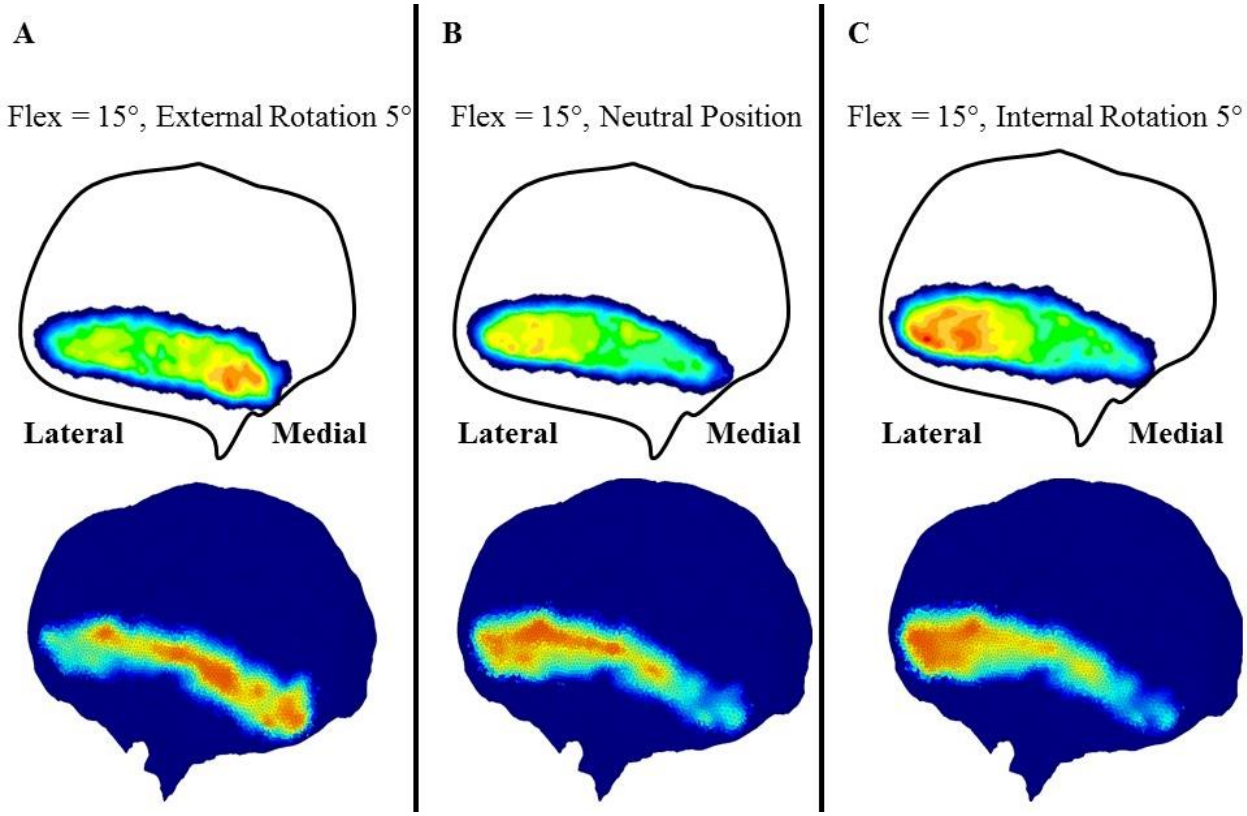

Figure 4.15. Experimental (top) and computational (bottom) patellofemoral stress distributions for specimen #2 at 15° knee flexion and varying degrees of femoral rotation (A = 5° internal rotation; B = neutral femoral alignment; C = 5° of external rotation)

Quantitatively, the computational model did an excellent job of predicting the experimental stresses. The lateral facet mean contact stress ranged from 0.26 MPa – 0.55 MPa experimentally vs. 0.21 – 0.57 MPa computationally. The lateral facet peak contact stress ranged from 0.42 MPa – 1.13 MPa experimentally vs. 0.41 MPa – 1.26 MPa computationally. The medial facet mean contact stress ranged from 0.23 MPa – 0.36 MPa experimentally vs. 0.17 MPa – 0.61 MPa computationally. The medial facet peak contact stress ranged from 0.39 MPa – 0.86 MPa experimentally vs. 0.37 MPa – 0.98 MPa computationally. Overall, strong correlations were observed for both lateral facet mean contact stress ($r = 0.71$, $p = 0.02$) and lateral facet peak contact stress ($r = 0.90$, $p < 0.001$) between the experimental and computational measures. When assessing medial facet stress, a moderate, but non-significant correlation was found between the

experimental and computational mean contact stress ($r = 0.54$, $p = 0.11$); however, a strong correlation was found between the experimental and computational peak contact stress ($r = 0.92$, $p < 0.001$). A summary of the data for specimen #2 can found in Table 4.2.

4.1.2.3 Lateral to medial ratio of contact stress

The lateral to medial ratio of joint contact stress was calculated to estimate the ability of the DEA model to predict the contact stress distribution from the pressure sensor. In general, both mean and peak lateral to medial facet contact stress for both the DEA model and experimental data were greater than a value of 1.0, indicating greater lateral facet loading (Figure 4.16). Both mean contact stress and peak contact stress ratios were less than 1 at the externally rotated positions (0° and 15°) for the DEA model and experimental data, indicating greater medial facet loading. For specimen #1, moderate to strong correlations were observed for the lateral to medial ratio of mean contact stress ($r = 0.68$, $p = 0.02$) and peak contact stress ($r = 0.70$, $p = 0.01$) between the DEA model and experimental data. Similarly for specimen #2, moderate to strong correlations were observed for the lateral to medial ratio of mean contact stress ($r = 0.85$, $p = 0.002$) and peak contact stress ($r = 0.63$, $p = 0.049$) between the DEA model and experimental data.

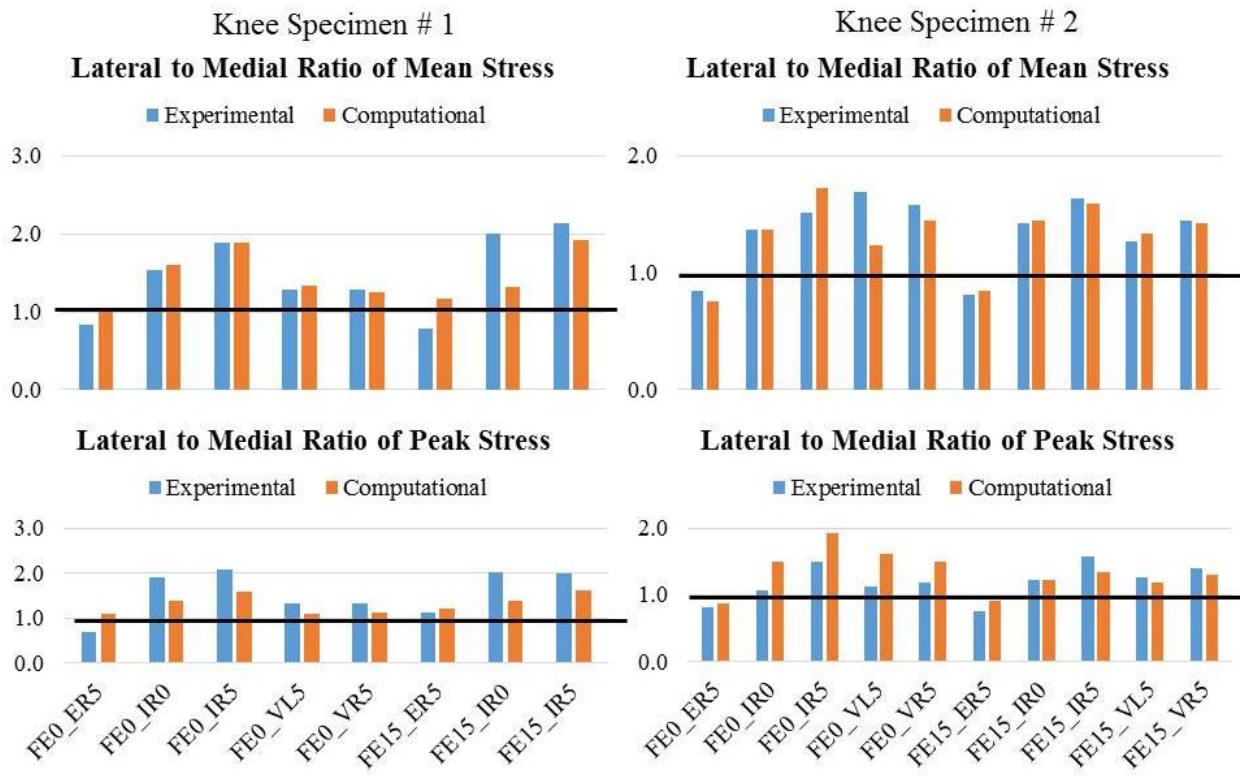

Figure 4.16. Lateral to medial facet ratio of mean (top) and peak (bottom) contact stress between DEA model and experimental data for specimen #1 (left) and specimen #2 (right) across multiple joint positions: FE = flexion angle, IR0 = neutral femoral alignment, IR5 = internal femoral rotation 5°, ER5 = external femoral rotation 5°, VL5 = valgus 5°, VR5 = varus 5°

4.1.2.4 Bland-Altman analysis

A Bland-Altman analysis was performed on the lateral to medial facet ratio of mean and peak contact stress between the experimental and computational data. The Bland-Altman analysis is useful when comparing two different measuring techniques to assess measurement bias and establish limits of agreement (LOA) of the data points. This analysis is performed by plotting a scatterplot of the difference between the two paired measurements (computational – experimental), known as bias, on the Y-axis and plotting the average of the measures on the X-axis [214, 215]. This analysis determines the agreement between two measurement techniques while identifying potential bias within a system. For validating measurement from one technique

using another, 95% of the data points should be within the upper and lower LOA while maintaining a “small” mean bias (i.e. close to 0).

The Bland-Altman analysis for this study was performed on the lateral to medial facet ratios to assess how well the computational model was able to estimate the contact stress distribution from the pressure sensors at each joint position. This analysis was performed for mean contact stress and peak contact stress for both knee specimens. The results can be seen in Figure 4.17.

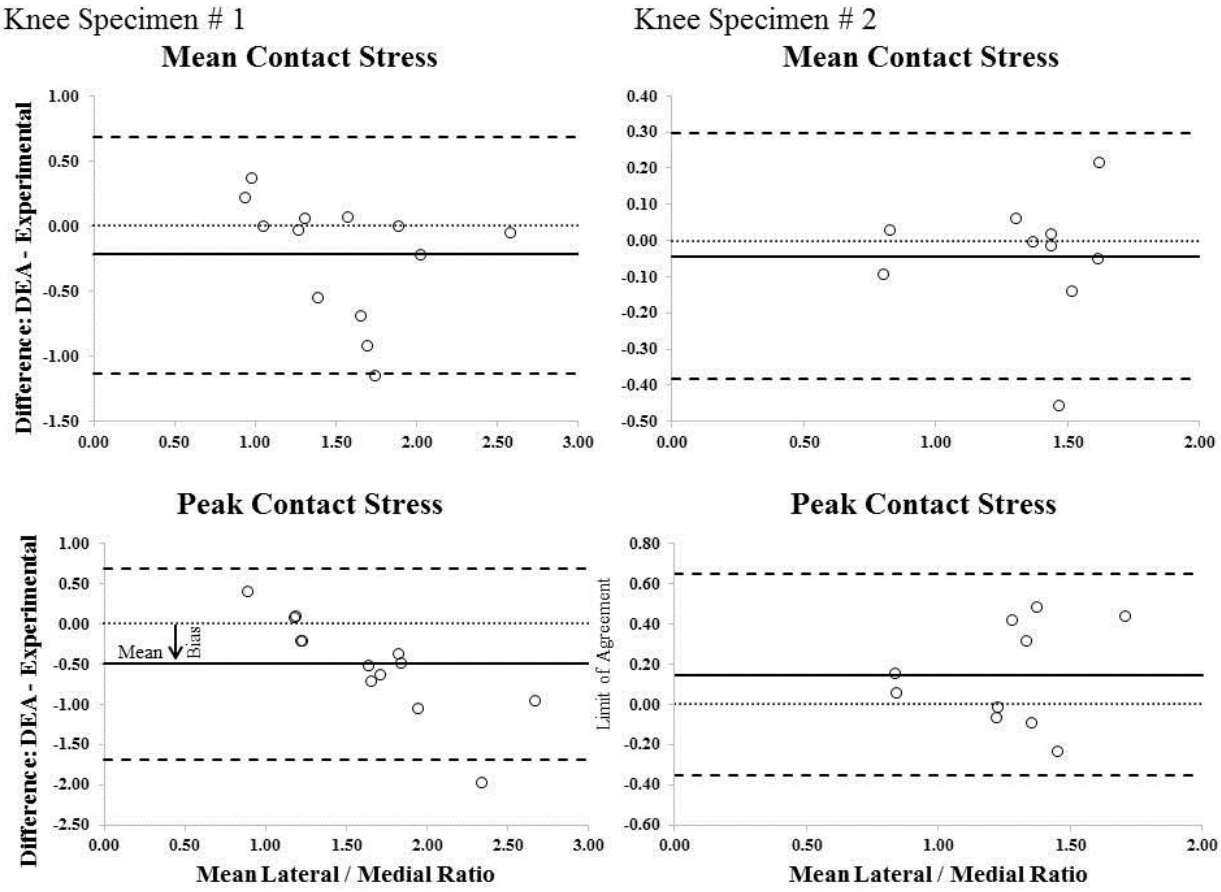

Figure 4.17. Bland-Altman plots of differences between DEA and experimental measures vs. the mean of the two methods in measuring lateral to medial facet contact stress ratio. Plots are shown for mean contact stress (top) and peak contact stress (bottom) lateral to medial facet ratio for specimen #1 (left) and specimen #2 (right)

For specimen # 1, the measurement bias for the lateral to medial facet ratio of the mean contact stress was -0.22 (95% confidence limits of agreement: -1.13 to 0.68). The measurement bias for the lateral to medial facet ratio of the peak contact stress was -0.50 (95% confidence limits of agreement: -1.69 to 0.68). For specimen # 2, the bias between the DEA model and experimental data was much lower. The measurement bias for the lateral to medial facet ratio of the mean contact stress was -0.04 (95% confidence limits of agreement: -0.38 to 0.30) and for peak contact stress was 0.14 (95% confidence limits of agreement: -0.35 to 0.64).

4.1.3 Discussion

The objective of this study was to develop a subject-specific modeling framework employing the DEA method driven by knee joint kinematics to estimate patellofemoral joint contact. Additionally, a secondary objective was to validate this modeling framework by comparing DEA-computed contact stresses with those measured experimentally at multiple knee flexion positions. In this study, the DEA model stress distributions were qualitatively similar to the experimental pressure distributions, both in relative magnitude and location of contact. The changes in joint contact stress distributions due to changes in femoral rotation at different flexion angles were also predicted by the DEA model. A correlation analysis confirms a strong relationship between the experimental and computational contact stress values. Finally, a Bland-Altman analysis was performed to assess the measurement bias of the lateral to medial facet stress ratios predicted by the DEA model and establish limits of agreement.

In general, the DEA model predicted greater contact stresses in terms of mean and peak contact stress compared to the experimentally measured contact pressures, regardless of the facet joint. This is consistent with prior DEA-based modeling studies, where DEA has been shown to overestimate contact stress values for different joints [149, 151, 155, 218]. This tendency to overestimate contact stress is in part due to the independent nature of each spring within the model, where deformation throughout the articulating surface at each spring has no effect on the neighboring springs. This is a gross simplification of the highly non-linear contact happening at the joint interface; however, this simplification can bypass many challenges associated with FEA and complex contact modeling.

Additionally, the DEA model estimates of stress in the current study are highly dependent on the material property values (i.e. cartilage elastic modulus, E, and Poisson's ratio, v) chosen

for the springs. The relationship between stress and cartilage elastic modulus is a linear relationship, meaning if the elastic modulus is increased by 2-fold, the stress will increase by 2-fold as well. The elastic modulus for the articular cartilage of the patellofemoral joint has been found to have wide-ranging values, dependent on the type of testing (indentation vs. confined compression) and the rate of loading [104, 219, 220]. The elastic modulus in the current study was on the "low end" of modulus compared to other modeling studies [135, 155]. However, the choice of the material properties in the current study was appropriate based on the range of material properties described in the literature and the age of the specimen. A detailed assessment of the effect of varying material properties of the springs on outcome mean and peak contact stress can be found in Appendix C.

Upon inspecting the stress values closer, a reduction of the elastic modulus by one half for specimen #1 would have brought the absolute magnitudes of mean and peak contact stress from the DEA model closer to the experimental data, which indicates potential differences in cartilage material properties between the two knee joint specimens for this validation study. Ultimately, the primary goal of this model was to reproduce the distribution of the stress patterns as opposed to matching the exact magnitude of stress. These DEA models are intended to be used to evaluate the effect of different rehabilitation treatments on joint contact patterns, with the goal of reducing excessive compartmental loading and restoring more even stress throughout the knee joint. For this reason, the ratio of the mean and peak contact stresses, not the magnitude, were used as primary surrogates of evaluating the model's ability to predict the experimental contact pressure distribution.

In general, the DEA model underestimated the lateral to medial contact stress ratio, indicating that the model was more evenly loaded (less lateral facet contact stress) compared to

the experimental data. Despite this, the model predicted the changes in the contact stress across both facets with the changes in femoral rotation, indicating the model's sensitivity to small changes in rotation. In support of this, the model predicted the changes in mean and peak contact stress on each facet as a result of the different rotational positions within 15% - 19% of the experimental data, respectively. This has important implications as this validated model is intended to be used with individuals with patellofemoral dysfunction to estimate stress during functional tasks. To this end, it has been found that the range of motion during tasks such as gait have been reported to be on the order of 0.8° - 4° in terms of tibiofemoral adduction and femoral rotation, respectively, and 2.5° of patellar tilt [70, 221]. If this model is to be utilized with highly accurate in-vivo kinematics, like those collected using biplane fluoroscopy methods, the model must be validated at these joint positions. This study demonstrates the model's ability to do estimate patellofemoral stress at these functionally relevant positions.

When assessing the ability of the DEA model to predict the experimental lateral to medial ratio of contact stress, the model performed quite well. The lateral to medial ratios of the contact stress were well correlated and the bias was relatively small when averaged for both mean and peak contact stress across the two specimens (-0.16). This is the first study to attempt to validate the lateral to medial facet ratio of the contact stress in the patellofemoral joint at the tested joint positions using displacement-driven DEA models. Comparing the results from the current study with prior modeling studies looking at the effect of hamstrings loading on patellofemoral stress distribution [154] and patellofemoral joint stress loading during gait simulated from musculoskeletal models [222, 223], the ratio of facet stresses are within a similar range (1.25 – 1.80). It should be noted that these studies were either at higher flexion angles (40°) or did not report the knee joint angle (tibiofemoral flexion as a % of stance phase of gait), but still provide

a reference for the stress ratios estimated from the current displacement-driven modeling framework.

Prior validation studies employing force-controlled DEA models have been performed in the patellofemoral joint [154, 155]. These studies validated the ratio of the lateral patellar facet forces and stresses due to changes in either surgical procedure or added hamstrings loading, with the primary validation criteria being correlated model results with experimental data ($r^2 = 0.79$) or reporting no significant difference between the model and experimental results. While these measures provide information as to the association between the model and experimental data, they do not directly assess the differences between the results as with the Bland-Altman analysis.

Studies using the Bland-Altman analysis as a metric for validating DEA-based model estimates of stress have been performed in the hip joint [224]. This study reported errors in model estimates of contact stress ranging from 20% - 25%, employing a Bland-Altman analysis to determine the amount and direction of bias in the model. They concluded excellent agreement between their model and experimental results, as 95% of their data was within the limits of agreement. The model results from the current study predicted joint contact stress changes across the joint positions (within 20%) as well as demonstrated minimal bias in the facet ratio relative to the experimental data. An important consideration of using Bland-Altman analysis is that there is no "accepted" value for validation, but rather the technique establishes limits of agreement which provide a range of values through which the model can reliably predict experimental results (95% confidence). The limits of agreement for ratios of the stress in the current study ranged from -0.40 to 0.64 for mean and peak contact stress. These limits of agreement, in addition to the mean bias in the model, must be considered when applying the model to assess differences in patient populations or rehabilitation treatments.

One critical observation must be referenced regarding this study. The bias and relative errors between the DEA model and experimental data were significantly reduced in specimen #2 compared to specimen #1. Part of these differences can be explained by the testing order of these knees. Specimen #1 was the first knee to be tested in the knee testing system of the current study. There was an appreciable learning curve with the testing methodology that was markedly improved when testing specimen #2. Potential experimental errors associated with measured kinematics and contact mechanics were more controlled with additional tests.

Additionally, it should be discussed that the current DEA model is dependent on the accuracy of two measurement systems: 1) the experimentally measured kinematics and 2) the image segmentation and co-registration technique. The experimental kinematic tracking accuracy is reported to be on the order of sub-millimeter and sub-degree in all 6 DOFs. The image segmentation and co-registration technique is limited only by the quality of the image acquisition technique. The current model was developed from MR images with a 0.4 x 0.4 mm2 pixel size and slice thickness of 0.7 mm, which is deemed to be excellent for operating these displacement-based DEA models.

This modeling framework and validation study must be reviewed considering the limitations associated with the system. First, the stresses measured experimentally and, thus, estimated by the model were lower than prior studies with similar testing systems [87, 120, 187]. It is important to note that pressure based systems, like the one used in this study, have been reported to potential exhibit errors in peak contact pressure estimations between 10% - 15% [225, 226], which is important as the experimental data was treated as the "gold standard" for the comparing model estimates of stress and may explain some of the variability between the model and experimental data. The current study utilized a pulley system with physiologic loads that

were chosen for safety purposes. Additionally, the current test system does not allow for dynamic actuation of the muscle tendons with increased flexion, which will contribute greatly to the "natural" patellofemoral joint kinematic profile as well as the contact stresses. However, the goal of this study was to validate the DEA model based on the input kinematics at the different flexion positions. Regardless of the simulated muscle forces, the resulting kinematics were the primary driver for the current model. This is a very attractive aspect of the DEA modeling framework proposed here, as this model does not require assumptions of active (i.e. muscle) and passive (i.e. ligament/soft tissue) forces to properly load the model. These forces are incorporated into the final kinematic positions of the rigid bones.

4.1.4 Summary

The current modeling framework is the first to employ displacement driven DEA methods to estimate patellofemoral joint contact stress at multiple knee joint positions. Additionally, this study has demonstrated validation of this framework in terms of facet-specific contact stress and stress distribution. Future studies will utilize these models with accurate in-vivo dynamic biplane fluoroscopy techniques to estimate patellofemoral joint stress during functional tasks. These models have the ability to address clinically relevant questions related to patellofemoral OA by evaluating currently existing treatment methods and developing new rehabilitation strategies for these individuals.

5.0 AIM3: IMPLEMENTATION OF DEA MODEL IN INDIVIDUALS WITH AND WITHOUT PATELLOFEMORAL OA

5.1 EVALUATION OF A VALIDATED DEA MODELING FRAMEWORK TO ESTIMATE IN-VIVO, SUBJECT-SPECIFIC PATELLOFEMORAL JOINT CARTILAGE STRESS DURIGN GAIT

5.1.1 Introduction

Osteoarthritis (OA) is the most common joint disorder, incurring pain and disability in millions of people worldwide [1]. While OA predominantly occurs in the tibiofemoral joint with a 50% lifetime risk [2], OA of the patellofemoral joint has gained recent attention as it has been shown to occur independent of tibiofemoral joint OA and may be as common, if not more common, than tibiofemoral OA [32, 33]. Additional evidence has shown that the prevalence of mixed tibiofemoral and patellofemoral OA in older adults with painful knees is significantly greater (40%) than either patellofemoral OA (24%) or tibiofemoral OA (4%) in isolation [31]. Currently, there is no cure for OA and most non-operative treatment options involve prevention or minimization of disease progression [5]. OA of the patellofemoral joint affects approximately 25% of the population [34], having even higher rates (> 30%) in adults over 60 [196], and yet despite its high prevalence, the etiology of patellofemoral OA remains poorly understood.

It is well observed that the OA, particularly patellofemoral OA, leads to significant alterations in the surface congruity between the patella and femur, which can lead to a disruption in the normal contact mechanics at the joint, potentially eliciting pain at the subchondral bone. In support of this theme, patellofemoral OA and the cascading structural abnormalities resulting from the disease have been shown to be significantly associated with increased pain at the knee joint [227-229]. A study performed in 777 participants with knee pain found that increasing radiographic severity was associated with significant functional limitations [230]. It is believed that pain and disability caused by increased joint contact stress at the articular and subchondral surfaces due to malalignment and maltracking. A study by McWalter et al. [231] found significant associations between tibiofemoral alignment (varus/valgus) and patellar kinematic changes with patellofemoral OA in older adults. This study concluded that patellofemoral tracking is vital to understanding the relationship between knee joint mechanics and patellofemoral OA.

To this end, Farrokhi et al. [70] measured significant differences in terms of increasing lateral patellar tilt and medial translation in individuals with mixed tibiofemoral and patellofemoral OA compared to healthy controls. The conclusions from this prior study were that individuals with patellofemoral OA altered their movement patterns in order to off-load their lateral facet, potentially placing the medial patellar facet at risk. However, there are no current methods for directly evaluating how these changes in kinematics affect the underlying joint contact mechanics. Prior studies have attempted to quantify patellofemoral joint contact stress during walking through the use of a mathematical model combined with externally measured kinetics [38] as well as using advanced dynamic magnetic resonance imaging (MRI) techniques [125, 232]. However, these studies lack the ability to either incorporate subject-specific

geometry or simulate functional loading scenarios of daily activities. A greater understanding of the changes in the mechanical environment due to the OA process, particularly during daily, functional tasks, would allow for improved treatment development for those individuals with patellofemoral OA.

Computational modeling is an attractive solution for studying the effect of joint injuries and diseases on joint mechanics, particularly in the patellofemoral joint. Current models of the patellofemoral joint include utilizing finite element techniques [37, 135, 207, 208], discrete element methods [146, 155], or utilize a combination of subject-specific musculoskeletal computer models with either of the other two modeling methods [140, 212]. Existing models require estimations of muscle and soft-tissue passive forces to drive contact between the articular surfaces. Additionally, solving the non-linear contact at the articular interface can be a significant bottle neck in terms of computational processing time, limiting the real-time clinical applicability. Employing discrete element models driven by highly accurate kinematic data can bypass several of these force-based assumptions and provide estimates of the joint contact stress during functional tasks. The use of subject-specific geometry and knee joint kinematics as inputs to drive models would allow for researchers and clinicians to better understand joint contact mechanics during functional tasks and provide a novel tool for prescribing and evaluating subject-specific rehabilitative treatment solutions.

The objective of this study was to employ a validated discrete element model driven by subject-specific knee joint kinematics for assessing in vivo changes in patellofemoral contact mechanics during a downhill walking task. Specifically, this study sought to compare joint contact stress distributions between individuals with patellofemoral OA and disease free controls. Based on findings from our prior study [70], we hypothesized that individuals with OA

would exhibit decreased lateral facet joint contact stress in terms of mean contact stress, peak contact stress, and lateral to medial facet ratio of contact stress. Additionally, we aimed to identify the joint contact stress loading profile in these individuals during the loading response phase (LR) of downhill gait.

5.1.2 Methods

5.1.2.1 Subject characteristics

Subjects were recruited from the University of Pittsburgh's Claude D. Pepper Older Adults Independence Center Research Registry. This Registry includes over 2,000 Pittsburgh residents above the age of 60 who have previously consented to be contacted by researchers. Subjects for this study consisted of two main groups: 1) subjects (n = 5) demonstrating evidence of either patellofemoral OA of grade II or greater confirmed by radiographic evidence according to the Kellgren and Lawrence (KL) scale [233] and who met the American College of Rheumatology clinical classification criteria for knee OA [234], and 2) subjects (n = 6) without knee OA (KL radiographic grade $\leq$ 1) who reported no history of knee pain to serve as a control group. Subjects were excluded from this study if they: 1) suffered any ligamentous or traumatic knee injury; 2) had received any major orthopaedic joint arthroplasty for their hip, knee or ankle; 3) had been diagnosed with any neurological disorders that affect the lower extremity; 4) required the use of an assistive device to ambulate a distance of 30 m; and 5) had reported two or more falls within the past year. All participants signed a consent form approved by the Institutional Review Board of the University of Pittsburgh prior to participation in the study.

5.1.2.2 Clinical data

The 24-item Western Ontario and McMaster Universities (WOMAC) OA index and the 14-item Activities of Daily Living Scale (ADLS) were used to collect knee-specific information on symptoms and impairment with activities of daily of living. The WOMAC has been established as a reliable, disease-specific tool for evaluating pain, stiffness, and physical function in individuals with knee OA [235-237]. Briefly, each item on the WOMAC has 5 response options (ranging from none to extreme) and yields total subscale scores for pain (5 questions, range 0 – 20), stiffness (2 questions, range 0 – 8), function (17 questions, range 0 – 68), and a total composite score (24 questions, range 0 – 96). Higher scores on the WOMAC indicate increased severity of the symptoms or functional limitations.

The ADLS consists of 14 questions which measure the range of symptoms and functional limitation during different daily activities as a result of different diseases at the knee joint [238]. Consisting of 6 responses (ranging from none to extreme), the ADLS scores are transformed to a 0 – 100 point scale with 100 indicating the absence of symptoms or functional deficits. This tool has been proven to be a reliable instrument in ascertaining symptoms and functional limitations resulting from disorders of the knee [238, 239]. In addition to self-reported scores on knee pain and function, knee joint range of motion (knee flexion/extension) measured using a goniometer and maximum voluntary isometric knee extension torque measured using a Biodex System 3 dynamometer were collected for each individual. All measurements of knee extension torque were an average of 3 trials and normalized to subject's body weight (BW). An intraclass correlation coefficient ($ICC_{2,3}$) of 0.97 (95%CI: 0.94 – 0.98) was obtained for this study. Measurements of knee joint range of motion using a goniometer have been reported to produce excellent ICCs of between 0.84 and 0.93 [240].

5.1.2.3 Dynamic Stereo X-ray testing

Dynamic Stereo X-ray (DSX) methods were used to quantify three-dimensional (3D) TF and PF joint kinematics using biplane radiographic images. The DSX system consists of two x-ray generators (100 kW, CPX 3100CV; EMD Technologies, Quebec, Canada), two 40 cm image intensifiers (Thales, Neuilly-sur-Seine, France), and two high-speed 4 megapixel digital video cameras (Phantom v10, Vision Research, Wayne, New Jersey, USA), all of which were synchronized together to allow for simultaneous collection of x-ray data in two planes. The X-ray gantries were configured with their beam paths intersecting at 60 degrees in a plane parallel to the floor. For the current study, radiographs were generated with a 1 ms pulse width at 100 Hz, with a maximum radiographic exposure protocol of 90 kVp/200 mA and a 1 s collection time (100 ms total X-ray exposure) per trial.

Participants' knees were imaged during a downhill gait condition (7% grade, 0.75 m/s) on an instrumented treadmill (Bertec Corp., Columbus, OH). A downhill gait condition was implemented to elicit a functional task that is reported as difficult and demanding for patients with knee OA and has been suggested to increase knee flexion angle, vertical ground reaction force and knee joint moments [180, 241, 242]. Additionally, a relatively slow gait velocity of 0.75 m/s was chosen for our experimental set up based on pilot results demonstrating that most patients with knee OA had difficulty walking downhill at higher gait speeds. Participants were positioned within the biplane x-ray system such that the knee of interest would remain within the system's 3D imaging volume throughout the loading response phase of gait. Loading response is a critical time period associated with high demands on the knee joint and reports of dynamic alignment change in patients with knee OA [243, 244]. For subjects with knee OA, the knee in which they reported symptoms or the most painful knee in bilateral cases was designated as the

test knee. For control participants, the knee from the dominant lower limb was designated as the test knee. For each subject, an average of 3 individual gait trials was collected. The loading response phase was defined as the first 20% of the stance phase of gait after heel contact, which was determined utilizing both the patient kinematics and ground reaction force profile [176].

5.1.2.4 Calculation of joint kinematics

Prior to testing, all participants underwent computed tomography (CT) imaging of their knee. The CT field of view was approximately 28 x 28 cm2, slice thickness ranged from 0.6 to 1.25 mm, and the in-plane resolution was approximately 0.55 mm per pixel. The CT images of the tibia, femur, and patella were manually segmented and custom software (MATLAB R2014, The MathWorks, Natick, MA) was used to perform feature-based interpolation to create 3D bone models. Briefly, anatomical coordinate systems are assigned to each bone based on user-defined anatomical landmarks which are then utilized to calculate transformation matrices to relate the anatomical coordinate systems to the global reference frame of the CT environment.

The 3D positions and orientations of the femur and patella were measured from the biplane x-ray images using a model-based tracking technique. This technique involves applying a ray-tracing algorithm to project two 2-dimensional digitally reconstructed radiographs (DRRs) from the CT-based bone models on each fluoroscopic image of the two planes collected from the DSX system. The in-vivo position and orientation of the bones are estimated by using a software suite which allows for virtual translation and rotation of each DRR to simultaneously match each frame of the biplane radiographic images. Using an image correlation to find the optimum orientation that matches each radiographic image, 3D orientations of the patella and femur are determined for all frames of each trial. The final step in this process involves creation of a series of affine transformation matrices relating laboratory coordinate systems to the CT defined

anatomical coordinate systems to calculate 3D knee joint kinematics of the patella relative to the femur [69, 245]. These transformations were one of the inputs to the current study modeling technique.

The specific kinematics quantified for this study included patellar shift (i.e., medial-lateral translation relative to the femur), flexion (i.e. rotation about a medial-lateral axis relative to the femur), tilt (i.e. rotation about the patella's long axis), and spin (i.e. angular position relative to the patella's anterior-posterior axis). This experimental approach has previously been shown to have excellent accuracy for quantifying TF and PF joint motion with measurement bias of better than 0.5° - 1.0° for rotations and 0.3 – 0.7 mm for translations and measurement precision of better than 0.4° - 0.9° for rotations and 0.1 – 0.7 mm for translations.

5.1.2.5 Subject-specific model

Several steps were taken in order to generate subject-specific bone and cartilage geometry, as well as developing the discretized mesh of the patellofemoral joint for each individual. The framework for the models developed in this study can be described as follows: 1) create subject-specific geometry and discrete element mesh; 2) perform MR to CT shape matching methods for model transformation; 3) apply DSX kinematic transformations to MR model; and 4) run the DEA simulation. All data was obtained prior to experimental data collection and segmentation of subject-specific geometry was performed by the same individual.

Subject-specific geometry and discrete element mesh

In addition to obtaining CT scans, high resolution, sagittal plane MR images were taken for each individual. A 3.0-T scanner (MAGNETOM Trio; Siemens Medical Solutions USA, Inc, Malvern, PA) was used to acquire a sagittal 3-D double-echo steady state with water excitation

(SAG 3D-DESS WE) scan of both knee joints. Coronal multiplanar reformats were performed from the SAG 3D-DESS WE scans and used for segmentation of the femoral and tibial cartilage. The SAG 3D-DESS WE MR scan parameters were as follows: in-plane resolution, 0.365 × 0.456 mm; repetition time, 16.3 milliseconds; echo time, 2.8 milliseconds; flip angle, 25°; matrix, 384 × 384; field of view, 14 × 14 cm; slice thickness, 0.7 mm; scan time, 10 minutes 36 seconds.

The MR images were semi-automatically segmented (Mimics®, Materialise, Leuven, Belgium) in order to separate femur and patellar bone and cartilage geometries using methods described in Chapter 4.1.1.1. A mesh refinement was performed on the surface geometry of the bones and articular cartilage using meshing software (Hypermesh, Altair Engineering Inc., Troy, MI). Tetrahedral, shell elements were created for the bones and articular cartilage with an average element size of 1mm similar to the methods employed in the prior validation study described in Chapter 4.0

Perform MR to CT shape matching algorithm

In order to relate the MR-based geometrical models (containing cartilage) to the CT-based models used in the DSX tracking system, a 3D co-registration algorithm was applied to both the femur and patella using Geomagic Studio 12 (©2013 Geomagic Studio, 3DSystems, Rock Hill, SC, USA). A manual n-point registration was performed by selecting several landmarks (7 for the femur; 6 for the patella) on the CT 3D bone model and then choosing the same points on the surface of the 3D MR bone models. For the femur, the selected landmarks included the following: lateral/medial epicondyle, lateral/central/medial trochlear groove, and ant/post femoral notch (Figure 5.1). For the patella, the selected landmarks included the following: inferior apex, lateral and medial border, anterior/posterior base, and the inferior spine of the median ridge on the posterior patella. Based on recommendations from two clinicians, the

specific landmarks used in this study were chosen due to the ability to distinctly identify these landmarks despite the potential variability in patellar and femoral bone geometry across different subject groups.

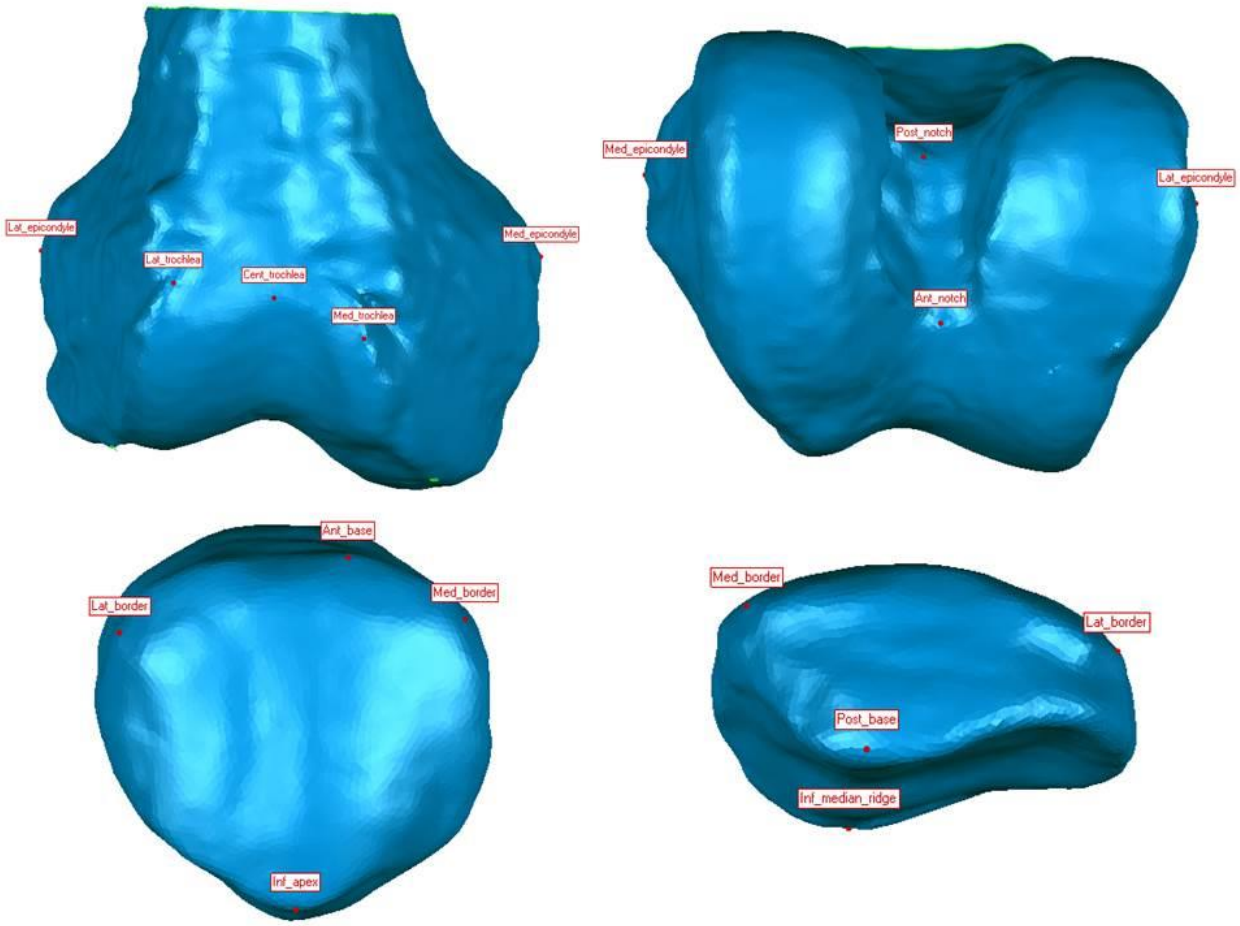

Figure 5.1. Anatomical landmarks from one sample subject in the current study. Landmarks for the femur (top) and patella (bottom) were selected to provide initial alignment between MR and CT bone models

These landmarks were used to provide a close, initial estimate of the final position of the MR relative to the CT to apply an automatic global registration process. The automatic global registration process minimizes the co-registration error between the two 3D models by using an iterative closest point algorithm (ICP). Briefly, the objects are brought into a roughly aligned (matched) position. The test object (MR model) is sampled and the closest points are computed

on the reference (CT) to each sample point. Next, a least-squares method to minimize the distances between the sample pairs is performed over all of the rigid motions that could potentially realign the two objects (Figure 5.2). This is performed on an iterative basis until the smallest error (average and root mean square error (RMS)) is achieved over the model. The average (± SD) error in this co-registration process for the bones across the two subject groups in this study was 0.73 (± 0.21) mm. Additional information from this best-fit algorithm can be seen in Table 5.1. The output of this best-fit alignment procedure is a transformation matrix to relate the MRI-based model coordinate system to the CT coordinate system (MRI-CT).

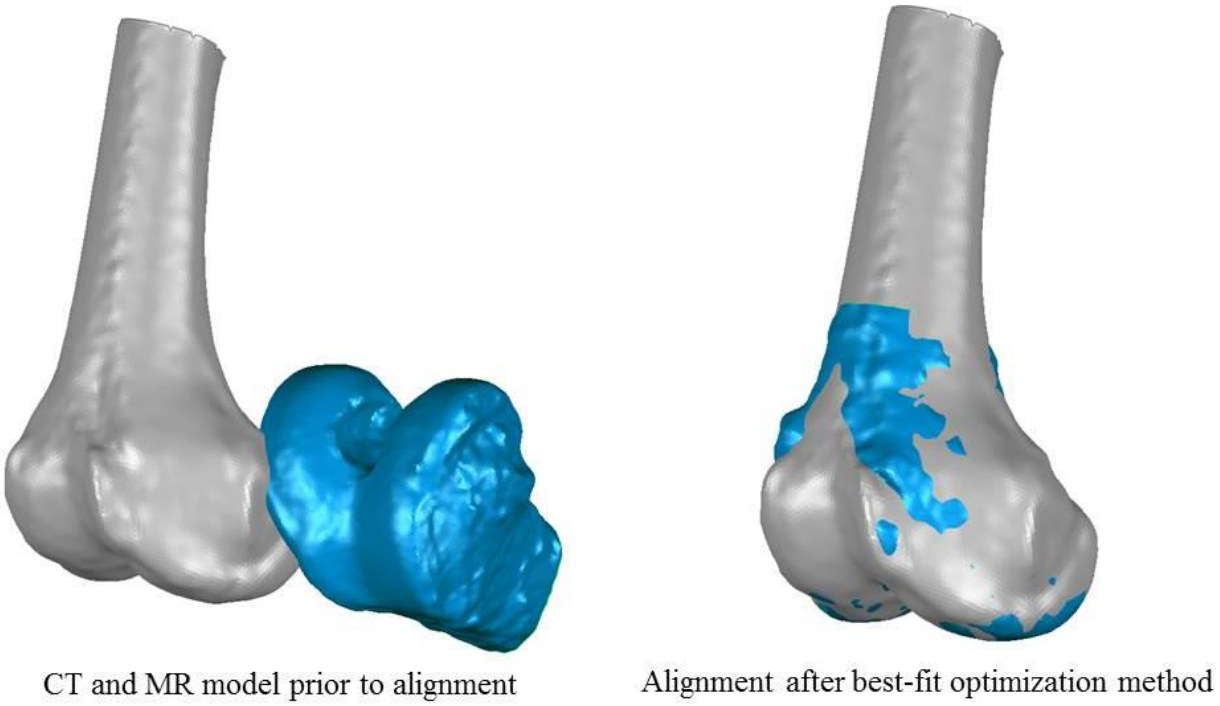

Figure 5.2. Result of best-fit shape matching algorithm. The MR model (blue) is fit to the CT-based model (grey) based on root mean squared error minimization of the coordinate points over the model

Table 5.1. Shape matching error between MR and CT-based models

	Patella	Femur
Average Error (mm)	0.72	0.74
RMSE (mm)	0.30	0.13

Application of DSX kinematics to MR models

In order to position the MR-based DEA model into the experimental positions measured from the DSX tracking system, a series of transformation matrices was needed to relate the geometry across the three primary coordinate systems: 1) the DSX experimental (lab) system with which all data was collected on each individual during the downhill walking task; 2) the CT-based coordinate system, which is utilized in conjunction with the DSX system to measure the patellofemoral kinematics; and 3) the MRI-based coordinate system with which the DEA models were developed. One output of the model-based tracking process is a transformation matrix relating the laboratory coordinate system to the CT coordinate system (lab-CT) of each bone for every time frame throughout each trial. This lab-CT transformation matrix was used in combination with the MRI-CT transformation matrix described above to relate the position of each bone in the MRI coordinate system to the laboratory system (MRI-lab). The femoral transformation was applied to both the femoral bone and cartilage, while the patellar transformation was applied to the patella and patellar cartilage. Once applied, these transformations positioned the bones and their respective cartilage into the final position measured during the experimental tests. A detailed description of this process can be found in Appendix D.

5.1.2.6 DEA simulation

The DEA algorithm for this study was implemented in MATLAB (2016a, The MathWorks, Natick, MA) and has been described in detail. Briefly, subject-specific articular cartilage thickness (both femoral and patellar) was calculated by the program using methods previously described. Overlapping elements resulting from the application of the kinematic transformation matrices were determined using a nearest neighbor algorithm as part of a penetration analysis. This algorithm searched from the patellar articular surface to the femoral articular surface for potential elements whose surface outward normal were nearly anti-parallel (i.e. ~ -1), indicating surface overlap/penetration. A linear system of independent springs were then generated at the centroid of each element in the regions of overlap and provided user-defined material properties (E = 2 MPa, v = 0.45 [144]). The previously described linear elastic spring model was implemented to calculate patellofemoral joint contact stress, which was divided into medial and lateral patellar facets by drawing a line from the inferior apex to the most superior point on the base of the patella. Contact stress distributions in terms of lateral to medial patellar facet ratio were also calculated. All outcome variables were analyzed at 0%, 25%, 50%, 75%, and 100% of the loading response (LR) phase of downhill gait, identified as the region of gait from heel contact to peak knee flexion angle/moment [176].

5.1.2.7 Statistical analysis

Descriptive statistics were calculated and the normality of the distributions of all continuous variables was checked. A logarithmic transformation [246] was applied as several outcome variables did not pass normality. As a first pass of the model's ability to predict patellofemoral joint stress during downhill walking, contact stress distributions were compared qualitatively between the OA and control group. Chi-square tests were performed on gender

between groups and analysis of variance (ANOVA) was used to determine group differences in clinical scores as well as knee extensor strength and range of motion. A 2 x 5 (group by percentage of loading response) factorial ANOVA was performed on model estimates of contact stress and stress ratio to find the effect of 0%, 25%, 50%, 75%, and 100% of the loading response phase of downhill gait, with percentage of loading response as the repeated measure. For all factorial ANOVA test results, only significant main group effects were reported if there were no significant interactions. A $p < 0.05$ was considered statistically significant. All statistical tests were performed in SPSS 22 (IBM, Armonk, NY).

5.1.3 Results

Overall, ANOVA and chi-square tests did not discover any significant differences in subject characteristics between the two groups. Subject demographics can be found in Table 5.2.

Table 5.2. Mean subject demographics

Demographics	**Control (n = 6)**	**OA (n = 5)**	**p-value**
Age (years)	67.7 (5.4)	69.8 (9.1)	0.640
Female (%)	2 (33)	2 (40)	0.819
Height (cm)	177.8 (13.0)	173.2 (2.2)	0.454
Weight (kg)	74.0 (9.4)	84.1 (16.6)	0.232
BMI (kg/m2)	23.4 (2.4)	28.0 (5.2)	0.082
OA=osteoarthritis; BMI=body mass index; values are mean (SD) or N (%)			

5.1.3.1 Clinical data results

Comparisons of the WOMAC scores demonstrated significant associations in terms of increased (worse) total WOMAC score in individual with patellofemoral OA (mean ± SD, 6.6 ± 4.7) compared to the controls (mean ± SD, 0.7 ± 1.8). Similarly, the patellofemoral OA group exhibited increased WOMAC physical function (mean ± SD, 1.6 ± 1.2 vs 0.3 ± 0.7) and WOMAC stiffness (mean ± SD, 1.6 ± 1.2 vs 0.3 ± 0.7) scores compared to the control group. Additionally, the patellofemoral OA group exhibited significantly decreased extension range of motion (mean ± SD, -3.0 ± 5.9 vs 5.1 ± 5.1) and total knee range of motion (mean ± SD, 123.5 ± 14.2 vs 141.7 ± 7.9) compared to the control group. A summary of the clinical data can be found in Table 5.3.

Table 5.3. Average clinical outcomes

Clinical Outcome Measures	**Control (n = 6)**	**OA (n = 5)**	**p-value**
WOMAC total score	0.7 (1.8)	6.6 (4.7)	0.021
WOMAC physical function score	0.3 (0.7)	1.6 (1.2)	0.044
WOMAC pain score	0.3 (0.7)	1.6 (1.2)	0.058
WOMAC stiffness score	0.2 (0.4)	3.4 (2.5)	0.011
ADLS score	66.8 (7.2)	57.4 (7.5)	0.078
Knee extension strength, Nm/kg	0.4 (0.1)	0.4 (0.1)	0.667
Flexion range of motion, degrees	136.6 (4.9)	126.5 (15.6)	0.165
Extension range of motion, degrees	5.1 (5.1)	-3.0 (5.9)*	0.037
Total knee range of motion, degrees	141.7 (7.9)	123.5 (14.2)	0.024
OA=osteoarthritis; values are mean (SD);*negative values indicate flexion contracture			

5.1.3.2 Patellofemoral joint contact stress distribution during downhill walking

Qualitatively, there were markedly different contact stress distributions between the individuals, both across the groups and even within the groups (Figure 5.3). In general, regardless of the group, individuals exhibited greater lateral facet contact stress throughout the loading response phase of downhill gait. Individuals also demonstrated increased contact near the end of loading response (100% LR) compared to early portions of loading response (HC). When making comparisons between groups, greater contact was observed in the control group compared to the OA group, although the contact patterns were highly dependent on each individual.

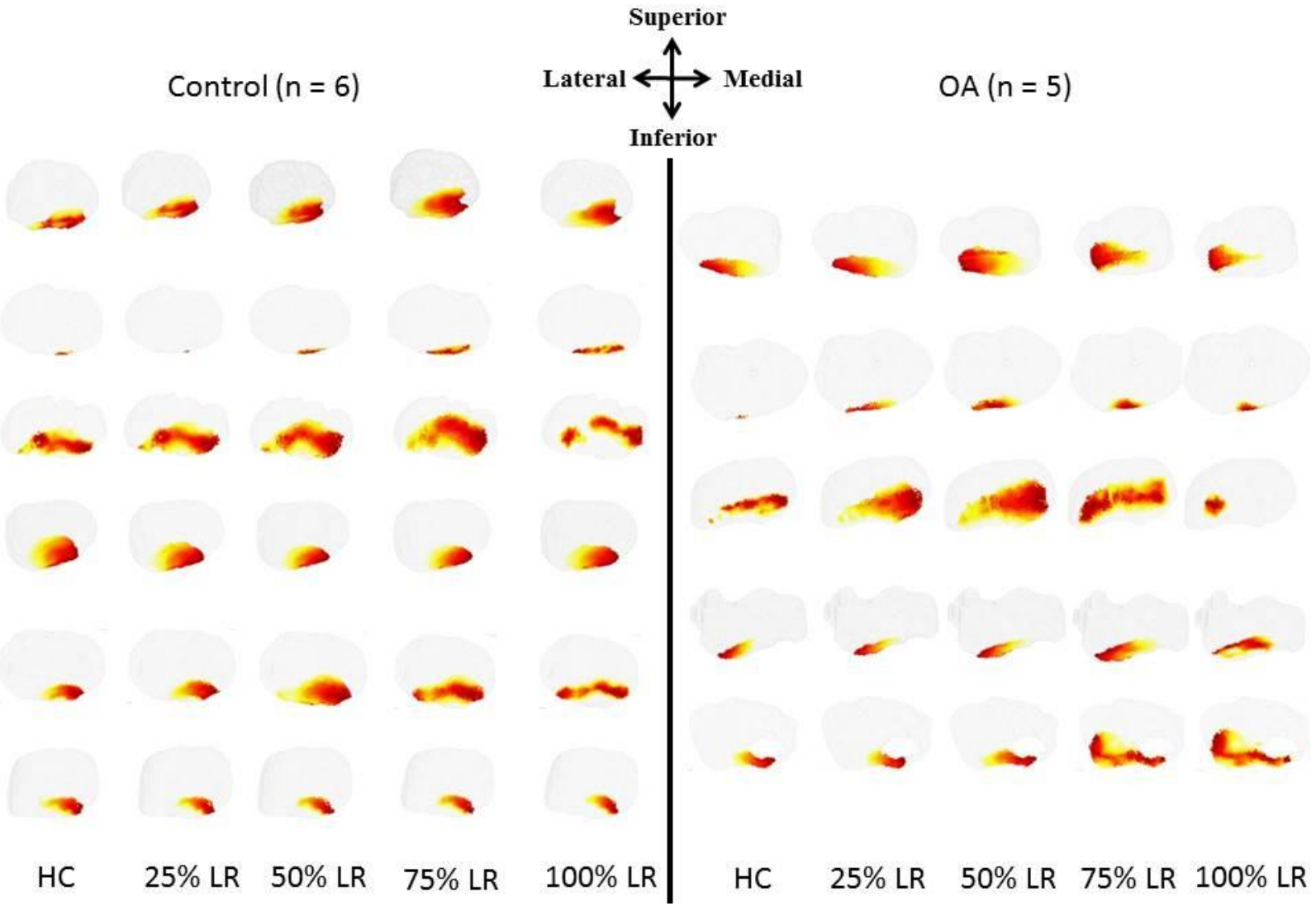

Figure 5.3. Patellofemoral joint contact stress distribution for the control group (left) and OA group (right) for each individual subject (top-down). The joint contact stress distributions were generated at five discrete time points throughout the loading response (LR) phase of downhill walking. HC = Heel contact

The ANOVA results revealed a significant group x time interaction for lateral facet peak contact stress ($F_{4,36}$ = 3.302, p 0.021). The interaction effect was such that the lateral facet peak stress for the control group increased from heel contact (4.81 MPa) to 50% LR (6.87 MPa, difference = 2.06 MPa), at which point it decreased back to stress levels slightly below heel contact (3.96 MPa) at the end of loading response. The OA group, however, demonstrated a rapid increase in their lateral facet peak stress from heel contact (3.86 MPa) to 25% LR (5.83 MPa; difference = 1.97 MPa), at which point the peak stress dropped dramatically from 25% LR to the end of loading response (1.70 MPa, difference = 4.13 MPa decrease). There were no other group or interaction effects for the remaining variables.

The ANOVA also revealed a significant main effect of time for the lateral facet mean contact stress ($F_{4,36}$ = 11.925, $p < 0.001$). A post-hoc analysis revealed significant decreased mean joint contact stress at the end of loading response compared to the earlier time points: heel contact (mean difference = 1.71 MPa, p = 0.02), 25% loading response (mean difference = 2.39 MPa, $p < 0.001$), 50% loading response (mean difference = 2.47 MPa, $p < 0.001$), and 75% loading response (mean difference = 1.71 MPa, p = 0.003). This observation was observed for the medial facet mean and peak contact stresses (Figure 5.4). No differences due to time, group or an interaction were observed for the lateral to medial facet ratio of both the mean contact stress and peak contact stress (Figure 5.5).

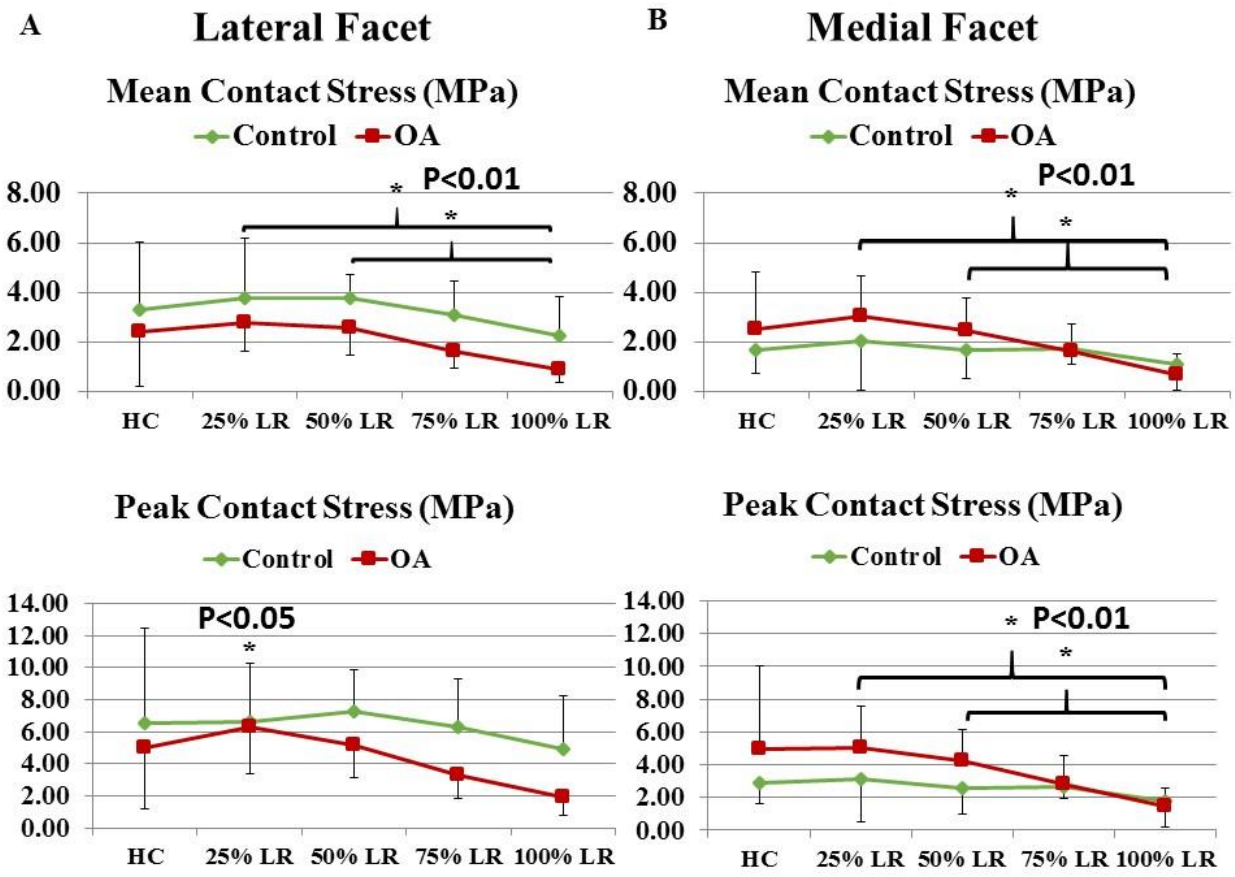

Figure 5.4. DEA stress for both A) lateral and B) medial facets of control and OA groups during the loading response (LR) phase of a downhill walking task; HC = heel contact

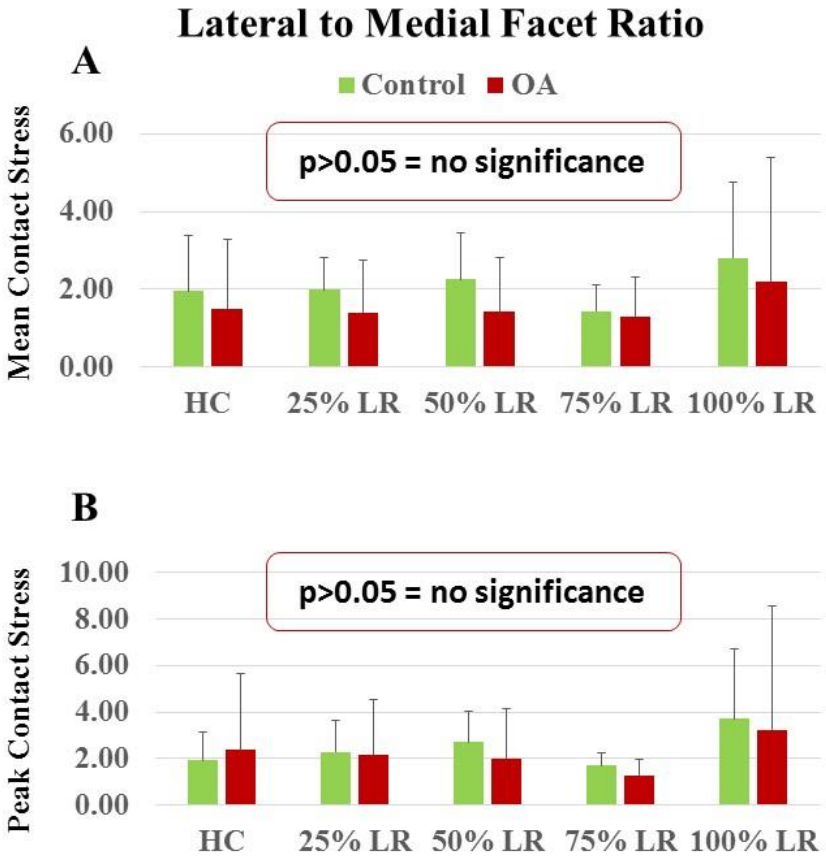

Figure 5.5. DEA estimate of lateral to medial facet ratio for A) mean and B) peak contact stress

5.1.4 Discussion

The primary objective of this study was to employ a validated DEA model of the patellofemoral joint to estimate joint contact stress during a functional task such as gait. This is the first study to implement subject-specific DEA models utilizing highly accurate patellofemoral kinematics to estimate knee joint stress in individuals with and without patellofemoral OA during a downhill walking task. A secondary goal was to determine whether the model could discern differences in the loading patterns in individuals with and without patellofemoral OA. We had hypothesized individuals with patellofemoral OA would exhibit increased lateral facet patellofemoral stress

compared to their disease-free counterparts. This hypothesis was partially supported by the results presented, in that individuals with patellofemoral OA had an initial dramatic increase in lateral facet peak contact stress during early loading response to a relatively similar magnitude as the control subjects. This drastic increase in stress during the early portions of the gait cycle may be a pattern of excessive, rapid trauma to the articular surface, which could potentially progress the degeneration in the joint. Future studies will need to evaluate the long-term relationship between these joint stress changes and cartilage health.

In contrast to the lateral facet contact stress, there was no significant difference in the medial facet contact stress or the lateral to medial facet ratio between these groups. Lack of any statistical difference can be partially attributed to the small sample of patients in this study. Utilizing the mean and standard deviation values for both groups averaged across the time points, effect sizes of the differences between these groups were calculated (Table 5.4). These results show that there are moderate to strong effects of the contact stresses between the two groups estimated from the DEA model.

Descriptively, individuals with patellofemoral OA exhibited increased medial patellar facet contact stresses compared to the control subjects in early loading response (Figure 5.4). While not statistically significant, it bears merit to discuss this relationship considering the descriptive aspect of this study in applying knee joint kinematics to assess changes in knee joint stress. Looking at the average tibiofemoral joint kinematics in terms of tibiofemoral internal/external rotation and average patellofemoral tilt excursions between these two groups (Figure 5.6), individuals with patellofemoral OA were more internally rotated than the controls at early loading response, which may be indicative of the increased lateral facet peak stress observed in this study. Looking at the patellofemoral tilt angle, however, individuals with

patellofemoral OA were more medially tilted than the control subjects. This could be indicative of the unique stress profiles seen in these two groups and future studies will need to investigate the effect of these two combined motions on resulting stress. Regardless, these trends are interesting and show promise that there may be a relationship between the kinematics and stress.

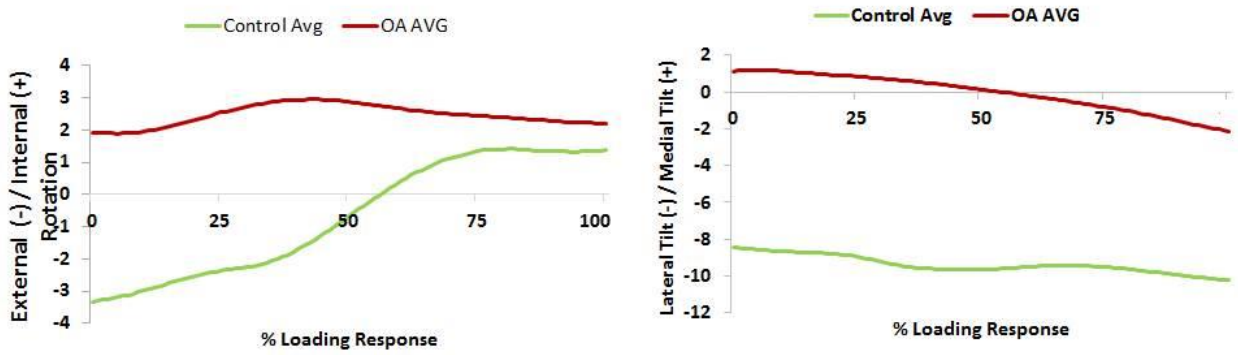

Figure 5.6. Comparison of tibiofemoral transverse plane rotation (left) and patellofemoral tilt (right)

Table 5.4. Cohen's d test statistic of DEA outcome measures

	Control (n = 6)	OA (n = 5)	Cohen's d
Lateral Facet Mean Stress, MPa	3.25 (1.68)	2.05 (1.01)	0.87
Lateral Facet Peak Stress, MPa	6.34 (3.50)	4.33 (2.04)	0.70
Medial Facet Mean Stress, MPa	1.62 (0.86)	2.08 (1.20)	-0.44
Medial Facet Peak Stress, MPa	2.57 (1.06)	3.71 (2.23)	-0.65
Lateral / Medial Ratio Mean Stress	1.99 (1.12)	1.52 (1.63)	0.34
Lateral / Medial Ratio Peak Stress	2.35 (1.39)	2.13 (2.64)	0.10
OA=osteoarthritis; values are mean (SD)			

The clinical data in this study present interesting results that may in part explain the stress results. First, while there were significant differences between the patellofemoral OA and control group in terms of passive knee range of motion and several of the clinical scores, the knee extension strength as measured isometrically was not different between this subset of individuals. It is well known that knee OA is significantly associated with muscle weakness [92, 93], and muscle weakness in combination with joint pain commonly leads to a "quadriceps avoidance" and knee joint stiffening gait pattern often seen in patients with OA [247]. It could be that the sub sample of individuals in the patellofemoral OA group were able control their joint loading at similar levels to the control group, which may explain a lack of statistical significance in some of the model-based variables in this study. The effect of muscle weakness on altered joint stress merits further scrutiny in future studies.

There is limited data in the literature of the in situ joint contact stresses during gait, making comparisons of the current model-estimated stresses to prior studies challenging. The range of stress values (0.74 MPa – 7.95 MPa) generated from the displacement-driven DEA model in the current study is consistent to those measured from in vitro experimental tests [84, 87, 248]. Other computational models of the patellofemoral joint utilizing FEA techniques and musculoskeletal models have also generated joint contact stress magnitudes similar to the current study [135, 164, 207]. A study by Fernandez and colleagues [223] implemented a combined musculoskeletal and FE model of the knee joint to estimate tibiofemoral and patellofemoral stresses in one healthy male subject during an overground walking task. Estimates of lateral and medial patellofemoral peak stress occurred at a similar time point as the current study (10 – 18% of the gait cycle). Magnitudes of peak stress were reported as high as 11 MPa (current study peak stress = 7.95 MPa) and the lateral to medial patellofemoral stress ratio estimated during overground walking was approximately 1.8 (current study average ratio range = 1.52 – 2.35).

While this is the first study to employ displacement-driven DEA models during a downhill walking task utilizing the highly accurate kinematics from the current study's DSX system, there have been other groups that have applied various modeling techniques to estimate joint contact forces and stress during simulated walking [38, 212, 249-252]. A study by Brechter et al. implemented a combination of theoretical models with experimentally measured data to estimate the differences in patellofemoral joint reaction force and stress between patients with patellofemoral pain (PFP) and pain-free controls during gait [38]. Not only do our DEA-based model results in terms of the magnitude of the stresses fall within their results, but the loading profile exhibited by their two groups during gait showed a large increase in stress within the first 15% - 20% of the gait cycle. This pattern was also evident in a study by Adouni and colleagues

[212], which implemented a finite element model combined with musculoskeletal modeling techniques to estimate forces in the tibiofemoral and patellofemoral compartments. This study also generated increased patellofemoral forces at 25% of the stance phase of gait, which would fall relatively close to the 50% loading response portion of gait from the current study. While similarities between the joint stress profile from the current model with prior studies provides confidence in the model, future studies will need to validate the in vivo joint contact estimated from the model, perhaps by incorporating the use of dynamic MR imaging techniques.

Many of the existing FE and DEA models require several assumptions as to the contribution of active and passive, soft tissue forces within the FE model to properly model the native mechanics of the patellofemoral joint. We present a novel method incorporating accurate knee joint kinematics with a computationally efficient model to bypass these active and soft tissue forces, as the input kinematics to the model are the end results of these forces contributing to knee joint function. These displacement-driven DEA models provide an alternative method for investigating the effect of rehabilitation strategies (i.e. patellar bracing and taping) on joint contact stress.

In light of the modeling framework developed and its application to predicting in vivo joint stress, several limitations must be acknowledged. First, the modeling framework in this study is dependent on the overlapping cartilage regions to be able to estimate joint stress. A study by Fregly and co-workers discussed the utility of displacement-driven models and the sensitivity of these models to kinematic errors, reporting that errors by as much as ± 0.1 mm throughout the gait cycle in the tibiofemoral joint led to changes in the joint contact profile by as much as 200%, with greater kinematic errors leading to even greater model errors [210]. It should be noted that this study was performed in an instrumented tibiofemoral joint, where small

errors in the coordinate axis can lead to very large movements due to the size of the joint. While the accuracy of our kinematic system is on the order of sub-millimeter and sub-degree accuracy, we are primarily utilizing these models to determine changes in the ratio of the joint stress profile, as was performed in this study.

An additional limitation of the current DEA modeling technique in this study is that it is currently unable to estimate joint stress in regions of the articular cartilage where large lesions may exist as a result of the OA process. As seen in Figure 5.3, there were several individuals in the patellofemoral OA group who exhibited large cartilage lesions, primarily on the lateral facet. The current DEA model requires overlapping regions of the articular cartilage surfaces in order to generate springs and estimate contact stress. If contact is occurring in these regions of cartilage degeneration, yet there is no "apparent" overlap of cartilage due to missing regions, no calculations of stress are made in these areas. This is an important limitation as these regions consisting of cartilage lesions may undergo unique stress profiles, with potential for bone-on-bone contact and eliciting pain and further joint degeneration in these individuals. This requires further analysis in future studies.

A prior study has attempted to address the current study's limitation of modeling bone-on-bone contact. Cohen and colleagues [253] employed a rigid-body modeling technique to evaluate and find optimized surgical procedures for tibial tuberosity transfer. They incorporated a nonlinear stiffening effect due to "excessive" penetration, or bone-to-bone overlap, to account for the variable articular cartilage thickness and stiffening effect provided by the underlying bone. They did this to improve model predictions of joint contact. This nonlinear stiffening factor modification may aid in accounting for contact in regions with cartilage legions and future studies should explore validating this effect in knees with cartilage defects, such as severe OA.

It is also important to acknowledge that the current model only provides surface joint contact stress, particularly compressive stress. It is well known that articular cartilage (both collagen and chondrocytes) respond poorly to shear stress and strains [254]. Examining the effect of shear stress and strains on cartilage function is more suitable for FEA-based modeling methods, as the current model is unable to estimate shear stresses and strains. Despite this limitation, understanding the changes at the joint contact surfaces resulting from different rehabilitation treatments remains unknown and has important clinical implications. The current DEA-based modeling framework allows for estimation of joint contact stress during functional tasks, with the goal of applying these techniques to evaluate and develop subject-specific rehabilitation treatments. The model from the current study detected meaningful changes throughout the gait cycle in individuals with and without patellofemoral OA, demonstrating the potential to employ these displacement-driven models in large-scale cohort studies to better develop treatments for individuals with patellofemoral dysfunction.

5.1.5 Summary

The DEA modeling framework described in this study was able to determine differences in the joint loading patterns in individuals with patellofemoral OA compared to disease free controls. The utility of these models in distinguishing subject-specific differences in knee joint contact mechanics has limitless applications. Due to the simplified, yet efficient method for calculating stress in the current study framework, these models have potential near real-time clinical utility to track changes in joint stress as improvements in geometrical segmentation and automated kinematic tracking techniques are made. These models will be used in the future to better

understand the effect of different treatment strategies on patellofemoral joint mechanics and aid in the development of subject-specific rehabilitation solutions.

6.0 SUMMARY AND CONCLUSIONS

OA of the patellofemoral joint is a significant clinical problem that has proven to be challenging to understand and resolve. Despite the growing body of literature attempting to understand the pathomechanics patellofemoral OA, management of the disease still remains a significant challenge. While multiple forms of treatment exist, most of the outcomes are limited in their findings and applications. One potential reason for this inconsistency is due in part to a lack of knowledge in understanding the primary driver in the OA process.

While the most widely accepted reason for the development and progression of OA is due to altered joint loading and subsequent cartilage degradation, there still exists a gap in being able to clearly define this relationship in the human knee joint. This gap is due to the challenges with measuring in vivo knee joint contact stresses during natural movement patterns. The primary objective of this dissertation was to develop a computational modeling framework driven by highly accurate, subject-specific knee joint motions, validate this framework in a controlled laboratory setting, and, finally, implement these models in assessing altered patellofemoral joint loading in individuals with patellofemoral OA. These objectives were achieved by carrying out three studies.

6.1 REVIEW OF THE WORK

A reliable knee joint testing system was required to develop and validate this modeling framework. The primary objective of study #1 was to develop a sophisticated testing system for simultaneously measuring patellofemoral joint kinematics and joint contact mechanics under complex patellofemoral and tibiofemoral loading conditions. This testing system was developed to simulate loading patterns similar to those seen during activities such as walking. Patellofemoral joint kinematics and joint contact mechanics were collected using established digitization and pressure sensor technology. The effects of tibiofemoral flexion and femoral alignment on patellofemoral joint contact pressure were explored. Repeated measures of these outcome parameters were conducted. The results of the study demonstrated excellent repeatability of patellofemoral joint kinematic tracking (ICC > 0.9) and patellofemoral joint contact pressure measurements (< 9% variability). Based on these findings, the system proved to be reliable to allow for measurement of kinematics to drive a patellofemoral computational model for estimating joint contact stress and validate this model using the experimentally measured pressures.

The purpose of study #2 was to develop a subject-specific modeling framework that could estimate joint contact stress solely from the input of relative bone to bone joint positioning. This dissertation chose to employ discrete element modeling techniques due to the advantages associated with implementing these models in a small time-scale and potential to utilize them across large population-based studies in the future. Two specimen-specific, discrete element models were generated and tested for the modeling framework. This framework implemented a highly accurate cross-registration technique with the bone surface models and experimentally collected kinematics to drive the computational models. Discrete element techniques utilized

penetration analysis techniques estimate the overlapping cartilage resulting from positioning of the bones as a surrogate of cartilage deformation and joint contact stress. Validation of the modeling framework was performed by comparing the joint contact stress estimated from each model to experimental contact pressures. The model demonstrated excellent joint contact distribution profiles similar to the experimental data. Quantitatively, the model showed general agreement across the two knee joints tests. Bland-Altman plots were calculated to establish the bias and limits of agreement of the model in predicting the facet ratio of contact stress in each knee. Results from the analysis found a mean bias of -0.16 across the two knee joints. Based on the analyses presented, the model's ability to predict the patellofemoral contact stress was validated.

The main purpose of study #3 was to implement the validated modeling framework during a downhill walking to compare the in-vivo patellofemoral stress patterns in two groups: five individuals with patellofemoral OA and six pain-free control subjects with no signs of patellofemoral OA. Highly accurate knee joint kinematics were acquired using a biplane fluoroscopy system while individuals walked on a declined, instrumented treadmill. Sophisticated image registration techniques were combined with the experimental kinematics to use as input to discrete element model, driving contact of the articular surfaces throughout the loading response phase of gait. Patellofemoral joint contact stress estimated from the model was compared between the two groups as well as over time. Results revealed that individuals with patellofemoral OA walked with a dramatic increase (58%) in lateral facet peak stress within the first 25% of the loading response phase of gait compared to the control group (38%), who walked with relatively similar levels of stress throughout the entire loading response of gait. These findings suggest that individuals with patellofemoral OA were unable to control the rate of

loading on their lateral facet in early loading response. An additional finding was that joint contact stress for both groups exhibited a distinct pattern of increased joint loading from heel contact to 25% of the loading response phase of gait, followed by a steady decrease to stress levels lower than those at heel contact. This study presented a novel framework for estimating in vivo patellofemoral joint contact stress during a functional task and demonstrated the model's ability to distinguish joint contact characteristics within two groups of individuals.

6.2 IMPLICATIONS OF KINEMATICALLY-DRIVEN DEA MODEL

Although the 3 studies conducted as part of this dissertation were descriptive in general, the modeling framework developed has far reaching applications in addressing clinical problems associated with patellofemoral dysfunction. The discrete element modeling framework presented in this dissertation is the first to employ highly accurate kinematics combined with subject-specific articular geometry to predict joint contact stress changes during functional knee joint positions. This was implemented in individuals with and without patellofemoral OA during a downhill walking task. The data collected as part of study #3 can serve as preliminary data for future studies aimed at investigating the effect of different rehabilitative programs and treatment solutions on changes in patellofemoral joint stress, which is currently unavailable.

The modeling framework developed in this dissertation provides a unique tool that can be implemented to aid our current understand of altered joint motions on underlying joint contact stress. With continuing technological advances in segmentation and imaging techniques, it may even be possible to utilize this modeling framework to provide near real-time feedback of joint stress during functional tasks. Future directions for these models include incorporating and

validating these models at deeper knee flexion angles, while also adjusting the model to account for potential bone-to-bone contact, particularly as one major target population for these models are individuals with patellofemoral OA. Additionally, future work can investigate different activities at deeper flexion angles, particularly stair ascent, descent and chair rising tasks, as these tasks are known to be challenging for individuals with patellofemoral OA. Particularly, it is important to understand how joint contact stress is associated with self-reported clinical measures, such as pain, stiffness and function. Future use of these models can explore how self-reported baseline levels of pain, stiffness and function correlate with joint stress during these functional activities, and if currently used rehabilitation methods (i.e. bracing) are able to reduce joint stress and pain in these individuals throughout these tasks. Understanding the associations between joint stress and self-reports of stiffness and pain would be critical for clinicians to better recommend appropriate treatment.

The knowledge gained from this dissertation is an important step towards improving our current treatment paradigms in OA. Current guidelines have been clinically shifting towards a "patient-specific" approach to treating patellofemoral pathologies. This dissertation provides an additional tool for assessing the effect of altered patellofemoral motions on joint contact mechanics. The long term goal of these models is to generate additional information for clinicians to provide the best patient care on an individual-to-individual basis.

APPENDIX A

IN VITRO TESTING PROTOCOL

This appendix includes additional information on the testing protocol, calibration, data processing and raw data.

A.1.1 Testing Protocol

1. **Knee Specimen preparation**
    a. 24 hours in advanced, retrieve intact knee specimen from the freezer in lab and thaw
    b. Retrieve red "biohazard" bag and write the following information about the specimen on the bag:
        a. I.D #, Left/Right knee, gender, age: _____
    c. Slowly and carefully dissect skin/soft tissue from tibia and femur, keeping the ligaments and tendons intact
    d. Once all soft tissue has been removed, isolate the quadriceps tendons
        a. Find the fibers of the rectus femoris, vastus lateralis, and vastus medialis and slowly separate them
        b. "Clean" the tendons of all remaining soft tissue for clamp preparation
    e. Upon dissection and cleaning of the knee specimen, measure approximately 20 – 25 cm of tibia-femur bone to be kept. Remove the distal end of the tibia and proximal end of the femur
    f. Use a metal screw to fix the fibula to the tibia at the distal end
    g. Cut a portion of X-ray film that will act as a barrier/guide for epoxy putty to be used at the distal end of tibia and proximal end of femur

h. In a separate container, mix epoxy base "Bondo" with "Cream Hardener" adhesive compound. Stir thoroughly and evenly. Pour mixture into X-ray film around distal tibia, making sure there are no air bubbles forming in epoxy. Allow 5 min to set
i. Repeat step i for the proximal femur segment

2. Registration Block preparation

a. Upon completion of specimen preparation (Step 1), registration blocks (green cubes) must be added to the specimen knee for 3D digitization
b. Using plastic container, baking soda, and super glue, mix a tsp of baking soda to super glue and place over the region of interest for fixation: ***NOTE***: Area of the bone for registration block fixation must be COMPLETELY cleaned and dry
c. Place registration block on the most center part of the patella and most medial portion of the tibia and femur, closest to their joint line
d. Once dissection has been completed, place knee **carefully** in red biohazard bag and tie. If possible, place bag with knee in a container so as not to disrupt registration blocks

3. ****NOTE**:** Be sure to thaw the knee at least 12 hours before testing
4. Prepare the TekScan Sensors: See "**Protocol for Conditioning, Equilibration, and Calibration of TekScan Sensors**" Appendix A.1.2
5. Take X-Ray film and cut out two long rectangles (the width of the top part of the 4000 sensor and the length of about 4 inches)
6. Tape the X-Ray film onto the top of 4000 sensor with clear boxing tape
7. Move the computer with I-Scan open on the cart over near the jig
8. Attach the handle of the TekScan sensor onto the Velcro located below the distal part of the tibia on the jig
9. Keep the handle plugged into the USB port of the computer
10. Set-up Faro Arm system
    a. Open the case containing the Faro Arm
    b. Gently pull it out of the case (making sure to hold it by the base and the largest part of the arm)
    c. Place the base of the Faro Arm on the railing of the STAR IV in front of the distal part of the tibia in the jig
    d. Using the large blue clamps, clamp the base of the Faro Arm to the STAR IV
    e. Plug the power cord in from the Faro Arm to the power strip over by the computer
    f. Take the gray cord, and plug the non-USB side into the Faro Arm and the USB side into the USB port of the desktop with Geomagic
    g. From the little tool box located inside the casing of the Faro Arm, remove the 6 mm ball probe and screw it onto the tip of the Faro Arm
11. On the desktop, open and set-up Geomagic

12. Open Geomagic
13. Click “New” under the section “Tasks”
14. Once the Faro Arm is set-up and plugged in/turned on, go to the tab “Capture” and select “Scan”
15. Turn all 6 Degrees of Freedom in order to initialize the Faro Arm
16. Under the Dialog Box on the left-hand side under “Scanner Controls” select the second from the right picture to calibrate sensor
17. Change “current probe” to “6mm ball probe”
18. Click “edit” under “Compensation” and deselect “Guidance” and select “modify”
19. Select “Hole Compensation” and follow the instructions for calibration of the 6mm probe and click “ok” when finished
20. Under “Compensation status”, if “failed” appears, click “View log” at the bottom
21. Under the column “2 Sigma”, as long as the sigma error is below 0.0500 then the accuracy is acceptable. If it is greater, restart from step 15. (In order to pass, sigma error must be <0.002, but we don’t need accuracy to this degree)
22. Once completed, select “Single Point Articulation Test (SPAT)” and click “Yes” to use the invalid probe, follow the instructions to complete the test
23. Click “Ok” for compensation, click “Yes” to use an invalid prove, click “Ok” under the dialog box to return to the main screen
24. Set-up a local coordinate system within Geomagic:
25. Under the “Capture” tab within the “collect” box select the bright lime green picture of a plane
26. Using the Faro arm, digitize between 25 and 50 points on your x-axis of the surface (aka your YZ plane)
27. Lift up your probe, press the red button once, then collect 25-50 points on your y-axis of the surface (aka your XZ plane)
28. Repeat for your z-axis (aka your XY plane) and click the red button twice to end data point collection with the Faro arm
29. Click the “Features” tab, select “Point” and select “3 Planes”
30. For Plane 1 scroll to your x-axis plane, for Plane 2 scroll to your y-axis plane, for Plane 3 scroll to your z-axis plane
31. Click “Apply” and “Ok” to exit the dialog box
32. Next, click the “Tools” tab, select “Coordinate Systems” and “Create by Definition”
33. Under “Input Type” Select the picture of the plane
34. Under “Definition” scroll to your x-axis plane, select “Y-Z” and “Add definition”
35. Scroll to your y-axis plane, select “X-Z” and “Add definition”
36. Scroll to your z-axis plane, select “X-Y” and “Add definition”
37. Click “Ok” to exit the dialog box
38. Put Gloves on
39. Lay down surgical paper on a dissection table

40. Obtain the knee from the freezer (do not touch freezer door with any hands wearing gloves). Unwrap and set on the surgical paper.
    a. Lay the knee out and inspect to make sure the blocks are all stationary
41. Pick knee up, and manually with hands (one hand on the femur and one on the tibia) bend the knee from 0 to 90 degrees of flexion slowly 10 times
42. Attach the counter weight cables to the end of the jig that is hanging and loop them over the respective pulleys
43. Attach the 25 lb dumbbell to each of the two cables
44. Release the large black screws on the edge of the free hanging part of the jig to allow it to freely move up and down (using the largest allen wrench)
45. While one person picks up the knee, have the other person unscrew the screws that hold the cylinders that hold the femur and tibia in place so the knee can go in easily
46. Place the tibia in the horizontally sliding cylinder. Screw the cylinder in so that it is completely vertical
47. Move the cylinder with the tibia horizontally until it is directly under the other cylinder
48. Place the femur in the cylinder and screw in so that the knee is now in the jig at 0 degrees of flexion
49. Using the Faro Arm, digitize the anatomical coordinate system
    a. Digitize the Femur
    b. In Geomagic, click the picture of the green point under the "Capture" tab and the "collect" box
    c. Digitize the most medial and lateral points on the condyles (for the ML axis).
    d. Digitize an anterior, posterior, medial, and lateral point on the axis of the femur (a little more proximal than the condyles) to make a ring around the bone. Do this twice.
    e. Rename points: _____
    f. Digitize the Tibia
    g. Digitize most medial and lateral points on the condyles.
    h. Digitize an anterior, posterior, medial, and lateral point on the axis of the tibia. Do this twice.
    i. Rename points:_____
    j. Digitize the Patella
    k. Digitize the most proximal and distal points of the patella.
    l. Digitize the most medial point of the patella
    m. Rename points: _____
50. Perform the "Intact Kinematics"
    a. Attach the cable-clips from weights to the quadriceps tendons
    b. Ensure the correct quadriceps angles are being used in the coronal plane (19^0 VL and 47^0 VMO)
    c. Randomly select an order for the angles (0, 30, 60, 90) of flexion and position the knee in the first angle with the assistance of a goniometer

d. Apply 35 kg compressive load to the tibiofemoral joint by loading 20 kg, 10 kg, and 5 kg weights on top of vertical sliding component of knee jig
e. Apply tensile loads to the quadriceps tendons
    i. Vastus Medialis: 12 lbs
    ii. Vastus Intermedius: 20 lbs
    iii. Vastus Lateralis: 18 lbs
    iv. Digitize the registration blocks (digitize the 3 x, y, z planes labels on each of the three cubes: 9 planes total)
f. Rename planes: _____

_____

_____

_____

g. Unload the 3 quadriceps loads, **then** the compressive load
h. Move the knee to the next angle of flexion with the help of the goniometer
i. Repeat steps e-g for all angles of flexion
j. Remove the knee from the jig and place it back on the table
k. Repeat steps 48-49 two more times for three total "Intact Kinematics" tests at each flexion angle

51. Remove the knee from the jig and place it back on the surgical paper
52. Turn the knee over in order to make an incision posteriorly
53. Make an incision on the posterior side of the knee under the meniscus at each of the medial and lateral compartments
54. Make an incision above the patellofemoral joint
55. Coat sensors surface with Vaseline gently (this improves flexibility and longevity)
56. Insert the 4000 sensor into the tibiofemoral joint on each side under the meniscus carefully (do not suture yet)
57. Insert the 5051 sensor in the patellofemoral joint right on the surface of the patella
    a. Suture the edges where possible to the tissue around the patella (4 if possible)
    b. Super glue the knots so they hold
58. Pick the knee up and insert it back into the jig at 0^0 of flexion
59. Insert the 4000 sensor into the handle and make sure the real-time window is active
60. Position the sensors in the joint by pressing on different areas of the joint to make sure it is located in there exactly correct
61. Suture the sensor sides in place to the surrounding tissue (2 or 3 per side)
62. Secure the knots with super glue
63. Using the Faro Arm, digitize the anatomical coordinate system
    a. Digitize the Femur

b. In Geomagic, click the picture of the green point under the "Capture" tab and the "collect" box
c. Digitize the most medial and lateral points on the condyles (for the ML axis).
d. Digitize an anterior, posterior, medial, and lateral point on the axis of the femur (a little more proximal than the condyles) to make a ring around the bone. Do this twice.
e. Rename points: _____
f. Digitize the Tibia
g. Digitize most medial and lateral points on the condyles.
h. Digitize an anterior, posterior, medial, and lateral point on the axis of the tibia. Do this twice.
i. Rename points: _____
j. Digitize the Patella
k. Digitize the most proximal and distal points of the patella.
l. Digitize the most medial point of the patella
m. Rename points: _____

64. Perform the "Capsule-Cut Kinematics"
    a. Attach the cable-clips from weights to the quadriceps tendons
    b. Ensure the correct quadriceps angles are being used in the coronal plane (19^0 VL and 47^0 VMO)
    c. Randomly select an order for the angles (0, 30, 60, 90) of flexion and position the knee in the first angle with the assistance of a goniometer
    d. Apply 35 kg compressive load to the tibiofemoral joint by loading 20 kg, 10 kg, and 5 kg weights on top of vertical sliding component of knee jig
    e. Apply tensile loads to the quadriceps tendons
        i. Vastus Medialis: 12 lbs
        ii. Vastus Intermedius: 20 lbs
        iii. Vastus Lateralis: 18 lbs
    f. Digitize the registration blocks (digitize the 3 x, y, z planes labels on each of the three cubes: 9 planes total)
    g. Rename planes: _____
_____
_____
    h. Insert the 4000 sensor into the handle and take a snap shot of the reading
    i. Remove the 4000 sensor from the handle and insert the 5051 sensor, take a snap shot of the reading
    j. Unload the 3 quadriceps loads and the compressive load
    k. Move the knee to the next angle of flexion with the help of the goniometer
    l. Repeat steps e-g for all angles of flexion

m. Remove the knee from the jig and place it back on the table
n. Repeat steps 63-64 two more times for three total "Capsule-Cut Kinematics" tests at each flexion angle

65. Perform "Internal-External Rotation Kinematics"
    a. Attach the cable-clips from weights to the quadriceps tendons
    b. Ensure the correct quadriceps angles are being used in the coronal plane (19^0 VL and 47^0 VMO)
    c. Randomly select an order for the angles (0, 30, 60, 90) of flexion and position the knee in the first angle with the assistance of the goniometer
    d. Apply 35 kg compressive load to the tibiofemoral joint by loading 20 kg, 10 kg, and 5 kg weights on top of the vertical sliding component of the knee jig
    e. Apply tensile loads to the quadriceps tendons
        i. Vastus Medialis: 12 lbs

        ii. Vastus Intermedius: 20 lbs

        iii. Vastus Lateralis: 18 lbs

    f. Internally rotate the Femur holder 5 degrees by twisting the holder based on the marked angle and tightening the screw behind to keep it in place
    g. Digitize the registration blocks (digitize the 3 x, y, z planes labels on each of the three cubes: 9 planes total)
    h. Rename planes: _____

_____

_____

    i. Insert the 4000 sensor into the handle and take a snap shot of the reading
    j. Remove the 4000 sensor from the handle and insert the 5051 sensor, take a snap shot of the reading
    k. Unload the 3 quadriceps loads and the compressive load
    l. Move the knee to the next angle of flexion with the help of the goniometer
    m. Repeat f-m for internal rotation of 10 degrees, external rotation of 5 degrees, and external rotation of 10 degrees
    n. Repeat steps f-n for all angles of flexion
    o. Remove the knee from the jig and place it back on the table
    p. Repeat steps 64 two more times for three total "Internal-External Rotation Kinematics" tests at each flexion angle
66. Remove the knee from the jig and place it back on the surgical paper
67. Properly store the specimen
    a. Wrap gauze around the tendons and most of the knee area
    b. Dampen the gauze with saline

c. Wrap the knee in the skin (make sure the cubes are still visible)
d. Wrap a clean blue surgical paper around the entire area of the skin and tape it together
e. Place all of it in the red biohazard bag and tie
f. Place in a larger red bag and securely tie
g. Place in freezer

68. Dispose of everything in the correct containers
    a. Sharp items should be washed and sit in bleach
    b. Gloves, surgical paper, gauze, and anything that can be disposed of goes in the red biohazard bag
69. Clean items used in the experiment
    a. Put clean gloves on
    b. Wipe sensors down with bleach and soap mixture
    c. Clean tools, table, and knee jig with warm water and 10% bleach

A.1.2 Tekscan Sensor Protocol

Conditioning (approximately 30-45 minutes)

1. Plug in, turn on, and set-up Laptop
    a. Open "I-Scan"
    b. Go to "Options", click "Select Sensor", scroll to the correct sensor (choose between 4000 and 5051)

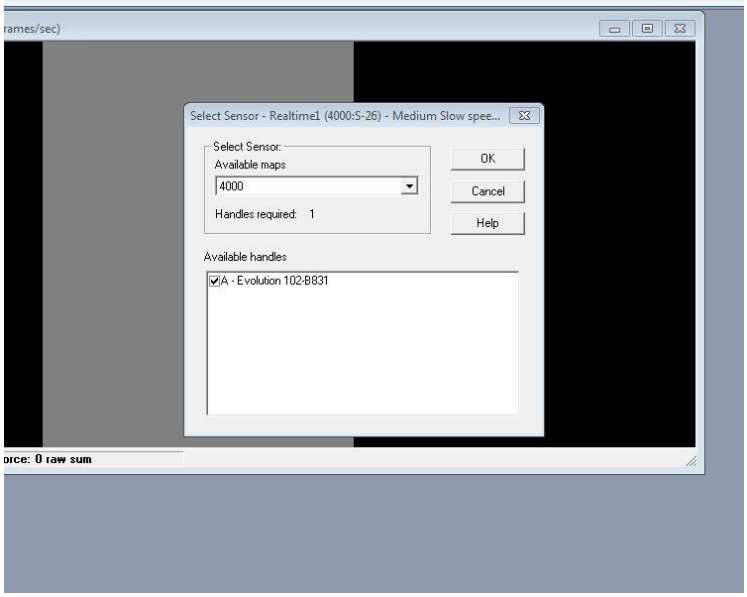

    c. Go to "Tools", click "Adjust Sensitivity", and select correct sensitivity
        i. If using the 4000 sensor, use S-26 sensitivity
        ii. If using the 5051 sensor, use S-33 sensitivity

d. Plug USB end of the sensor handle into the computer USB port

2. Power on the material testing machine
    a. Select the “compression test: in vitro PF study” testing scheme
    b. Attach flat metal platen to the base of the material testing maching
    c. Affix the round circular platen to the crosshead of the material testing machine
    d. Double-check the loading profile for the compression test (300 N, 10 cycles) and the loading rate (< 10 mm / min).
3. Insert the sensor into the handle (Note: Make sure you have the correct side up, it is labeled on the sensor)
    a. When the sensor is in the handle correctly, a green light will turn on at the top of the handle
    b. Readjust sensor by opening the handle back up and repositioning the sensor in the handle until the green light turns on (The screen will say “Sensor Misaligned” until this is done correctly)

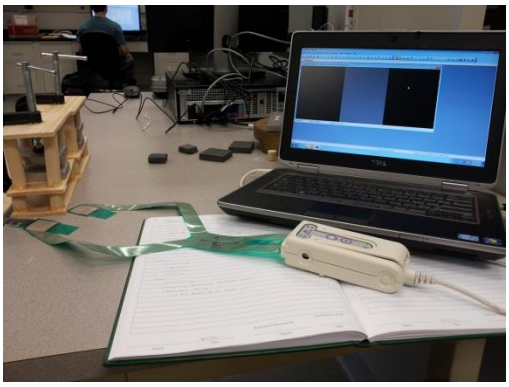

4. Position the sensor on the flat platen of the material testing machine
    a. Place the sensor on the lower metal plate so that the majority of the sensels are laying on it
    b. Place the correct sized padding (pre-cut up pieces that are almost the exact size of the sensel surface) directly on the surface of the sensor between the sensor and the top metal plate
        i. Make sure the padding is completely between the two metal plates so that all the force goes through the surface area of the padding
        ii. Test this by compressing the top plate manually using the “jog down” feature on the material testing machine
5. Apply a load of 300 N to the sensor
    a. Run the compression test to begin loading the sensor until the Real-time I-Scan window shows the coloring approximately Yellow-Green coloring the shape of the padding
        i. Take care to ensure that **NO PORTION** of the metal platens will come into contact (*CAUTION: Do not overload the load cell).

ii. If the shape of the padding does not show up completely, adjust the position of the sensor and padding next time to get the full compression desired

b. Continue the full test to load and unload 10 times

Equilibration (approximately 10-15 minutes)

1. Transfer the Laptop with sensor still in the sensor handle still plugged into the computer to the movable cart

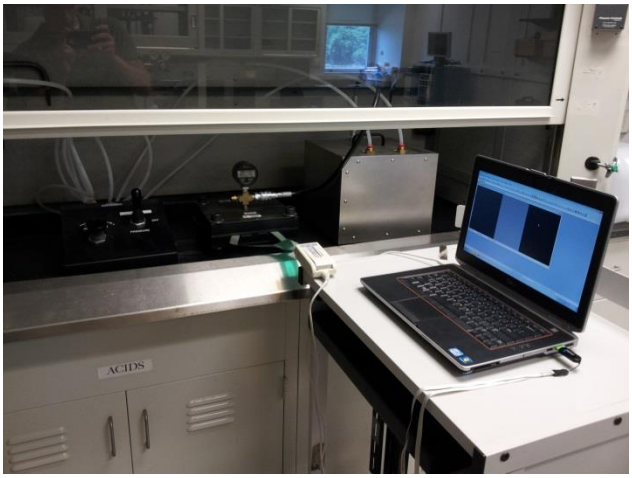

2. Move the cart over to the hood with the equilibration device
3. Lift up the hood window slightly and turn on the equilibration device
   a. Turn on the air in the hood by twisting the air knob on the left counter-clockwise
   b. Turn on the Pressure reading device in the very sensor by simply pressing the "On/off" button
   c. On the controller box (the further left most box), push the joystick in the center position (not releasing or applying any pressure – it should be there currently)
   d. Make sure the knob is very easy to twist – if not, twist counterclockwise until it is
4. Insert the TekScan sensor into the pressure applicator (the centermost box)
   a. Make sure the sensor goes in right-side up
   b. Put the sensor in until the only visible part is the uniform rectangular portion (no more no less)

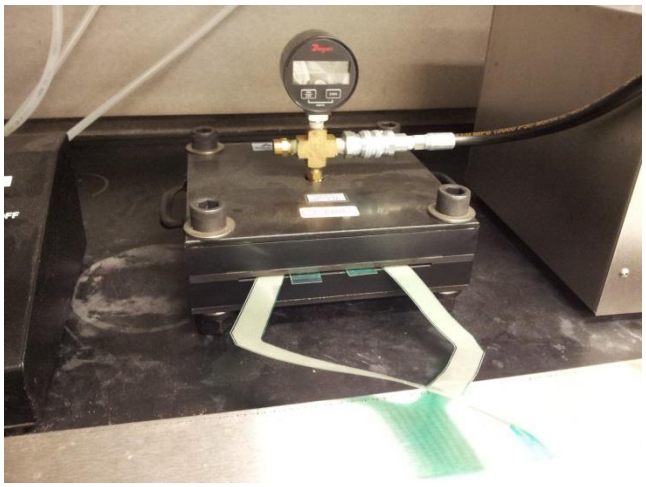

5. In I-Scan, open Equilibration procedure
    a. Click “Tools”
    b. Select “Equilibration”

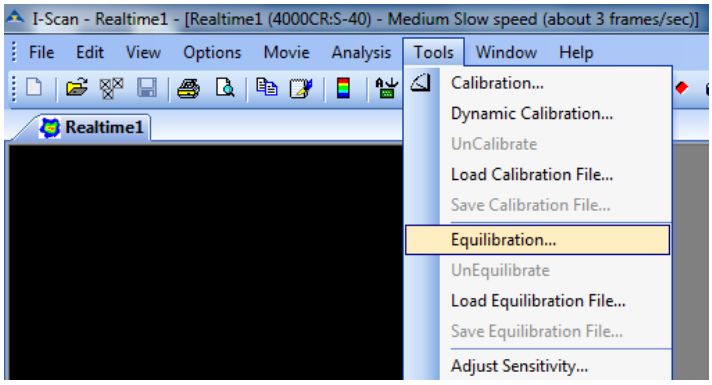

    i. If “UnEquilibrate” is an option, click this first
    ii. If “UnEquilibrate” was an option, it was previously equilibrated at least once
    c. In the Equilibration dialog box, select “Equilibrate-1”
    d. Change the “Begin equilibrating in” to 30 seconds

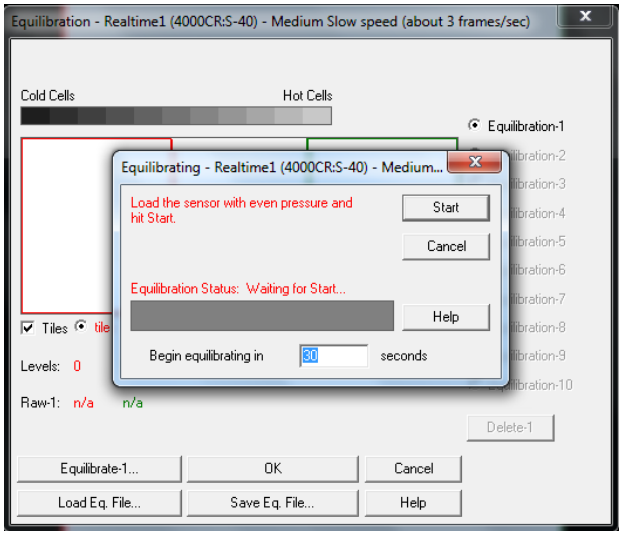

6. With the equilibration device, apply 150 PSI for 10 seconds, and then go down to 25 PSI
   a. Move the joystick downward
   b. Twist the knob clockwise slowly until the center reading goes to at least 150 PSI
   c. Let it sit at 150 PSI to remove air bubbles for 10 seconds
   d. Twist the knob counterclockwise to go back down to 25 PSI where it bounces around 24.7-25.3 PSI
   e. In the I-Scan window, click "Start"
7. Next, click "Equilibration-2" and go through step 6 with 50 and 75 PSI
8. Save the Equilibration file
   a. Click "Save Eq File"
   b. Label the file accordingly, and click "Save": _____
   c. (add picture)

Calibration (approximately 10-12 minutes)

1. Load the equilibration file
   a. Go to "Tools" and select "Load Equilibration File"
   b. Choose the correct file that you saved for equilibration and select "Open"
   c. It should say it has found data, press "Ok"
2. Begin Calibration
   a. Go to "Tools" and select "Calibration"

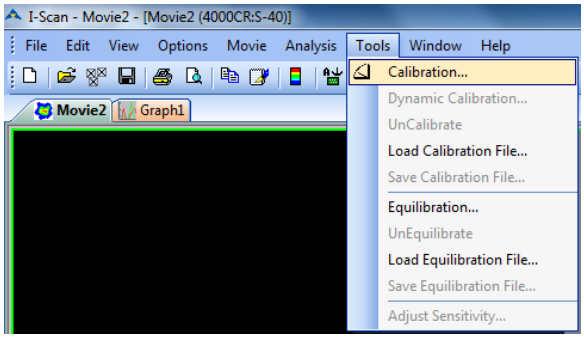

b. Select “Add” and enter 50 N as your known force

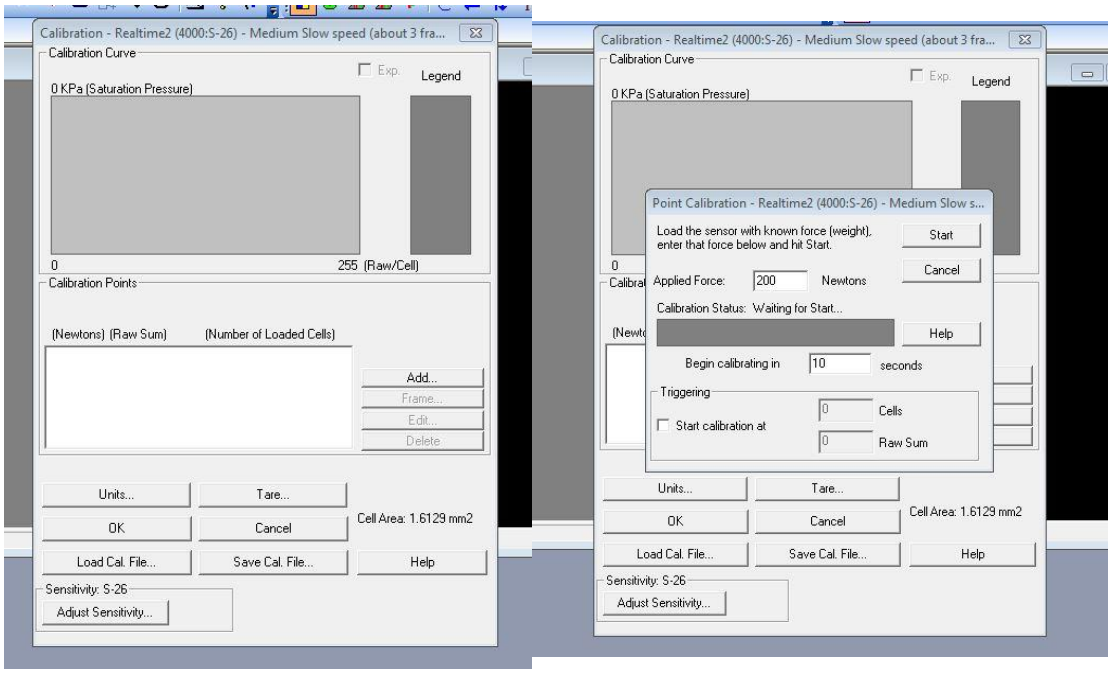

c. Apply 50 N to the TekScan sensor
    a. Power on the material testing machine
    b. Select the “calibration test: in vitro PF study” testing scheme
    c. Attach flat metal platen to the base of the material testing maching
    d. Affix the round circular platen to the crosshead of the material testing machine
    e. Affix the round circular platen to the crosshead of the material testing machine
    f. Double-check the loading profile for the compression test (50 N, hold 45 seconds, ramp to 200 N, hold 45 seconds) and the loading rate (< 10 mm / min).
d. During the 50 N loading profile, click “Add load” to the Teckscan calibration curve (see above image). Enter “50 N” and click “Add” when the material testing machine has applied 50 N
    i. Apply 50 N worth of force and click Start to begin calibrating
e. Select “Add” and enter 200 N as your known force

f. Apply 200 N to the TekScan sensor as part of the second step of the calibration protocol

3. Click “Save Cal File”
   a. Save the file under a name that specifies the sensor and the forces used: _____
   b. At this point, the sensor can be placed on the material testing machine to assess the sensor accuracy by applying known loads and reading the measured force.

APPENDIX B

DISCRETE ELEMENT COMPUTATIONAL ALGORITHM

This appendix contains calculations and MATLAB code used in the development and calculation of subject-specific contact stress from each model. The following section requires two major inputs: 1) subject-specific geometry, from CT or MRI, and 2) subject-specific kinematics, in the form of affine transformation matrices. This section was utilized with Aim 2 and Aim 3 to estimate patellofemoral joint contact stress throughout different ranges of knee joint motion. The primary outputs of this code are: 1) contact area, 2) mean contact stress, and 3) peak contact stress for both the medial and lateral patellar facets.

B.1.1 STL Import and Triangulation

The following code imports the femoral cartilage and divides the surface into articular and subchondral sides by fitting a sphere to the entire surface and identifying elements on either side based on the dot product between the line from each element to the center of the sphere and their surface normal. Articular surface: dot product = -1 (i.e. anti-parallel), Subchondral surface: dot product = +1 (parallel).

```
%% Triangulation of unloaded surfaces
%Unloaded Surfaces
```

```
[fcart_v1, fcart_f1, fcart_n] = stl_read(fcart_file);
[fcart_v2, fcart_f2] = patchslim(fcart_v1,fcart_f1);
%Femur Bone
[fbone_v1, fbone_f1, fcart_n] = stl_read(femur_file);
[fbone_v2, fbone_f2] = patchslim(fbone_v1,fbone_f1);
%Perform a triangulation to get triangulation class to allow for easy
manipulation and searching
fbone = triangulation(fbone_f2,fbone_v2(:,1),fbone_v2(:,2),fbone_v2(:,3));
fbone_norm = faceNormal(fbone);
fbone_IC = incenter(fbone);

fcart = triangulation(fcart_f2,fcart_v2(:,1),fcart_v2(:,2),fcart_v2(:,3));
fcart_norm = faceNormal(fcart);
fcart_IC = incenter(fcart);

%Femoral Articular Cartilage Definition of articular and subchondral faces
[Center,Radius] = SphereFit(fcart.Points); %Fit a sphere to our femur
Center_mat = repmat(Center,length(fcart.ConnectivityList),1);
Center_to_IC_vec = Center_mat - fcart_IC;
for ii = 1:length(Center_to_IC_vec)
    Center_to_IC_norm_vec(ii,:) =
Center_to_IC_vec(ii,:)./norm(Center_to_IC_vec(ii,:));
end
Center_to_IC_dotval = dot(fcart_norm,Center_to_IC_norm_vec,2);
fcart_artFace_elem_temp = fcart.ConnectivityList(Center_to_IC_dotval<0,:);
%Find the matching points for the new elements
for ii = 1:length(fcart_artFace_elem_temp)
    v_art_temp(ii*3-2:ii*3,:) =
fcart.Points(fcart_artFace_elem_temp(ii,:),:);
    f_art_temp(ii,:) = [ii*3-2,ii*3-1,ii*3];
end
[v_art_new, art_indexm, art_indexn] =  unique(v_art_temp, 'rows');
fcart_artFace_elem = art_indexn(f_art_temp);

fcart_subchFace_elem_temp = fcart.ConnectivityList(Center_to_IC_dotval>=0,:);
%Find the matching points for the new elements
for ii = 1:length(fcart_subchFace_elem_temp)
    v_subch_temp(ii*3-2:ii*3,:) =
fcart.Points(fcart_subchFace_elem_temp(ii,:),:);
    f_subch_temp(ii,:) = [ii*3-2,ii*3-1,ii*3];
end
[v_subch_new, subch_indexm, subch_indexn] =  unique(v_subch_temp, 'rows');
fcart_subchFace_elem = subch_indexn(f_subch_temp);
```

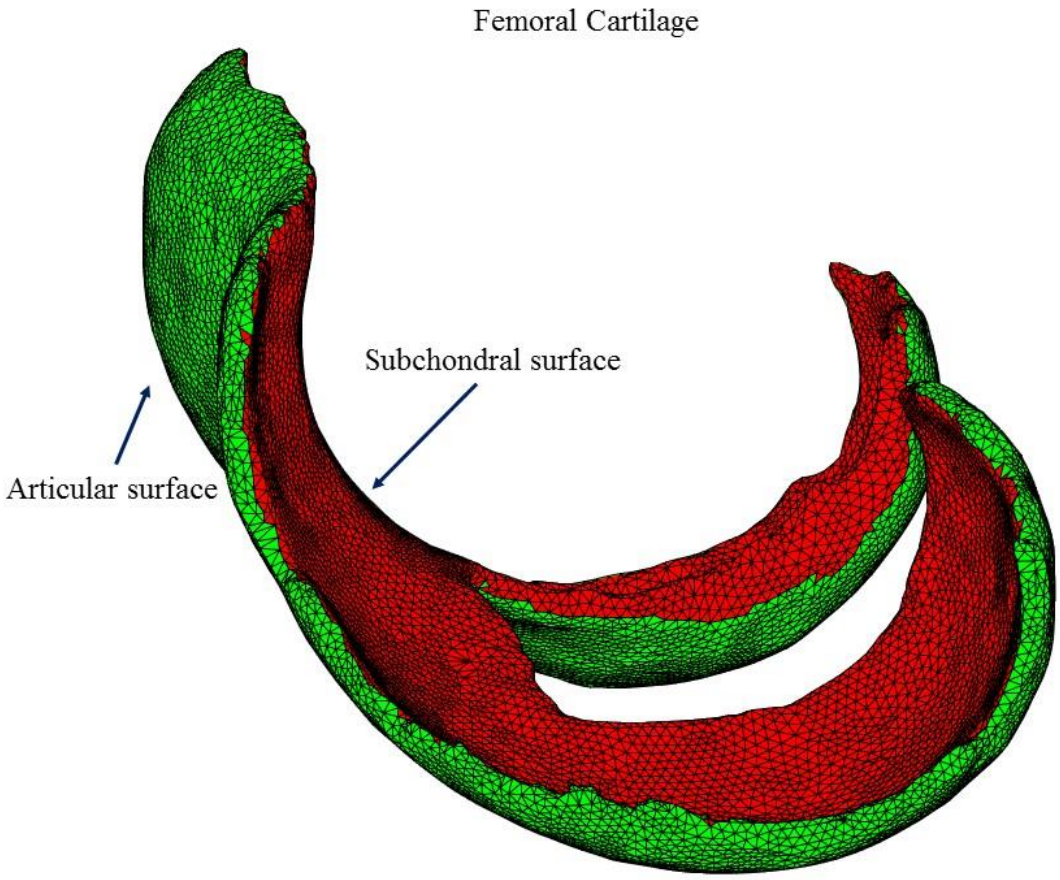

Figure B.1. Femoral cartilage divided into articular and subchondral faces

*Note STL_read is a download from the Mathworks website

```
function [vnew, fnew] = patchslim(v, f)
% PATCHSLIM removes duplicate vertices in surface meshes.
%
% This function finds and removes duplicate vertices.
%
% USAGE: [v, f]=patchslim(v, f)
%
% Where v is the vertex list and f is the face list specifying vertex
% connectivity.
%
% v contains the vertices for all triangles [3*n x 3].
% f contains the vertex lists defining each triangle face [n x 3].
%
% This will reduce the size of typical v matrix by about a factor of 6.
%
% For more information see:
%  http://www.esmonde-white.com/home/diversions/matlab-program-for-loading-
stl-files
%
```

```
% Francis Esmonde-White, May 2010

if ~exist('v','var')
    error('The vertex list (v) must be specified.');
end
if ~exist('f','var')
    error('The vertex connectivity of the triangle faces (f) must be
specified.');
end

[vnew, indexm, indexn] =  unique(v, 'rows');
fnew = indexn(f);
```

The following code separates the patellar cartilage STL file into articular and subchondral surfaces by using the sagittal image plane that each MR scan was taken to find all element normal in either the positive (articular) or negative (subchondral) directions. The primary sagittal axis is the global "y-axis"

```
%Patella Components
%Patella Cartilage
[pcart_v1, pcart_f1, pcart_n] = stl_read(pcart_file);
[pcart_v2, pcart_f2] = patchslim(pcart_v1,pcart_f1);
%Patella Bone
[patella_v1, patella_f1, patella_n] = stl_read(patella_file);
[patella_v2, patella_f2] = patchslim(patella_v1,patella_f1);

primary_dir_axis = 2; %Assign the primary direction axis for the ant/post
direction of the knee

pcart_unloaded =
triangulation(pcart_f2,pcart_v2(:,1),pcart_v2(:,2),pcart_v2(:,3));
pcart_unloaded_norm = faceNormal(pcart_unloaded);
pcart_unloaded_IC = incenter(pcart_unloaded);
[pcart_artFace_unloaded,pcart_subchFace_unloaded] =
SeparateFaces2(pcart_unloaded.ConnectivityList,pcart_unloaded.Points,pcart_un
loaded_norm,-0.3,primary_dir_axis);
pbone_unloaded =
triangulation(patella_f2,patella_v2(:,1),patella_v2(:,2),patella_v2(:,3));
pbone_unloaded_norm = faceNormal(pbone_unloaded);
pbone_unloaded_IC = incenter(pbone_unloaded);
%We want to calculate the articular cartilage surface and articular bone
%surface connections.  We need to trinagulate the bone surface.
pcart_artFace_UL_IC = incenter(pcart_artFace_unloaded);pcart_subchFace_UL_IC
= incenter(pcart_subchFace_unloaded);


function [upp_TR,low_TR] = SeparateFaces2(f,v,n,min,dir_axis)
%Separate front and back faces of geometry object using face normals.
%Output variables upp_TR and low_TR are triangulation data for easy
```

```
%implementation of search methods.

l = length(f);
fvc = zeros(l,3);
j = 1;
k = 1;
upp = zeros(l,1+size(f,2)+size(v,2));   %Pre allocate our vectors for
improved performance
low = zeros(l,1+size(f,2)+size(v,2));

for i = 1:l
    if n(i,dir_axis) > min        %If primary direction axis component of
normal vector greater than min
       fvc(i,:) = [0 1 0]; %green-upper surface
       upp(j,:) = [i f(i,:) n(i,:)];    %Stores the index, faces (1-3) and
normal vector of face in matrix
       v_upp(j*3-2:j*3,:) = v(f(i,:),:);
       f_upp(j,:) = [j*3-2,j*3-1,j*3];
       j = j+1;
    else
       fvc(i,:) = [1 0 0]; %red-lower surface
       low(k,:) = [i f(i,:) n(i,:)];
       v_low(k*3-2:k*3,:) = v(f(i,:),:);
       f_low(k,:) = [k*3-2,k*3-1,k*3];
       k = k+1;
    end
end

[v_upp_new, upp_indexm, upp_indexn] =  unique(v_upp, 'rows');
fnew_upp = upp_indexn(f_upp);
[v_low_new, low_indexm, low_indexn] =  unique(v_low, 'rows');
fnew_low = low_indexn(f_low);
upp_TR =
triangulation(fnew_upp,v_upp_new(:,1),v_upp_new(:,2),v_upp_new(:,3));
low_TR =
triangulation(fnew_low,v_low_new(:,1),v_low_new(:,2),v_low_new(:,3));
figure;patch('Faces',f,'Vertices',v,'FaceVertexCData',fvc,'FaceColor','flat')
; %Plot the faces based on the fvc color vector
grid on
axis equal
```

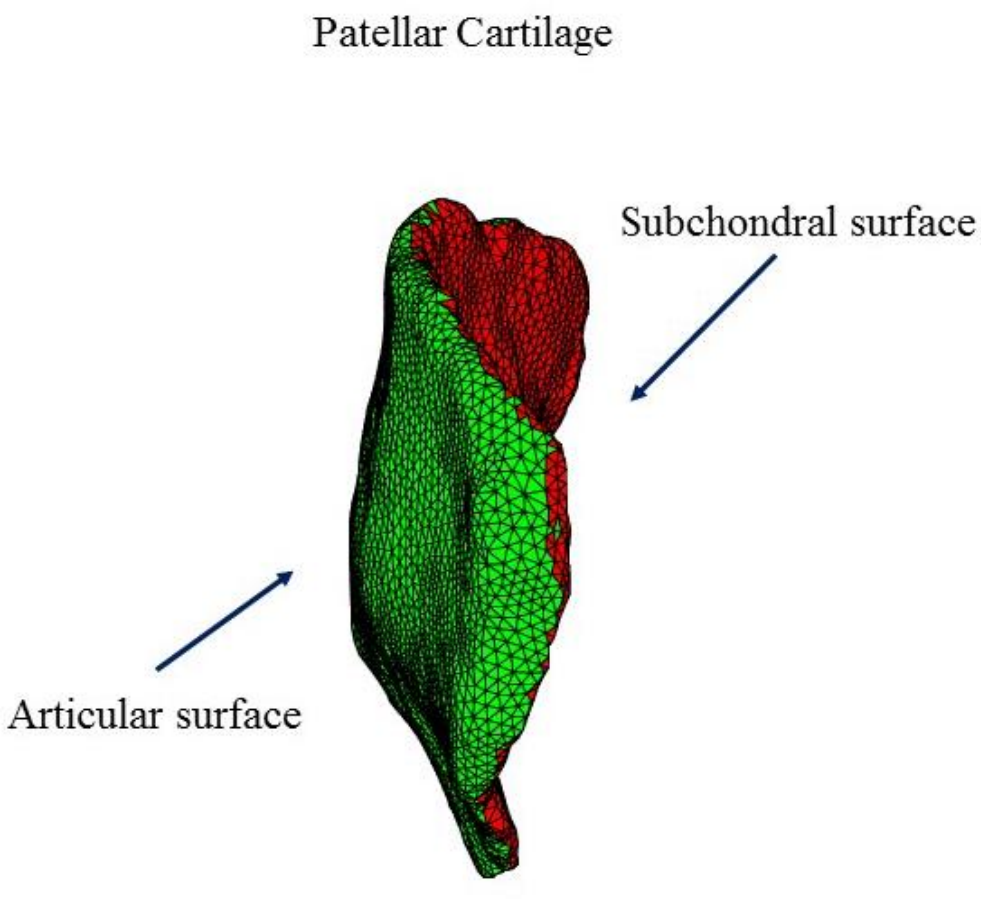

Figure B.2. Patellar cartilage divided into articular and subchondral faces

B.1.2 Cartilage Thickness Calculation

The following code will go through each patellar and femoral cartilage surface and calculate the individual element thickness using a nearest neighbor function built in to MATLAB.

```
%We want to calculate the articular cartilage surface and articular bone
%surface connections.  We need to trinagulate the bone surface.
fcart_artFace_IC = incenter(fcart_artFace);fcart_subch_IC =
incenter(fcart_subchFace);
fcart_artFace_norm = faceNormal(fcart_artFace);fcart_subch_norm =
faceNormal(fcart_subchFace);
% fbone_art_IC = incenter(fbone_artFace);fbone_subch_IC =
incenter(fbone_subchFace);

%Calculate femoral cartilage thickness
[fcart_k,fcart_thick] = nearestNeighbor(fbone,fcart_artFace_IC);
```

```
%Plot Thickness colormap
figure;[fcart_thick_sort,fcart_artFace_elem_sort,fcart_thick_cmap_scaled] =
cmap_plot(fcart_artFace,fcart_thick,fcart_thick,'Thickness (mm)');

%We want to calculate the articular cartilage surface and articular bone
%surface connections.  We need to trinagulate the bone surface.
pcart_artFace_UL_IC = incenter(pcart_artFace_unloaded);pcart_subchFace_UL_IC
= incenter(pcart_subchFace_unloaded);
%Thickness calculation using nearestNeighbor from Patella Cart
%to Patella Bone:
[pcart_thick_k,pcart_thick] =
nearestNeighbor(pbone_unloaded,pcart_artFace_UL_IC);
%Plot Thickness colormap
figure;[pcart_thick_sort,pcart_artFace_elem_sort,pcart_thick_cmap_scaled] =
cmap_plot(pcart_artFace_unloaded,pcart_thick,pcart_thick,'Thickness (mm)');
```

B.1.3 Division of Patellar Cartilage: Medial/Lateral Facet

The following code requires manual input to determine the superior, inferior and medial/lateral points that define the patellar cartilage in order to generate a body-based local coordinate system to divide the cartilage surface into medial and lateral facets.

```
%% Generating local coordinate system to define medial and lateral facets
%Use the unloaded position to ID the proper vertices for superior, inferior,
%medial and lateral points. Then run the below code 1 time to get the
%med/lateral element IDs

%Create local coordinate system for dividing elements into medial and
%lateral facet joints
%Use manual points to define the medial/lateral cartilage: Ideally, this
%should be done in the unloaded cartilage to ID the proper vertex point.

%Plot to define the sup/inf and med/lat anatomical points for LCS
figure;patch('Faces',pcart_artFace_unloaded.ConnectivityList,'Vertices',pcart
_artFace_unloaded.Points,'FaceColor','cyan');
hold on;axis
equal;patch('Faces',fbone.ConnectivityList,'Vertices',fbone.Points,'FaceColor
','magenta')
```

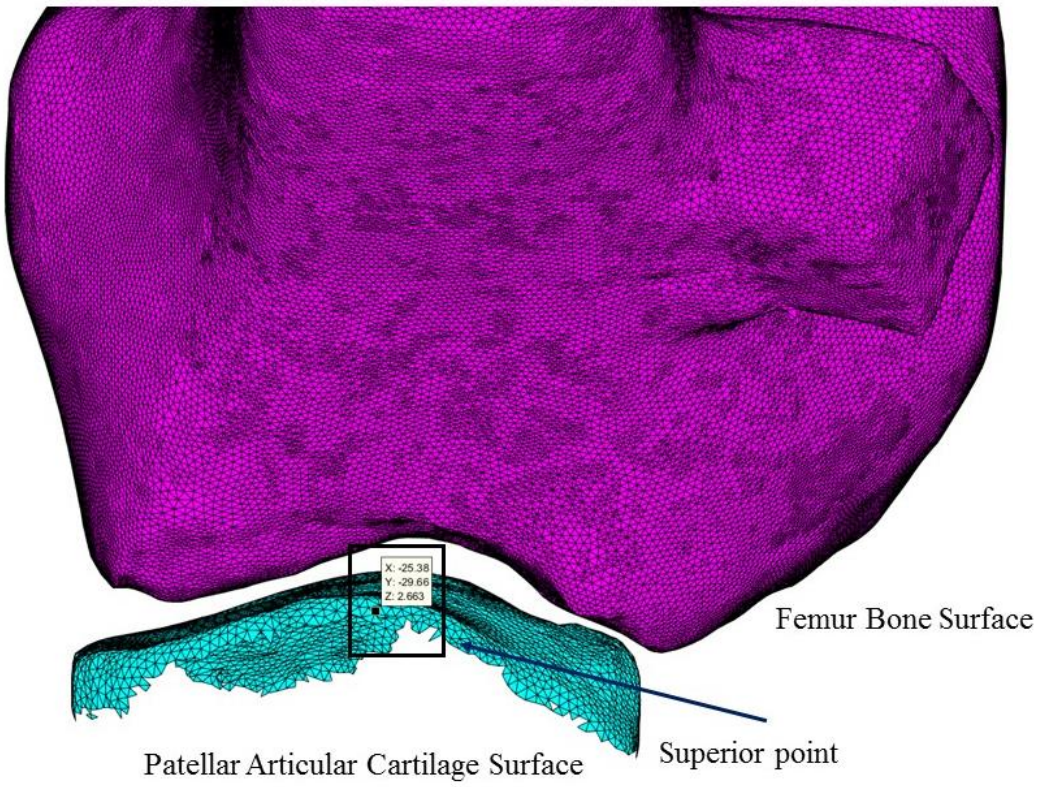

Figure B.3. Manual identification of patellar landmarks (superior point)

This process is performed for the inferior, medial and lateral points on the patellar surface. Running the following code will then generate a local coordinate system for the patellar cartilage and is used to divide the cartilage into medial/lateral facets using a project plane cut through the superior-to-inferior points.

```
%Plot to define the sup/inf and med/lat anatomical points for LCS

%MD Knee: T1 Data
superior_point = [-27.68,-29.92,34.38];inferior_point = [-26.48,-32.91,-
1.927];
supPoint_vertexID = nearestNeighbor(pcart_artFace_unloaded,superior_point)
infPoint_vertexID = nearestNeighbor(pcart_artFace_unloaded,inferior_point)

medial_point = [-4.607,-39.31,19.9];lateral_point = [-51.63,-36.11,19.89];
medPoint_vertexID = nearestNeighbor(pcart_artFace_unloaded,medial_point)
latPoint_vertexID = nearestNeighbor(pcart_artFace_unloaded,lateral_point)
supPoint = pcart_artFace_unloaded.Points(supPoint_vertexID,:);
infPoint = pcart_artFace_unloaded.Points(infPoint_vertexID,:);
supinf_midpt = (supPoint+infPoint)./2;
```

```
% medPoint_vertexID = 8203;
% latPoint_vertexID = 69;
medPoint = pcart_artFace_unloaded.Points(medPoint_vertexID,:);
latPoint = pcart_artFace_unloaded.Points(latPoint_vertexID,:);
medlat_midpt = (medPoint+latPoint)./2;

pat_lcs_medlat_vec = latPoint - medlat_midpt;%lateral is positive
pat_lcs_antpost_tempvec = supinf_midpt - medlat_midpt;
pat_lcs_origin = medlat_midpt +
dot(pat_lcs_antpost_tempvec,pat_lcs_medlat_vec,2)./dot(pat_lcs_medlat_vec,pat
_lcs_medlat_vec,2).*pat_lcs_medlat_vec;
pat_lcs_supinf_vec =
cross(pat_lcs_antpost_tempvec,pat_lcs_medlat_vec);%superior is positive for
right knee
pat_lcs_antpost_vec = cross(pat_lcs_supinf_vec,pat_lcs_medlat_vec);%anterior
is positive

pat_lcs_medlat = pat_lcs_medlat_vec./sqrt(sum(pat_lcs_medlat_vec.^2,2));%x-
axis
pat_lcs_antpost =
pat_lcs_antpost_vec./sqrt(sum(pat_lcs_antpost_vec.^2,2));%y-axis
pat_lcs_supinf = pat_lcs_supinf_vec./sqrt(sum(pat_lcs_supinf_vec.^2,2));%z-
axis

cent_pat = pat_lcs_origin'; %Origin of local patellar coordinate system
norm_x_pat = pat_lcs_medlat'; %X-axis of patella LCS defined in global
norm_y_pat = pat_lcs_antpost'; %Y-axis of patella LCS defined in global
norm_z_pat = pat_lcs_supinf'; %Z-axis of patella LCS defined in global

R_mat_patLCS = [norm_x_pat,norm_y_pat,norm_z_pat];
T_trans_patLCS = [eye(3),-cent_pat;0,0,0,1];
T_Rot_patLCS = [R_mat_patLCS,[0;0;0];0,0,0,1];
pcart_artFace_v = pcart_artFace_unloaded.Points;
pcart_LCS_prep = [pcart_artFace_v, ones(size(pcart_artFace_v,1),1)];
%Homogeneous construction
for ii = 1:length(pcart_LCS_prep)
    pcart_LCS_newpos(ii,:) =
transpose(inv(T_Rot_patLCS)*T_trans_patLCS*pcart_LCS_prep(ii,:)');
end

pcart_artFace_LCS =
triangulation(pcart_artFace_unloaded.ConnectivityList,pcart_LCS_newpos(:,1),p
cart_LCS_newpos(:,2),pcart_LCS_newpos(:,3));
pcart_artFace_LCS_IC = incenter(pcart_artFace_LCS);pcart_artFace_LCS_norm =
faceNormal(pcart_artFace_LCS);
pt_plane_to_IC = pcart_artFace_LCS_IC;
pt_plane_to_IC_norm = sqrt(sum(pt_plane_to_IC.^2,2));
pt_plane_to_IC_normalized =
pt_plane_to_IC./[pt_plane_to_IC_norm,pt_plane_to_IC_norm,pt_plane_to_IC_norm]
;
yz_plane_mat = repmat([1,0,0],[length(pcart_artFace_LCS_IC),1]);

med_lat_div = dot(yz_plane_mat,pt_plane_to_IC_normalized,2);
med_lat_div_revised = med_lat_div;
```

```
%For both knees (right and left) lateral is always positive based on LCS
if strcmp(test_knee(end),'L') == 1 %If left knee, med elem are positive
    med_elem = pcart_artFace_LCS.ConnectivityList(med_lat_div<0,:);
    lat_elem = pcart_artFace_LCS.ConnectivityList(med_lat_div>0,:);
else %If we have a right knee, med elem will be positive
    med_elem = pcart_artFace_LCS.ConnectivityList(med_lat_div<0,:);
    lat_elem = pcart_artFace_LCS.ConnectivityList(med_lat_div>0,:);
end

antpost_x = [cent_pat(1)+10*norm_y_pat(1),cent_pat(1)];
antpost_y = [cent_pat(2)+10*norm_y_pat(2),cent_pat(2)];
antpost_z = [cent_pat(3)+10*norm_y_pat(3),cent_pat(3)];

medlat_x = [cent_pat(1)+10*norm_x_pat(1),cent_pat(1)];
medlat_y = [cent_pat(2)+10*norm_x_pat(2),cent_pat(2)];
medlat_z = [cent_pat(3)+10*norm_x_pat(3),cent_pat(3)];

supinf_x = [cent_pat(1)+10*norm_z_pat(1),cent_pat(1)];
supinf_y = [cent_pat(2)+10*norm_z_pat(2),cent_pat(2)];
supinf_z = [cent_pat(3)+10*norm_z_pat(3),cent_pat(3)];

xline =
[pcart_artFace_unloaded.Points(supPoint_vertexID,1),pcart_artFace_unloaded.Po
ints(infPoint_vertexID,1)];
yline =
[pcart_artFace_unloaded.Points(supPoint_vertexID,2),pcart_artFace_unloaded.Po
ints(infPoint_vertexID,2)];
zline =
[pcart_artFace_unloaded.Points(supPoint_vertexID,3),pcart_artFace_unloaded.Po
ints(infPoint_vertexID,3)];

%Plot to check my lines and coordinate system
figure;patch('Faces',pcart_artFace_unloaded.ConnectivityList,'Vertices',pcart
_artFace_unloaded.Points,'FaceColor','red');
axis equal;hold on;plot3(xline,yline,zline,'-y');
plot3(pcart_artFace_unloaded.Points(supPoint_vertexID,1),pcart_artFace_unload
ed.Points(supPoint_vertexID,2),pcart_artFace_unloaded.Points(supPoint_vertexI
D,3),'*b');
plot3(pcart_artFace_unloaded.Points(infPoint_vertexID,1),pcart_artFace_unload
ed.Points(infPoint_vertexID,2),pcart_artFace_unloaded.Points(infPoint_vertexI
D,3),'*b');
plot3(medPoint(1),medPoint(2),medPoint(3),'*b');plot3(latPoint(1),latPoint(2)
,latPoint(3),'*b');
plot3(medlat_midpt(1),medlat_midpt(2),medlat_midpt(3),'*g');
plot3(supinf_midpt(1),supinf_midpt(2),supinf_midpt(3),'*c');
plot3(cent_pat(1),cent_pat(2),cent_pat(3),'y*'); %plot the origin on cube
corner
plot3(cent_pat(1)+10*norm_x_pat(1),cent_pat(2)+10*norm_x_pat(2),cent_pat(3)+1
0*norm_x_pat(3),'b*');
plot3(cent_pat(1)+10*norm_y_pat(1),cent_pat(2)+10*norm_y_pat(2),cent_pat(3)+1
0*norm_y_pat(3),'b*');
plot3(cent_pat(1)+10*norm_z_pat(1),cent_pat(2)+10*norm_z_pat(2),cent_pat(3)+1
0*norm_z_pat(3),'b*');
plot3(medlat_x,medlat_y,medlat_z,'-g');plot3(antpost_x,antpost_y,antpost_z,'-
g');
plot3(supinf_x,supinf_y,supinf_z,'-g');
```

```
%Plot line and visualize left and right
figure;patch('Faces',pcart_artFace_unloaded.ConnectivityList,'Vertices',pcart
_artFace_unloaded.Points,'FaceColor','yellow');
axis equal;hold on;plot3(xline,yline,zline,'-y');
patch('Faces',med_elem,'Vertices',pcart_artFace_unloaded.Points,'FaceColor','
cyan');
patch('Faces',lat_elem,'Vertices',pcart_artFace_unloaded.Points,'FaceColor','
green');
plot3(pcart_artFace_unloaded.Points(supPoint_vertexID,1),pcart_artFace_unload
ed.Points(supPoint_vertexID,2),pcart_artFace_unloaded.Points(supPoint_vertexI
D,3),'*r');
plot3(pcart_artFace_unloaded.Points(infPoint_vertexID,1),pcart_artFace_unload
ed.Points(infPoint_vertexID,2),pcart_artFace_unloaded.Points(infPoint_vertexI
D,3),'*r');
view(0,0);
```

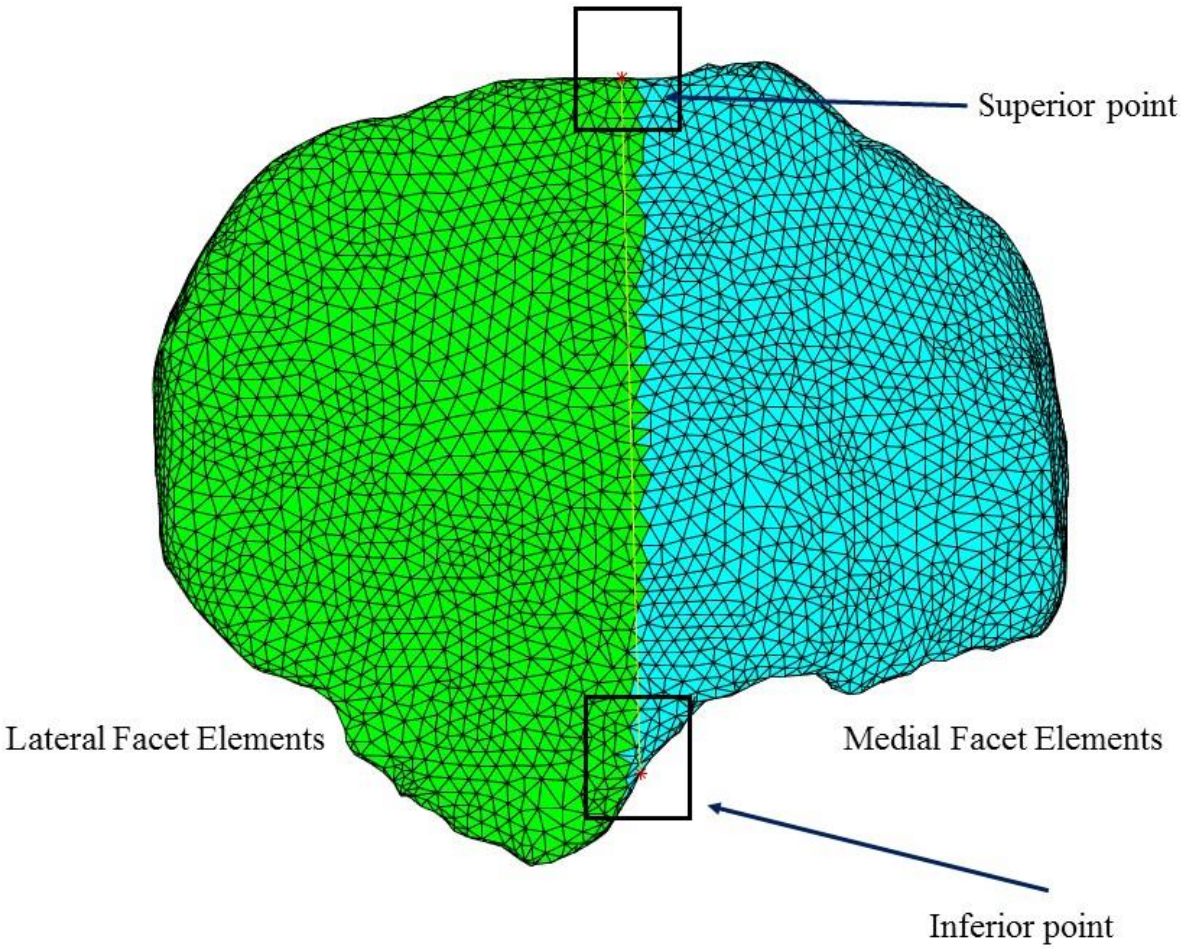

Figure B.4. Patellar cartilage division line separating lateral and medial facet elements

B.1.4 Application of Kinematics

The following code will apply the rigid transformation matrices calculated for the registration cubes and apply these transformations to position the MR-based model into the experimental local coordinate system (loaded position).

```
%% Load the Patella Catilage and Bone to new positions
%Transform our points from local to local by translating our data to the
%origin, rotating by unloaded matrix, then rotate by loaded state (change)
%and then re-rotate by original unloaded state.  Finally, translate to new
%position

%MD1108R Knee Directory/Data
load('MD1108R_Transformations_T1.mat');

cd(Matlabfolder_directory);
load_transform = P0_IR5;   %Possible loading transforms (depend on Knee):
P0_IR0,P0_ER5,P0_IR5,P15_IR0,P15_IR5,P15_ER5,P15_VR5
                                                                        %
P15_VL5,P30_IR0,P45_IR0,P60_IR0,P75_IR0,P90_IR0
T_loaded_wrt_global = Tms_FRB_MRI*Tms_PRB_wrt_FRB_MRI*load_transform;

cent_UL = Tms_PRB_MRI(2:4,1); %Origin of unloaded LCS
norm_x_UL = Tms_PRB_MRI(2:4,2); %X-axis of unloaded LCS
norm_y_UL = Tms_PRB_MRI(2:4,3); %Y-axis of unloaded LCS
norm_z_UL = Tms_PRB_MRI(2:4,4); %Z-axis of unloaded LCS

cent_L = T_loaded_wrt_global(2:4,1); %Origin of loaded LCS defined in global
norm_x_L = T_loaded_wrt_global(2:4,2); %X-axis of loaded LCS defined in
global
norm_y_L = T_loaded_wrt_global(2:4,3); %Y-axis of loaded LCS defined in
global
norm_z_L = T_loaded_wrt_global(2:4,4); %Z-axis of loaded LCS defined in
global

R_matUL = [norm_x_UL,norm_y_UL,norm_z_UL]; %Unloaded rotation matrix
R_matL = load_transform(2:4,2:4); %This is the local to local CS relative
change
T_trans1 = [eye(3),-cent_UL;0,0,0,1]; %Unloaded CS origin, relative to global
T_Rot1 = [R_matUL,[0;0;0];0,0,0,1]; %Homogeneous construction
T_Rot2 = [R_matL,[0;0;0];0,0,0,1]; %Homogeneous construction
T_trans2 = [eye(3),cent_L;0,0,0,1]; %Loaded CS origin, relative to global
pbone_v2_prep = [patella_v2 ones(size(patella_v2,1),1)]; %Homogeneous
construction
pcart_v2_prep = [pcart_v2 ones(size(pcart_v2,1),1)]; %Homogeneous
construction
pcart_artFace_v2_prep = [pcart_artFace_unloaded.Points
ones(size(pcart_artFace_unloaded.Points,1),1)]; %Homogeneous construction
pcart_subchFace_v2_prep = [pcart_subchFace_unloaded.Points
ones(size(pcart_subchFace_unloaded.Points,1),1)]; %Homogeneous construction
```

```
%Patella Bone transform
for ii = 1:length(pbone_v2_prep)
    pbone_newpos(ii,:) =
transpose(T_trans2*T_Rot1*T_Rot2*inv(T_Rot1)*T_trans1*pbone_v2_prep(ii,:)');
end
%Patella Cartilage transform
for ii = 1:length(pcart_v2_prep)
    pcart_newpos(ii,:) =
transpose(T_trans2*T_Rot1*T_Rot2*inv(T_Rot1)*T_trans1*pcart_v2_prep(ii,:)');
end
%Patella articulat and subchondral divided faces transform
for ii = 1:length(pcart_artFace_v2_prep)
    pcart_artFace_newpos(ii,:) =
transpose(T_trans2*T_Rot1*T_Rot2*inv(T_Rot1)*T_trans1*pcart_artFace_v2_prep(i
i,:)');
end
for ii = 1:length(pcart_subchFace_v2_prep)
    pcart_subchFace_newpos(ii,:) =
transpose(T_trans2*T_Rot1*T_Rot2*inv(T_Rot1)*T_trans1*pcart_subchFace_v2_prep
(ii,:)');
end

%Use the code below to check the orientation of the loaded position
%
figure;patch('Faces',patella_f2,'Vertices',patella_v2,'FaceColor','magenta');
% hold on;axis
equal;patch('Faces',patella_f2,'Vertices',pbone_newpos(:,1:3),'FaceColor','gr
een');
% patch('Faces',pcart_f2,'Vertices',pcart_v2,'FaceColor','cyan');
%
patch('Faces',pcart_f2,'Vertices',pcart_newpos(:,1:3),'FaceColor','yellow');
% plot3(cent_UL(1),cent_UL(2),cent_UL(3),'y*'); %plot the origin on cube
corner
%
plot3(cent_UL(1)+10*norm_x_UL(1),cent_UL(2)+10*norm_x_UL(2),cent_UL(3)+10*nor
m_x_UL(3),'r*');
%
plot3(cent_UL(1)+10*norm_y_UL(1),cent_UL(2)+10*norm_y_UL(2),cent_UL(3)+10*nor
m_y_UL(3),'r*');
%
plot3(cent_UL(1)+10*norm_z_UL(1),cent_UL(2)+10*norm_z_UL(2),cent_UL(3)+10*nor
m_z_UL(3),'r*');
% %These plot commands translate the origin by 10 units along each normal
% %direction
% plot3(cent_L(1),cent_L(2),cent_L(3),'y*'); %plot the origin on cube corner
%
plot3(cent_L(1)+10*norm_x_L(1),cent_L(2)+10*norm_x_L(2),cent_L(3)+10*norm_x_L
(3),'r*');
%
plot3(cent_L(1)+10*norm_y_L(1),cent_L(2)+10*norm_y_L(2),cent_L(3)+10*norm_y_L
(3),'r*');
%
plot3(cent_L(1)+10*norm_z_L(1),cent_L(2)+10*norm_z_L(2),cent_L(3)+10*norm_z_L
(3),'r*');
```

```
%Create our loaded data triangulation
pcart_loaded =
triangulation(pcart_f2,pcart_newpos(:,1),pcart_newpos(:,2),pcart_newpos(:,3))
;
pcart_loaded_norm = faceNormal(pcart_loaded);
pcart_loaded_IC = incenter(pcart_loaded);
pcart_artFace_loaded =
triangulation(pcart_artFace_unloaded.ConnectivityList,pcart_artFace_newpos(:,
1),pcart_artFace_newpos(:,2),pcart_artFace_newpos(:,3));
pcart_subchFace_loaded =
triangulation(pcart_subchFace_unloaded.ConnectivityList,pcart_subchFace_newpo
s(:,1),pcart_subchFace_newpos(:,2),pcart_subchFace_newpos(:,3));
pcart_artFace_L_IC = incenter(pcart_artFace_loaded);pcart_subchFace_L_IC =
incenter(pcart_subchFace_loaded);
pcart_artFace_loaded_norm =
faceNormal(pcart_artFace_loaded);pcart_subchFace_loaded_norm =
faceNormal(pcart_subchFace_loaded);
pbone_loaded =
triangulation(patella_f2,pbone_newpos(:,1),pbone_newpos(:,2),pbone_newpos(:,3
));
pbone_loaded_norm = faceNormal(pbone_loaded);
pbone_loaded_IC = incenter(pbone_loaded);
```

B.1.5 Penetration Algorithm

The following code implements a modified penetration algorithm once the experimental kinematics (above) have been applied. The algorithm uses the native MATLAB NearestNeighbor function and the KDTreeSearcher features over the patellar and femoral articular cartilage surfaces to find nearest neighbors, calculate the vector between those points, and use the dot product of this distance with the patellar cartilage element normal to determine penetration.

```
%Calculate Overlapping pairs using original mesh: IC to IC using for loop

clearvars pcart_to_fcart_distance overlap_vector overlap_norm_vec;
fcart_Mdl = KDTreeSearcher(fcart_artFace_IC);%Generate our KD Tree
pcart_to_fcart_k = zeros(length(pcart_artFace_L_IC),1);
pcart_to_fcart_distance = zeros(length(pcart_artFace_L_IC),1);
pcart_elem_tree_ind = zeros(size(pcart_artFace_loaded.ConnectivityList,1),1);
for ii = 1:length(pcart_artFace_L_IC)
    FB_pat = freeBoundary(pcart_artFace_loaded);%Check for freeEdge elements
    vert_ID = pcart_artFace_loaded.ConnectivityList(ii,:);
    [L_pcartElem_on_FB_1,L_FreeEdge_PatElemInd_1] =
ismember(vert_ID,FB_pat(:,1));
```

```
    [L_pcartElem_on_FB_2,L_FreeEdge_PatElemInd_2] =
ismember(vert_ID,FB_pat(:,2));
    if sum(L_pcartElem_on_FB_1)>=1 || sum(L_pcartElem_on_FB_2)>=1 %This code
uses NearestNeighbor for elements on edges of geometry
        [pcart_to_fcart_vertex_ind,pcart_to_fcart_distance(ii)] =
nearestNeighbor(fcart_artFace,pcart_artFace_L_IC(ii,:));
        temp_fcart_elem_vi =
vertexAttachments(fcart_artFace,pcart_to_fcart_vertex_ind); %This is a cell
with each row containing the elem ID's connected to each vertex
        temp_fcart_elem_IC =
fcart_artFace_IC(temp_fcart_elem_vi{1}(1:end),:);
        temp_pcart_IC =
repmat(pcart_artFace_L_IC(ii,:),size(temp_fcart_elem_IC,1),1);
        temp_pcart_to_fcart_ICvec = temp_fcart_elem_IC - temp_pcart_IC;
        temp_pcart_to_fcart_norm = sqrt(sum(temp_pcart_to_fcart_ICvec.^2,2));
        [min_dist,min_dist_ind] = min(temp_pcart_to_fcart_norm);
        pcart_to_fcart_distance(ii) = min_dist;
        pcart_to_fcart_k(ii) = temp_fcart_elem_vi{1}(min_dist_ind);
        pcart_elem_tree_ind(ii) = -1;
        clearvars KD_ind temp_nn_vector temp_nn_vector_norm
temp_nn_vector_normalized temp_dot_vector pot_elem min_dist min_dist_ind;
        continue;
    else
    [KD_ind,~] = rangesearch(fcart_Mdl,pcart_artFace_L_IC(ii,:),6.0);%We find
the KD Tree elements in fem cartilage that are within 4mm radius of problem
element
    temp_nn_vector = zeros(length(KD_ind{1}),3);
    for jj = 1:length(KD_ind{:})
        temp_nn_vector(jj,:) = fcart_artFace_IC(KD_ind{1}(jj),:) -
pcart_artFace_L_IC(ii,:);
    end
    temp_nn_vector_norm = sqrt(sum(temp_nn_vector.^2,2));
    temp_nn_vector_normalized =
temp_nn_vector./[temp_nn_vector_norm,temp_nn_vector_norm,temp_nn_vector_norm]
;
    temp_pcart_artFace_loaded_norm =
repmat(pcart_artFace_loaded_norm(ii,:),length(temp_nn_vector_norm),1);
    temp_dot_vector =
dot(temp_pcart_artFace_loaded_norm,temp_nn_vector_normalized,2);
    pot_elem = find(temp_dot_vector < -0.99);
    if isempty(pot_elem) == 1
        [pcart_to_fcart_vertex_ind,pcart_to_fcart_distance(ii)] =
nearestNeighbor(fcart_artFace,pcart_artFace_L_IC(ii,:));
        temp_fcart_elem_vi =
vertexAttachments(fcart_artFace,pcart_to_fcart_vertex_ind); %This is a cell
with each row containing the elem ID's connected to each vertex
        temp_fcart_elem_IC =
fcart_artFace_IC(temp_fcart_elem_vi{1}(1:end),:);
        temp_pcart_IC =
repmat(pcart_artFace_L_IC(ii,:),size(temp_fcart_elem_IC,1),1);
        temp_pcart_to_fcart_ICvec = temp_fcart_elem_IC - temp_pcart_IC;
        temp_pcart_to_fcart_norm = sqrt(sum(temp_pcart_to_fcart_ICvec.^2,2));
        [min_dist,min_dist_ind] = min(temp_pcart_to_fcart_norm);
        pcart_to_fcart_distance(ii) = min_dist;
        pcart_to_fcart_k(ii) = temp_fcart_elem_vi{1}(min_dist_ind);
        pcart_elem_tree_ind(ii) = 0;
```

```
        clearvars KD_ind temp_nn_vector temp_nn_vector_norm
temp_nn_vector_normalized temp_dot_vector pot_elem min_dist min_dist_ind;
        continue;
    end
    [min_dist,min_dist_ind] = min(temp_nn_vector_norm(pot_elem));
    pcart_to_fcart_distance(ii,1) = min_dist;
    pcart_to_fcart_k(ii,1) = KD_ind{1}(pot_elem(min_dist_ind));
    pcart_elem_tree_ind(ii) = 1;
    clearvars KD_ind temp_nn_vector temp_nn_vector_norm
temp_nn_vector_normalized temp_dot_vector pot_elem min_dist min_dist_ind;
    end
end

fcart_nn_IC = fcart_artFace_IC(pcart_to_fcart_k,:);
fcart_nn_norm = fcart_artFace_norm(pcart_to_fcart_k,:);
nn_vector = fcart_nn_IC - pcart_artFace_L_IC;
nn_norm_vec = zeros(length(nn_vector),3);
for ii = 1:length(nn_vector)
    if norm(nn_vector(ii,:)) > 15 %This assumes no springs greater than 6mm
        nn_norm_vec(ii,:) = [0.99,0.99,0.99];
        continue
    else
        nn_norm_vec(ii,:) = nn_vector(ii,:)./norm(nn_vector(ii,:));
    end
end

% overlap_dot_value_norms =
dot(pcart_artFace_loaded_norm(:,primary_dir_axis),fcart_nn_norm(:,primary_dir
_axis),2);
% overlap_dot_value_principal =
dot(pcart_artFace_loaded_norm(:,primary_dir_axis),nn_norm_vec(:,primary_dir_a
xis),2);
% overlap_dot_value = dot(pcart_artFace_loaded_norm,nn_norm_vec,2);


%Use this if model is off plane
overlap_dot_value_norms = dot(pcart_artFace_loaded_norm,fcart_nn_norm,2);
overlap_dot_value = dot(pcart_artFace_loaded_norm,nn_norm_vec,2);
% threshold_spring_princ = -0.5;format short;threshold_norms = -0.6;format
short;threshold= -0.6;format short;%For FE = 0
format short;threshold_norms = -0.7;format short;threshold= -0.7;format
short;%For FE = 0


k_elem_overlap = find((overlap_dot_value<threshold &
pcart_to_fcart_distance<10.0 & overlap_dot_value_norms<threshold_norms) |
(nn_norm_vec(:,primary_dir_axis)<threshold_norms &
overlap_dot_value_norms<threshold_norms) |
(overlap_dot_value_norms<threshold_norms & overlap_dot_value<threshold &
pcart_to_fcart_distance<10.0));


pcart_k_elem_masterindex =
zeros(size(pcart_artFace_loaded.ConnectivityList,1),1);
pcart_k_elem_masterindex(k_elem_overlap) = 1;
```

```
pcart_artFace_overlap_elem =
pcart_artFace_loaded.ConnectivityList(k_elem_overlap,:);


%Check overlap elements
figure;patch('Faces',fcart_artFace.ConnectivityList,'Vertices',fcart_artFace.
Points,'FaceColor','cyan');
axis equal;hold
on;patch('Faces',pcart_artFace_loaded.ConnectivityList,'Vertices',pcart_artFa
ce_loaded.Points,'FaceColor','yellow');
patch('Faces',pcart_artFace_overlap_elem,'Vertices',pcart_artFace_loaded.Poin
ts,'FaceColor','red');
view(153,2);
```

The result of this algorithm identifies elements in penetration and generates springs through those regions (Figure B.5).

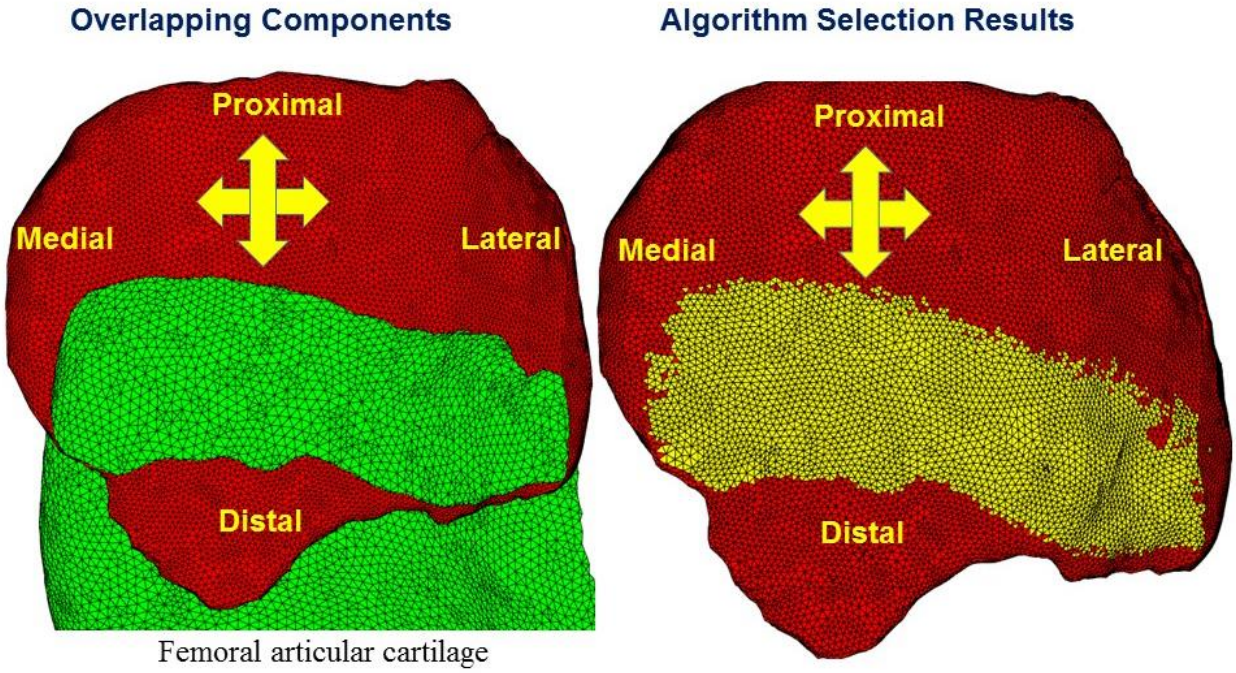

Figure B.5. Penetration algorithm selecting elements in overlap

This algorithm can be refined further to "smooth out" the selected edges and fill in any potential gaps or holes from the selection process using the following code:

```
%Refine_overlap function
```

```
 [overlap_elem_new_ind,pcart_artFace_overlap_elem_new] =
refineOverlap(pcart_artFace_loaded,pcart_artFace_overlap_elem,3);
figure;patch('Faces',fcart_artFace.ConnectivityList,'Vertices',fcart_artFace.
Points,'FaceColor','cyan');
axis equal;hold
on;patch('Faces',pcart_artFace_loaded.ConnectivityList,'Vertices',pcart_artFa
ce_loaded.Points,'FaceColor','yellow');
patch('Faces',pcart_artFace_overlap_elem_new,'Vertices',pcart_artFace_loaded.
Points,'FaceColor','red');view(153,2);
```

B.1.6 DEA Joint Contact Stress Calculation

The following code uses the overlapping regions to generate linear elastic springs and employ linear elastic theory to calculate joint contact area and stress (both mean and peak stress) for each facet region.

```
%Code for finding matching femoral cartilage thickness pairs if using the
%incenters of the femoral cartilage
fcart_overlap_thick = fcart_thick(pcart_to_fcart_k(overlap_elem_new_ind));
pcart_overlap_thick = pcart_thick(overlap_elem_new_ind);

%Combine our element to element thickness maps from the femoral and
%patellar cartilage
h_thickness = pcart_overlap_thick+fcart_overlap_thick;

Youngs_modulus = ones(length(d_overlap),1)*1.0;  %Define all E as 4 MPa
Poisson_ratio = ones(length(d_overlap),1)*0.42; %Define all v as 0.42; *Note
Elias used 0.45

%% Implement Linear Elastic Model Equation to calculate surface stress, p
%              (1-v)E                where v = Poisson_ratio
%      p = ------------- d              E = Youngs_modulus (MPa)
%           (1+v)(1-2v)h               h = unloaded thickness (mm)
%                                      d = overlap distance (mm)
% When deformation > 30%
%              (1-v)E                 where v = Poisson_ratio
%      p = ------------- ln(1-d/h)      E = Youngs_modulus (MPa)
%           (1+v)(1-2v)                h = unloaded thickness (mm)
%                                      d = overlap distance (mm)




pcart_stress = (((1-Poisson_ratio).*Youngs_modulus)./((1+Poisson_ratio).*(1-
2*Poisson_ratio))).*(d_overlap./(h_thickness));

%Stress calculation using logarithmic depth-dependent factor
```

```
% pcart_stress = -(((1-
Poisson_ratio).*Youngs_modulus)./((1+Poisson_ratio).*(1-
2*Poisson_ratio))).*log(1 - (d_overlap./(h_thickness)));


%Code to plot stress map on whole cartilage
% pcart_artFace_L_IC = incenter(pcart_artFace_loaded); %Run this command when
checking results
% test_knee = 'R';
pcart_stress_whole = zeros(length(pcart_artFace_L_IC),1);
pcart_stress_whole(overlap_elem_new_ind) = pcart_stress;
figure;[pcart_stress_sort,pcart_stress_elem_sort,pcart_stress_cmap_scaled] =
cmap_plot(pcart_artFace_loaded,pcart_stress,pcart_stress_whole,'Stress
(MPa)');

%% Calculate our contact variables for medial and lateral sides
%This includes pressure and area
if strcmp(test_knee(end),'L') == 1 %If left knee, med elem are negative
    med_pcart_stress = pcart_stress_whole(med_lat_div<0);
    lat_pcart_stress = pcart_stress_whole(med_lat_div>0);
else
    med_pcart_stress = pcart_stress_whole(med_lat_div<0);
    lat_pcart_stress = pcart_stress_whole(med_lat_div>0);
end

%Calculate area of contact
pcart_points = pcart_artFace_loaded.Points;
u_vec = pcart_points(pcart_artFace_overlap_elem_reduced(:,2),:) -
pcart_points(pcart_artFace_overlap_elem_reduced(:,1),:);
v_vec = pcart_points(pcart_artFace_overlap_elem_reduced(:,3),:) -
pcart_points(pcart_artFace_overlap_elem_reduced(:,1),:);
%Area of each triangle element is half the cross product norm
v_cross = cross(u_vec,v_vec);
tot_elem_area = sqrt(sum(v_cross.*v_cross,2))/2;

%Divide our area in medial and lateral facets
med_lat_overlap_div = med_lat_div(overlap_elem_new_ind);

if strcmp(test_knee(end),'L') == 1 %med elem are negative
    med_pcart_area = sum(tot_elem_area(med_lat_overlap_div<0));
    lat_pcart_area = sum(tot_elem_area(med_lat_overlap_div>0));
else
    med_pcart_area = sum(tot_elem_area(med_lat_overlap_div<0));
    lat_pcart_area = sum(tot_elem_area(med_lat_overlap_div>0));
end
%Sum area
pcart_whole_area = sum(tot_elem_area);

%Display our variables of interest
lat_pcart_area
med_pcart_area
mean(lat_pcart_stress(lat_pcart_stress~=0))
mean(med_pcart_stress(med_pcart_stress~=0))
max(lat_pcart_stress)
max(med_pcart_stress)
```

APPENDIX C

DEA MODEL SENSITIVITY

This appendix contains additional analyses looking at the effect of altering DEA input parameters of spring elastic modulus and Poisson's ratio on outcome mean and peak contact stress. This was conducted at several knee joint positions.

C.1.1 Effect of Elastic Modulus on DEA Stress

To explore the effect of changing the spring elastic modulus on outcome stress from the DEA model, several knee joint positions were processed with varying elastic moduli (0.5 MPa – 4.0 MPa). It was excpected that the elastic modulus would be linearly associated with the joint contact stress, as the springs are based on linear elastic foundation modeling.

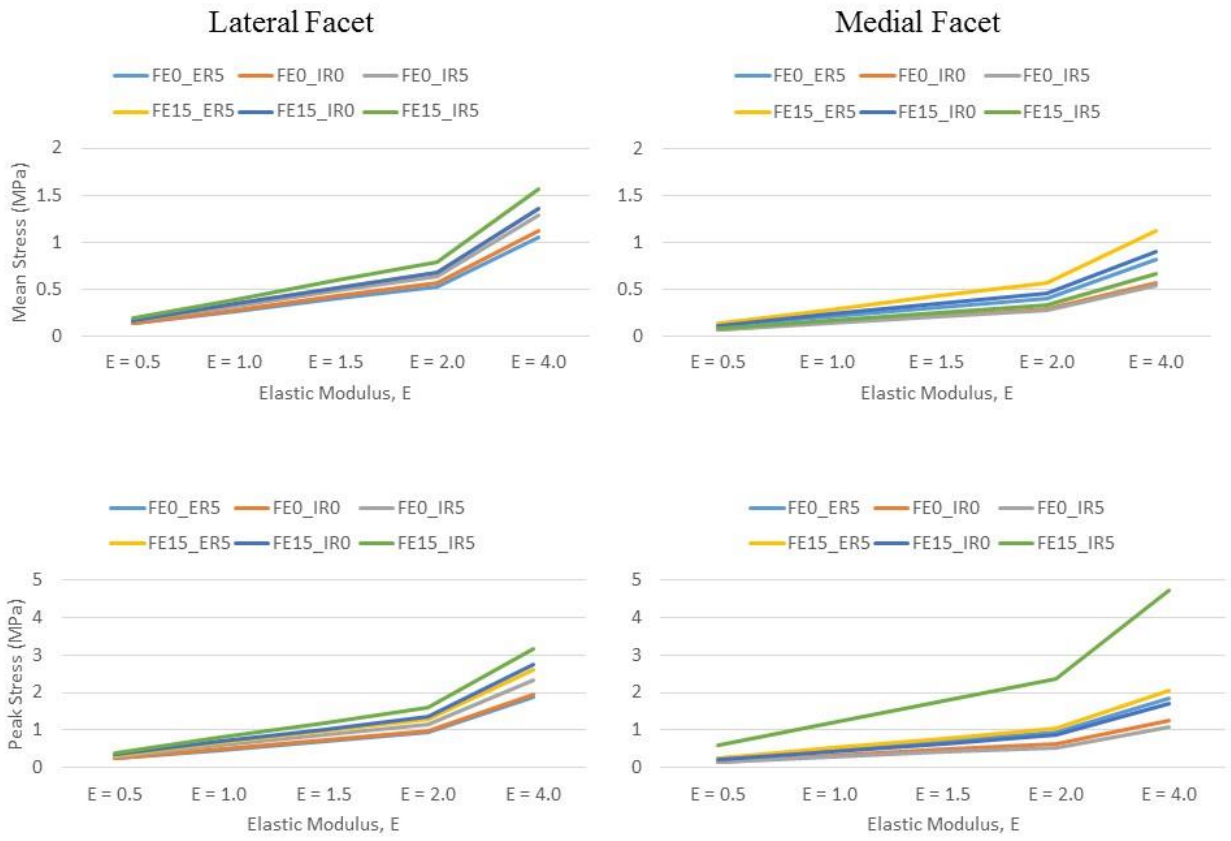

Figure C.1. Effect of altering elastic modulus on outcome stress for both patellar facets

C.1.2 Effect of Poisson's Ratio on DEA Stress

Similar to evaluating the effects of altering elastic modulus on the DEA-based outcome mean and peak contact stress, Poisson's ratio in each spring was altered in order to assess the sensitivity of the model to altering parameters. It was expected that Poisson's ratio would exhibit a non-linear relationship with stress, with higher values of Poisson's ratio to be associated with increased stresses.

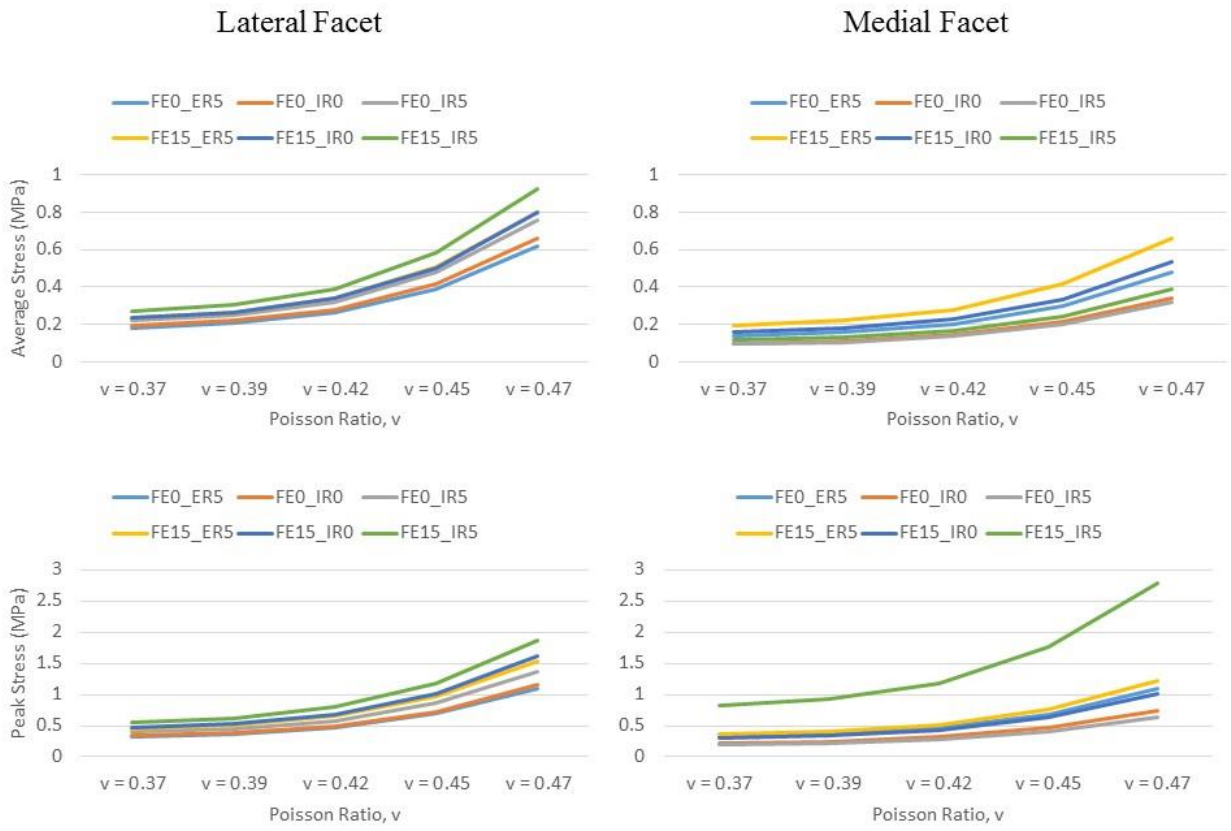

Figure C.2. Effect of altering Poisson's ratio on outcome stress for both patellar facets

C.1.3 Correlation Analysis for each Knee Specimen

The following table contains the outcome from the correlation analysis of the facet ratio from the DEA model for the in vitro validation study.

Correlation Analysis of Lateral to Medial Ratio Between Experimental and Computational Data

Data Set	Contact Area	Avg Stress	Peak Stress
Total Data (n = 23)	R = 0.270 P = 0.213	R = 0.676*‡ P < 0.001	R = 0.544* P = 0.007
Specimen 1 (n = 13)	R = 0.466 P = 0.108	R = 0.535 P = 0.59	R = 0.772* P = 0.002
Specimen 2 (n = 10)	R = 0.673* P = 0.033	R = 0.836* P = 0.003	R = 0.632* P = 0.05

* Significant at the 0.05 level

APPENDIX D

IN VIVO SHAPE MATCHING ALGORITHM

This appendix contains details for how to perform the best-fit shape matching algorithm for the femoral and patellar bones from the MR to CT based models. This is used in order to generate a rigid transformation matrix to navigate between the two modeling coordinate systems (Figure D.) and is important to generate in order to apply the DSX kinematics during functional tasks. Additionally, code for the application of these transformations is provided.

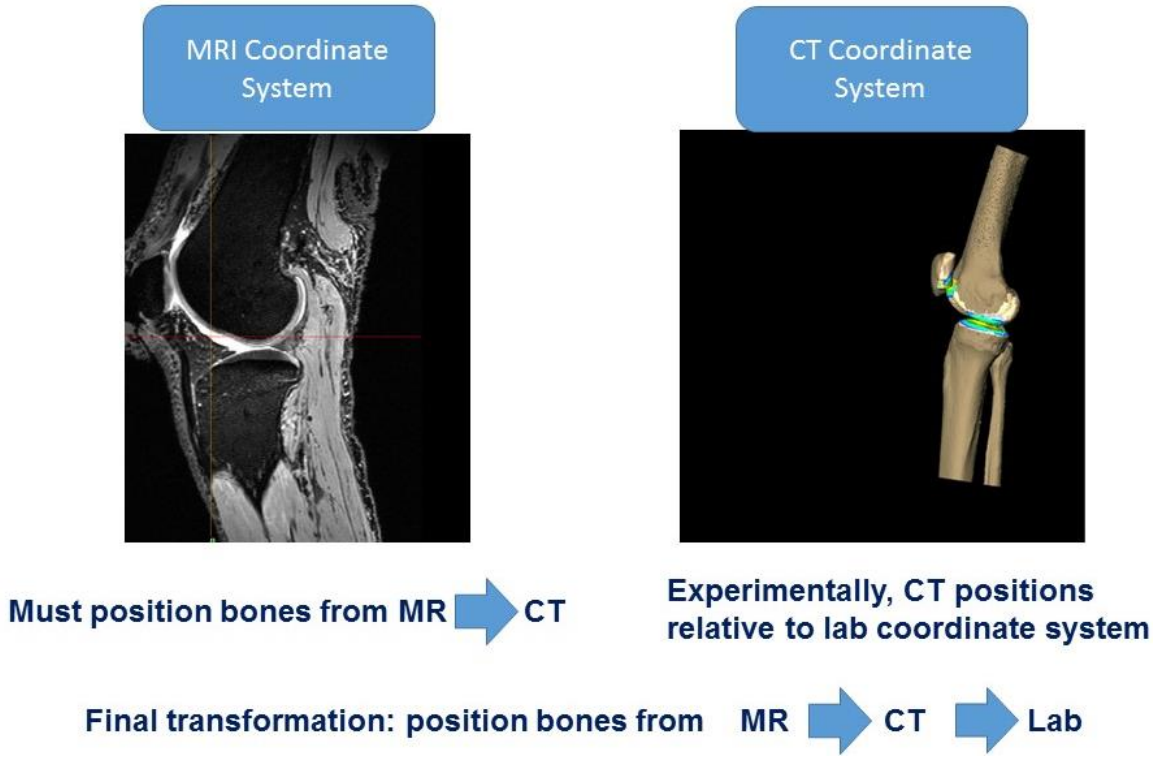

Figure D.1. Diagram describing transformation of DEA models from MR coordinate system to experimental CT-based coordinate system

D.1.1 Identify Anatomical Landmarks for Initial Alignment

After importing the CT and MRI models into Geomagic®, anatomical landmarks are defined on each model to perform an initial registration and alignment to better assist with the best-fit shape matching algorithm. The following landmarks were used for the femur bones: lateral and medial epicondyle, lateral/central/medial trochlear ridge, anterior and posterior femoral notch. Once these landmarks were defined, initial alignment was performed between the CT and MR models using the CT model as a reference (Figure D.2).

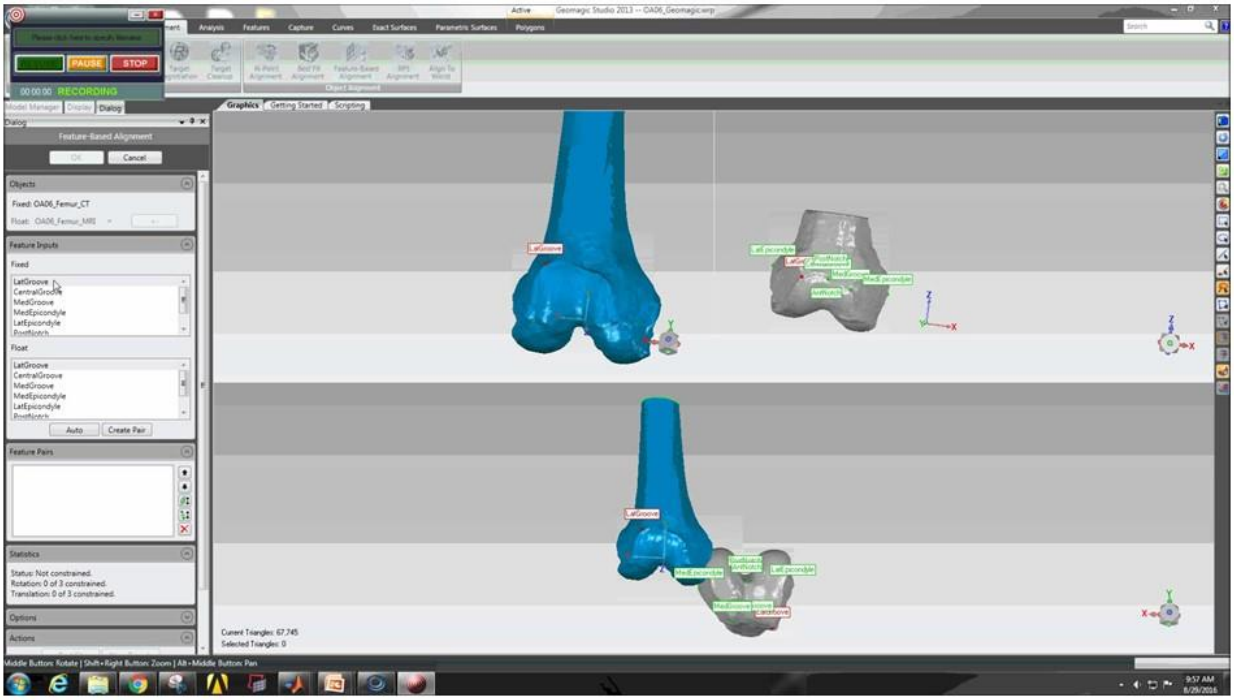

Figure D.2. Initial alignment of femoral bone using anatomical landmarks

For the patellar surfaces, the following anatomical landmarks were used: inferior apex, medial and lateral anterior border, posterior/superior patellar base, anterior/superior patellar base, and the posterior/inferior spine of the patella. Once these landmarks were defined for both the CT and MR models, the MR model was positioned to align with the CT model using these anatomical landmarks.

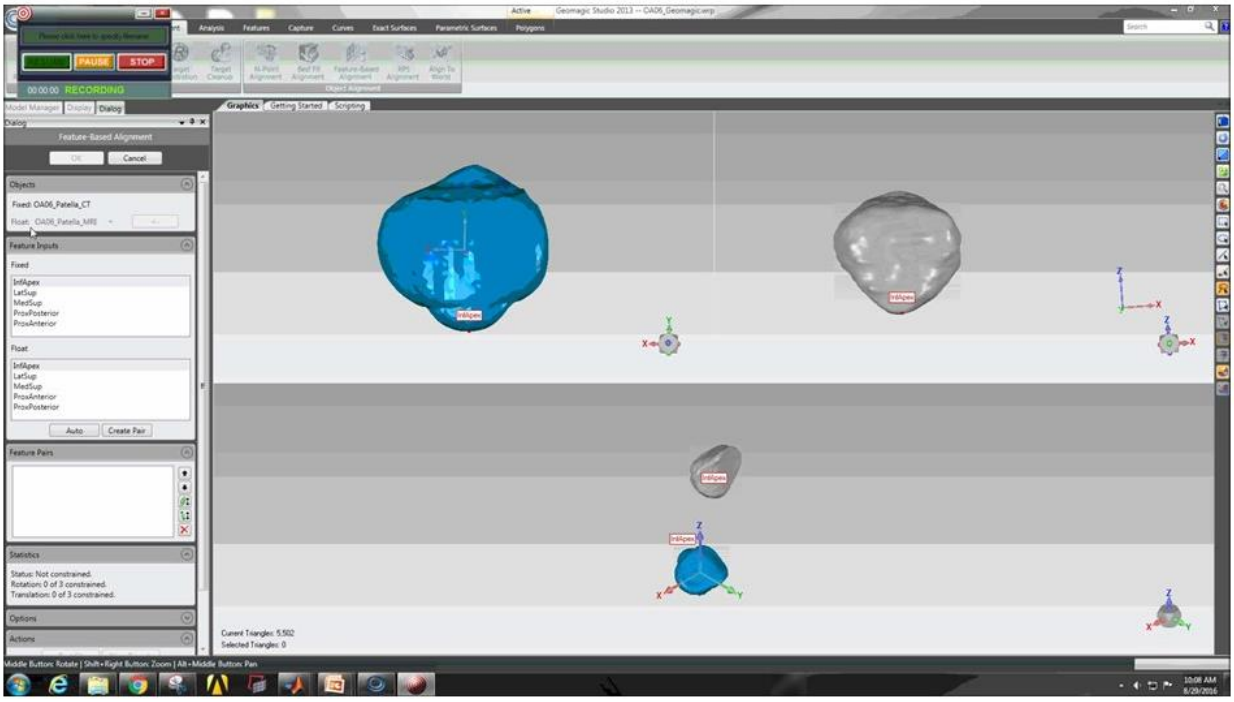

Figure D.3. Initial alignment of patellar bone using anatomical landmarks

D.1.2 Best-fit Shape Matching Algorithm

Once the femoral and patellar bone were initially aligned, a best-fit shape matching algorithm was employed in Geomagic®. The algorithm works by taking the object to be fit (MRI model) and minimizing the distance between the points throughout the object to the reference (CT model). The CT model was chosen as the reference object due to the increased resolution of the CT scanner in generating in-plane slices throughout each body compared to MRI (0.6 mm slice thickness vs. 0.7 mm). A tolerance can be set to define the minimum distance error for each point being matched. For the current study, a tolerance of 0.3 mm was used, to allow for small deviations in portions of the two geometries where there were differences in the curvature due to the differences in the imaging sources and segmentation methods. Once this best-fit algorithm has been performed, an average error across the fitted points and root mean square (RMS) error

of the individual points is generated, which indicates the quality of the fit. The objective was to minimize the average error and RMS error for the patella and femur for each individual, as large errors can affect the final positioning of the bones and alter DEA estimate of stress.

Table D.1. Individual results of best-fit shape matching algorithm

		Patella		Femur	
	Subject ID	Avg Error (mm)	RMS Error (mm)	Avg Error (mm)	RMS Error (mm)
Control	04	1.08	1.4	0.68	0.81
	07	0.45	0.57	0.88	1.52
	19	0.53	0.74	0.81	1.63
	24	0.50	0.66	0.81	1.08
	28	0.68	0.85	0.77	1.05
	30	0.50	0.61	0.66	0.84
OA	03	0.88	1.09	0.66	0.91
	06	0.57	0.78	0.66	0.89
	18	0.54	0.73	0.45	0.60
	25	1.36	1.98	0.96	1.46
	26	1.17	1.47	0.77	1.01

D.1.3 Application of In-Vivo Kinematics

Once the best-fit shape matching algorithm was performed, the output rigid transformation matrix was imported into the DEA code to rigidly transform the MR-based DEA model to each

of the loaded positions during the downhill walking task. The code below requires semi-manual input, requesting which trials and time points during the downhill walking was desired.

```
%% Load the Patella Catilage and Bone to new positions
%We need to import our MR --> CT transform from Geomagic and read in our
%.csv homogenoeous transformation files for the subject from the BDL
%dataset.

cd(fp);
%Start with loading the femur/patella MR to CT transforms
fileID_femur = fopen('Femur_MRI_to_CT_Transform.tfm');
C_femur = textscan(fileID_femur,'%f%f%f%f');
fclose(fileID_femur);
Tfemur_MR_to_CT = [C_femur{1},C_femur{2},C_femur{3},C_femur{4}];
%Patella
fileID_patella = fopen('Patella_MRI_to_CT_Transform.tfm');
C_patella = textscan(fileID_patella,'%f%f%f%f');
fclose(fileID_patella);
Tpatella_MR_to_CT = [C_patella{1},C_patella{2},C_patella{3},C_patella{4}];

%Run the OABRF_Transforms.m file located in the oabrf MATLAB folder dir or
%load the OABRF_Transforms.mat file
cd(Matlabfolder_directory);
load('OABRF_Transforms.mat');
subID = find(cellfun(@isempty,regexp(sub_list,test_subj(end-1:end)))==0);
trial = 'rdw3';
walk_frame = 10;
Tfemur_CT_to_lab = S_femur_Trans(subID).(trial).T_Femur_to_lab{walk_frame};
%Now the patella data
Tpatella_CT_to_lab =
S_patella_Trans(subID).(trial).T_Patella_to_lab{walk_frame};

%%%%%%%%%%%%%%%%%%
%MR --> CT transformations applied to the bone and cartilage
pbone_v2_prep = [patella_v2 ones(size(patella_v2,1),1)]; %Homogeneous
construction
pcart_v2_prep = [pcart_v2 ones(size(pcart_v2,1),1)]; %Homogeneous
construction
pcart_artFace_v2_prep = [pcart_artFace_unloaded.Points
ones(size(pcart_artFace_unloaded.Points,1),1)]; %Homogeneous construction
pcart_subchFace_v2_prep = [pcart_subchFace_unloaded.Points
ones(size(pcart_subchFace_unloaded.Points,1),1)]; %Homogeneous construction

fbone_v2_prep = [fbone_v2 ones(size(fbone_v2,1),1)]; %Homogeneous
construction
fcart_v2_prep = [fcart_v2 ones(size(fcart_v2,1),1)]; %Homogeneous
construction
fcart_artFace_v2_prep = [fcart_artFace.Points
ones(size(fcart_artFace.Points,1),1)]; %Homogeneous construction
fcart_subchFace_v2_prep = [fcart_subchFace.Points
ones(size(fcart_subchFace.Points,1),1)]; %Homogeneous construction
%Femur Bone transform
fbone_newpos = zeros(length(fbone_v2_prep),4);
for ii = 1:length(fbone_v2_prep)
```

```
    fbone_newpos(ii,:) =
transpose(Tfemur_CT_to_lab*Tfemur_MR_to_CT*fbone_v2_prep(ii,:)');
end
%Femur Cartilage transform
fcart_newpos = zeros(length(fcart_v2_prep),4);
for ii = 1:length(fcart_v2_prep)
    fcart_newpos(ii,:) =
transpose(Tfemur_CT_to_lab*Tfemur_MR_to_CT*fcart_v2_prep(ii,:)');
end
%Femur articular and subchondral divided faces transform
fcart_artFace_newpos = zeros(length(fcart_artFace_v2_prep),4);
for ii = 1:length(fcart_artFace_v2_prep)
    fcart_artFace_newpos(ii,:) =
transpose(Tfemur_CT_to_lab*Tfemur_MR_to_CT*fcart_artFace_v2_prep(ii,:)');
end
fcart_subchFace_newpos = zeros(length(fcart_subchFace_v2_prep),4);
for ii = 1:length(fcart_subchFace_v2_prep)
    fcart_subchFace_newpos(ii,:) =
transpose(Tfemur_CT_to_lab*Tfemur_MR_to_CT*fcart_subchFace_v2_prep(ii,:)');
end

%Patella Bone transform
pbone_newpos = zeros(length(pbone_v2_prep),4);
for ii = 1:length(pbone_v2_prep)
    pbone_newpos(ii,:) =
transpose(Tpatella_CT_to_lab*Tpatella_MR_to_CT*pbone_v2_prep(ii,:)');
end
%Patella Cartilage transform
pcart_newpos = zeros(length(pcart_v2_prep),4);
for ii = 1:length(pcart_v2_prep)
    pcart_newpos(ii,:) =
transpose(Tpatella_CT_to_lab*Tpatella_MR_to_CT*pcart_v2_prep(ii,:)');
end
%Patella articular and subchondral divided faces transform
pcart_artFace_newpos = zeros(length(pcart_artFace_v2_prep),4);
for ii = 1:length(pcart_artFace_v2_prep)
    pcart_artFace_newpos(ii,:) =
transpose(Tpatella_CT_to_lab*Tpatella_MR_to_CT*pcart_artFace_v2_prep(ii,:)');
end
pcart_subchFace_newpos = zeros(length(pcart_subchFace_v2_prep),4);
for ii = 1:length(pcart_subchFace_v2_prep)
    pcart_subchFace_newpos(ii,:) =
transpose(Tpatella_CT_to_lab*Tpatella_MR_to_CT*pcart_subchFace_v2_prep(ii,:)'
);
end
% %Use the code below to check the orientation of the loaded position
% figure;patch('Faces',patella_f2,'Vertices',patella_v2,'FaceColor',[1 1
0.5],'FaceAlpha',0.2);
% hold on;axis
equal;patch('Faces',fbone_f2,'Vertices',fbone_v2,'FaceColor','blue');
%
patch('Faces',pcart_f2,'Vertices',pcart_v2,'FaceColor','cyan');patch('Faces',
fcart_f2,'Vertices',fcart_v2,'FaceColor','yellow');
%
figure;patch('Faces',patella_f2,'Vertices',pbone_newpos(:,1:3),'FaceColor','g
reen');
```

```
% hold on;axis
equal;patch('Faces',pcart_f2,'Vertices',pcart_newpos(:,1:3),'FaceColor','yell
ow');
%
patch('Faces',fbone_f2,'Vertices',fbone_newpos(:,1:3),'FaceColor','magenta');
% patch('Faces',fcart_f2,'Vertices',fcart_newpos(:,1:3),'FaceColor','cyan');

%%%%%%%%%%%%%%%%%%%


%Create our loaded data triangulation
pcart_loaded =
triangulation(pcart_f2,pcart_newpos(:,1),pcart_newpos(:,2),pcart_newpos(:,3))
;
pcart_loaded_norm = faceNormal(pcart_loaded);
pcart_loaded_IC = incenter(pcart_loaded);
pcart_artFace_loaded =
triangulation(pcart_artFace_unloaded.ConnectivityList,pcart_artFace_newpos(:,
1),pcart_artFace_newpos(:,2),pcart_artFace_newpos(:,3));
pcart_subchFace_loaded =
triangulation(pcart_subchFace_unloaded.ConnectivityList,pcart_subchFace_newpo
s(:,1),pcart_subchFace_newpos(:,2),pcart_subchFace_newpos(:,3));
pcart_artFace_L_IC = incenter(pcart_artFace_loaded);pcart_subchFace_L_IC =
incenter(pcart_subchFace_loaded);
pcart_artFace_loaded_norm =
faceNormal(pcart_artFace_loaded);pcart_subchFace_loaded_norm =
faceNormal(pcart_subchFace_loaded);
pbone_loaded =
triangulation(patella_f2,pbone_newpos(:,1),pbone_newpos(:,2),pbone_newpos(:,3
));
pbone_loaded_norm = faceNormal(pbone_loaded);
pbone_loaded_IC = incenter(pbone_loaded);

fcart_loaded =
triangulation(fcart_f2,fcart_newpos(:,1),fcart_newpos(:,2),fcart_newpos(:,3))
;
fcart_loaded_norm = faceNormal(fcart_loaded);
fcart_loaded_IC = incenter(fcart_loaded);
fcart_artFace_loaded =
triangulation(fcart_artFace.ConnectivityList,fcart_artFace_newpos(:,1),fcart_
artFace_newpos(:,2),fcart_artFace_newpos(:,3));
fcart_subchFace_loaded =
triangulation(fcart_subchFace.ConnectivityList,fcart_subchFace_newpos(:,1),fc
art_subchFace_newpos(:,2),fcart_subchFace_newpos(:,3));
fcart_artFace_L_IC = incenter(fcart_artFace_loaded);fcart_subchFace_L_IC =
incenter(fcart_subchFace_loaded);
fcart_artFace_loaded_norm =
faceNormal(fcart_artFace_loaded);fcart_subchFace_loaded_norm =
faceNormal(fcart_subchFace_loaded);
fbone_loaded =
triangulation(fbone_f2,fbone_newpos(:,1),fbone_newpos(:,2),fbone_newpos(:,3))
;
fbone_loaded_norm = faceNormal(fbone_loaded);
fbone_loaded_IC = incenter(fbone_loaded);
```

```
figure;patch('Faces',fcart_artFace_loaded.ConnectivityList,'Vertices',fcart_a
rtFace_loaded.Points,'FaceColor','cyan');
axis equal;hold
on;patch('Faces',pcart_artFace_loaded.ConnectivityList,'Vertices',pcart_artFa
ce_loaded.Points,'FaceColor','yellow');
view(-13,0);
```

BIBLIOGRAPHY

1. Arden, N., & Nevitt, M. C. (2006). Osteoarthritis: epidemiology. *Best Practice & Research Clinical Rheumatology, 20*(1), 3-25.

2. Murphy, L., Schwartz, T. A., Helmick, C. G., Renner, J. B., Tudor, G., Koch, G., . . . Jordan, J. M. (2008). Lifetime risk of symptomatic knee osteoarthritis. *Arthritis Rheum, 59*(9), 1207-1213. doi: 10.1002/art.24021

3. Ma, V. Y., Chan, L., & Carruthers, K. J. (2014). Incidence, prevalence, costs, and impact on disability of common conditions requiring rehabilitation in the United States: stroke, spinal cord injury, traumatic brain injury, multiple sclerosis, osteoarthritis, rheumatoid arthritis, limb loss, and back pain. *Arch Phys Med Rehabil, 95*(5), 986-995 e981. doi: 10.1016/j.apmr.2013.10.032

4. Kotlarz, H., Gunnarsson, C. L., Fang, H., & Rizzo, J. A. (2009). Insurer and out-of-pocket costs of osteoarthritis in the US: Evidence from national survey data. *Arthritis & Rheumatism, 60*(12), 3546-3553.

5. Spector, T. D., Harris, P. A., Hart, D. J., Cicuttini, F. M., Nandra, D., Etherington, J., . . . Doyle, D. V. (1996). Risk of osteoarthritis associated with long-term weight-bearing sports: a radiologic survey of the hips and knees in female ex-athletes and population controls. *Arthritis & Rheumatism, 39*(6), 988-995.

6. Kim, S. (2008). Changes in surgical loads and economic burden of hip and knee replacements in the US: 1997–2004. *Arthritis Care & Research, 59*(4), 481-488.

7. Leskinen, J., Eskelinen, A., Huhtala, H., Paavolainen, P., & Remes, V. (2012). The incidence of knee arthroplasty for primary osteoarthritis grows rapidly among baby boomers: a population-based study in Finland. *Arthritis Rheum, 64*(2), 423-428. doi: 10.1002/art.33367

8. Flegal, K. M., Carroll, M. D., Ogden, C. L., & Curtin, L. R. (2010). Prevalence and trends in obesity among US adults, 1999-2008. *JAMA, 303*(3), 235-241. doi: 10.1001/jama.2009.2014

9. Cooper, C., Inskip, H., Croft, P., Campbell, L., Smith, G., McLaren, M., & Coggon, D. (1998). Individual risk factors for hip osteoarthritis: obesity, hip injury, and physical activity. *Am J Epidemiol, 147*(6), 516-522.

10. Lohmander, L. S., Gerhardsson de Verdier, M., Rollof, J., Nilsson, P. M., & Engstrom, G. (2009). Incidence of severe knee and hip osteoarthritis in relation to different measures of body mass: a population-based prospective cohort study. *Ann Rheum Dis, 68*(4), 490-496. doi: 10.1136/ard.2008.089748

11. Anderson, J. J., & Felson, D. T. (1988). Factors associated with osteoarthritis of the knee in the first national Health and Nutrition Examination Survey (HANES I). Evidence for an association with overweight, race, and physical demands of work. *Am J Epidemiol, 128*(1), 179-189.

12. Collins, D. (1949). The Pathology of Articular and Spinal Diseases Arnold: London.

13. Jaffe, H. L. (1972). Metabolic, degenerative, and inflammatory diseases of bones and joints.

14. Meachim, G., & Brooke, G. (1984). The pathology of osteoarthritis. *Osteoarthritis: diagnosis and management*, 29-42.

15. Lohmander, L. S., Ionescu, M., Jugessur, H., & Poole, A. R. (1999). Changes in joint cartilage aggrecan after knee injury and in osteoarthritis. *Arthritis Rheum, 42*(3), 534-544. doi: 10.1002/1529-0131(199904)42:3<534::AID-ANR19>3.0.CO;2-J

16. Maniwa, S., Nishikori, T., Furukawa, S., Kajitani, K., & Ochi, M. (2001). Alteration of collagen network and negative charge of articular cartilage surface in the early stage of experimental osteoarthritis. *Arch Orthop Trauma Surg, 121*(4), 181-185.

17. Otterness, I. G., Weiner, E., Swindell, A. C., Zimmerer, R. O., Ionescu, M., & Poole, A. R. (2001). An analysis of 14 molecular markers for monitoring osteoarthritis. Relationship of the markers to clinical end-points. *Osteoarthritis Cartilage, 9*(3), 224-231. doi: 10.1053/joca.2000.0379

18. Grodzinsky, A. J., Levenston, M. E., Jin, M., & Frank, E. H. (2000). Cartilage tissue remodeling in response to mechanical forces. *Annu Rev Biomed Eng, 2*, 691-713. doi: 10.1146/annurev.bioeng.2.1.691

19. Beaupre, G. S., Stevens, S. S., & Carter, D. R. (2000). Mechanobiology in the development, maintenance, and degeneration of articular cartilage. *J Rehabil Res Dev, 37*(2), 145-151.

20. Carter, D. R., Beaupre, G. S., Giori, N. J., & Helms, J. A. (1998). Mechanobiology of skeletal regeneration. *Clin Orthop Relat Res*(355 Suppl), S41-55.

21. Eckstein, F., Faber, S., Muhlbauer, R., Hohe, J., Englmeier, K. H., Reiser, M., & Putz, R. (2002). Functional adaptation of human joints to mechanical stimuli. *Osteoarthritis Cartilage, 10*(1), 44-50. doi: 10.1053/joca.2001.0480

22. Mow, V. C., Ratcliffe, A., & Poole, A. R. (1992). Cartilage and diarthrodial joints as paradigms for hierarchical materials and structures. *Biomaterials, 13*(2), 67-97.

23. Andriacchi, T. P., Mündermann, A., Smith, R. L., Alexander, E. J., Dyrby, C. O., & Koo, S. (2004). A framework for the in vivo pathomechanics of osteoarthritis at the knee. *Annals of biomedical engineering, 32*(3), 447-457.

24. Bellamy, N. (1986). The clinical evaluation of osteoarthritis in the elderly. *Clin Rheum Dis, 12*(1), 131-153.

25. Felson, D. T., Zhang, Y., Hannan, M. T., Naimark, A., Weissman, B. N., Aliabadi, P., & Levy, D. (1995). The incidence and natural history of knee osteoarthritis in the elderly. The Framingham Osteoarthritis Study. *Arthritis Rheum, 38*(10), 1500-1505.

26. Felson, D. T., Naimark, A., Anderson, J., Kazis, L., Castelli, W., & Meenan, R. F. (1987). The prevalence of knee osteoarthritis in the elderly. The Framingham Osteoarthritis Study. *Arthritis Rheum, 30*(8), 914-918.

27. Spector, T. D., Hart, D. J., & Doyle, D. V. (1994). Incidence and progression of osteoarthritis in women with unilateral knee disease in the general population: the effect of obesity. *Ann Rheum Dis, 53*(9), 565-568.

28. Lanyon, P., O'Reilly, S., Jones, A., & Doherty, M. (1998). Radiographic assessment of symptomatic knee osteoarthritis in the community: definitions and normal joint space. *Ann Rheum Dis, 57*(10), 595-601.

29. Ledingham, J., Regan, M., Jones, A., & Doherty, M. (1993). Radiographic patterns and associations of osteoarthritis of the knee in patients referred to hospital. *Ann Rheum Dis, 52*(7), 520-526.

30. Cicuttini, F., Spector, T., & Baker, J. (1997). Risk factors for osteoarthritis in the tibiofemoral and patellofemoral joints of the knee. *The Journal of rheumatology, 24*(6), 1164.

31. Duncan, R. C., Hay, E. M., Saklatvala, J., & Croft, P. R. (2006). Prevalence of radiographic osteoarthritis--it all depends on your point of view. *Rheumatology (Oxford), 45*(6), 757-760. doi: 10.1093/rheumatology/kei270

32. McAlindon, T., Cooper, C., Kirwan, J., & Dieppe, P. (1993). Determinants of disability in osteoarthritis of the knee. *Annals of the rheumatic diseases, 52*(4), 258-262.

33. Stefanik, J. J., Niu, J., Gross, K. D., Roemer, F. W., Guermazi, A., & Felson, D. T. (2013). Using magnetic resonance imaging to determine the compartmental prevalence of knee joint structural damage. *Osteoarthritis Cartilage, 21*(5), 695-699. doi: 10.1016/j.joca.2013.02.003

34. Tumia, N., & Maffulli, N. (2002). Patellofemoral pain in female athletes. *Sports Medicine and Arthroscopy Review, 10*(1), 69-75.

35. Thomas, M. J., Wood, L., Selfe, J., & Peat, G. (2010). Anterior knee pain in younger adults as a precursor to subsequent patellofemoral osteoarthritis: a systematic review. *BMC Musculoskelet Disord, 11*, 201. doi: 10.1186/1471-2474-11-201

36. Boling, M. C., Padua, D. A., Marshall, S. W., Guskiewicz, K., Pyne, S., & Beutler, A. (2009). A prospective investigation of biomechanical risk factors for patellofemoral pain syndrome: the Joint Undertaking to Monitor and Prevent ACL Injury (JUMP-ACL) cohort. *Am J Sports Med, 37*(11), 2108-2116. doi: 10.1177/0363546509337934

37. Farrokhi, S., Keyak, J., & Powers, C. (2011). Individuals with patellofemoral pain exhibit greater patellofemoral joint stress: a finite element analysis study. *Osteoarthritis and Cartilage, 19*(3), 287-294.

38. Brechter, J. H., & Powers, C. M. (2002). Patellofemoral stress during walking in persons with and without patellofemoral pain. *Medicine and science in sports and exercise, 34*(10), 1582-1593.

39. Goodfellow, J., Hungerford, D. S., & Zindel, M. (1976). Patello-femoral joint mechanics and pathology. 1. Functional anatomy of the patello-femoral joint. *Journal of Bone and Joint Surgery-British Volume, 58*(3), 287-290.

40. Dye, S. F. (2005). The pathophysiology of patellofemoral pain - A tissue homeostasis perspective. *Clinical orthopaedics and related research*(436), 100-110.

41. Fulkerson, J. P., & Buuck, D. A. (2004). *Disorders of the patellofemoral joint* (Vol. 4th). Philadelphia: Lippincott Williams & Wilkins.

42. Outerbridge, R. E., & Dunlop, J. A. (1975). The problem of chondromalacia patellae. *Clinical orthopaedics and related research, 110*(110), 177-196. doi: 10.1097/00003086-197507000-00024

43. Chang, A., Hayes, K., Dunlop, D., Song, J., Hurwitz, D., Cahue, S., & Sharma, L. (2005). Hip abduction moment and protection against medial tibiofemoral osteoarthritis progression. *Arthritis & Rheumatism, 52*(11), 3515-3519.

44. Sharma, L., Hurwitz, D. E., Thonar, E. J., Sum, J. A., Lenz, M. E., Dunlop, D. D., . . . Andriacchi, T. P. (1998). Knee adduction moment, serum hyaluronan level, and disease severity in medial tibiofemoral osteoarthritis. *Arthritis & Rheumatism, 41*(7), 1233-1240.

45. Zhang, Y., Hunter, D. J., Nevitt, M. C., Xu, L., Niu, J., Lui, L. Y., . . . Felson, D. T. (2004). Association of squatting with increased prevalence of radiographic tibiofemoral knee osteoarthritis: the Beijing Osteoarthritis Study. *Arthritis & Rheumatism, 50*(4), 1187-1192.

46. Kujala, U. M., Kettunen, J., Paananen, H., Aalto, T., Battié, M. C., Impivaara, O., . . . Sarna, S. (1995). Knee osteoarthritis in former runners, soccer players, weight lifters, and shooters. *Arthritis & Rheumatism, 38*(4), 539-546.

47. Duryea, J., Neumann, G., Niu, J., Totterman, S., Tamez, J., Dabrowski, C., . . . Beals, C. R. (2010). Comparison of radiographic joint space width with magnetic resonance imaging cartilage morphometry: analysis of longitudinal data from the Osteoarthritis Initiative. *Arthritis Care & Research, 62*(7), 932-937.

48. Norvell, D. C., Czerniecki, J. M., Reiber, G. E., Maynard, C., Pecoraro, J. A., & Weiss, N. S. (2005). The prevalence of knee pain and symptomatic knee osteoarthritis among veteran traumatic amputees and nonamputees. *Arch Phys Med Rehabil, 86*(3), 487-493. doi: 10.1016/j.apmr.2004.04.034

49. Utting, M., Davies, G., & Newman, J. (2005). Is anterior knee pain a predisposing factor to patellofemoral osteoarthritis? *The knee, 12*(5), 362-365.

50. Peat, G., Duncan, R. C., Wood, L. R., Thomas, E., & Muller, S. (2012). Clinical features of symptomatic patellofemoral joint osteoarthritis. *Arthritis Res Ther, 14*(2), R63. doi: 10.1186/ar3779

51. Creamer, P., Lethbridge-Cejku, M., & Hochberg, M. (2000). Factors associated with functional impairment in symptomatic knee osteoarthritis. *Rheumatology, 39*(5), 490-496.

52. Fox, J. M., & Del Pizzo, W. (1993). *The Patellofemoral joint*. New York: McGraw-Hill, Inc.

53. Hungerford, D. S., & Barry, M. (1979). Biomechanics of the patellofemoral joint. *Clinical orthopaedics and related research*(144), 9-15. doi: 10.1097/00003086-197910000-00003

54. Maroudas, A., Wachtel, E., Grushko, G., Katz, E. P., & Weinberg, P. (1991). The effect of osmotic and mechanical pressures on water partitioning in articular cartilage. *Biochim Biophys Acta, 1073*(2), 285-294.

55. Fox, A. J., Wanivenhaus, F., & Rodeo, S. A. (2012). The basic science of the patella: structure, composition, and function. *J Knee Surg, 25*(2), 127-141.

56. Ateshian, G., Soslowsky, L., & Mow, V. (1991). Quantitation of articular surface topography and cartilage thickness in knee joints using stereophotogrammetry. *J Biomech, 24*(8), 761-776.

57. Kwak, S. D., Colman, W. W., Ateshian, G. A., Grelsamer, R. P., Henry, J. H., & Mow, V. C. (1997). Anatomy of the human patellofemoral joint articular cartilage: surface curvature analysis. *J Orthop Res, 15*(3), 468-472. doi: 10.1002/jor.1100150322

58. Staubli, H. U., Durrenmatt, U., Porcellini, B., & Rauschning, W. (1999). Anatomy and surface geometry of the patellofemoral joint in the axial plane. *Journal of Bone and Joint Surgery-British Volume, 81*(3), 452-458.

59. Tecklenburg, K., Dejour, D., Hoser, C., & Fink, C. (2006). Bony and cartilaginous anatomy of the patellofemoral joint. *Knee Surg Sports Traumatol Arthrosc, 14*(3), 235-240. doi: 10.1007/s00167-005-0683-0

60. Thomee, R., Augustsson, J., & Karlsson, J. (1999). Patellofemoral pain syndrome: a review of current issues. *Sports Med, 28*(4), 245-262.

61. Grayson, T. (1990). Disorders of the patellofemoral joint: Baltimore (MD): Williams & Wilkins.

62. Amis, A. A., Senavongse, W., & Bull, A. M. (2006). Patellofemoral kinematics during knee flexion-extension: an in vitro study. *J Orthop Res, 24*(12), 2201-2211. doi: 10.1002/jor.20268

63. Draper, C. E., Besier, T. F., Fredericson, M., Santos, J. M., Beaupre, G. S., Delp, S. L., & Gold, G. E. (2011). Differences in patellofemoral kinematics between weight-bearing and non-weight-bearing conditions in patients with patellofemoral pain. *Journal of Orthopaedic Research, 29*(3), 312-317.

64. Souza, R. B., Draper, C. E., Fredericson, M., & Powers, C. M. (2010). Femur rotation and patellofemoral joint kinematics: a weight-bearing magnetic resonance imaging analysis. *J Orthop Sports Phys Ther, 40*(5), 277-285.

65. Powers, C. M., Shellock, F. G., & Pfaff, M. (1998). Quantification of patellar tracking using kinematic MRI. *J Magn Reson Imaging, 8*(3), 724-732.

66. Fellows, R. A., Hill, N. A., Gill, H. S., MacIntyre, N. J., Harrison, M. M., Ellis, R. E., & Wilson, D. R. (2005). Magnetic resonance imaging for in vivo assessment of three-dimensional patellar tracking. *J Biomech, 38*(8), 1643-1652. doi: 10.1016/j.jbiomech.2004.07.021

67. Sheehan, F. T., Zajac, F. E., & Drace, J. E. (1999). In vivo tracking of the human patella using cine phase contrast magnetic resonance imaging. *J Biomech Eng, 121*(6), 650-656.

68. Nha, K. W., Papannagari, R., Gill, T. J., Van de Velde, S. K., Freiberg, A. A., Rubash, H. E., & Li, G. (2008). In vivo patellar tracking: clinical motions and patellofemoral indices. *Journal of Orthopaedic Research, 26*(8), 1067-1074.

69. Bey, M. J., Kline, S. K., Tashman, S., & Zauel, R. (2008). Accuracy of biplane x-ray imaging combined with model-based tracking for measuring in-vivo patellofemoral joint motion. *J Orthop Surg Res, 3*, 38. doi: 10.1186/1749-799X-3-38

70. Farrokhi, S., Meholic, B., Chuang, W., Gustafson, J. A., Fitzgerald, G. K., & Tashman, S. (2015). Altered Frontal and transverse Plane Tibiofemoral Kinematics and Patellofemoral Malalignments During Downhill Gait in Patients with Mixed Knee Osteoarthritis. *J Biomech*.

71. Shih, Y. F., Bull, A. M., McGregor, A. H., & Amis, A. A. (2004). Active patellar tracking measurement: a novel device using ultrasound. *Am J Sports Med, 32*(5), 1209-1217. doi: 10.1177/0363546503262693

72. Shih, Y. F., Bull, A. M. J., McGregor, A. H., Humphries, K., & Amis, A. A. (2003). A technique for the measurement of patellar tracking during weight-bearing activities using ultrasound. *Proceedings of the Institution of Mechanical Engineers, Part H: Journal of Engineering in Medicine, 217*(6), 449-457. doi: 10.1243/09544110360729081

73. Katchburian, M. V., Bull, A. M., Shih, Y.-F., Heatley, F. W., & Amis, A. A. (2003). Measurement of patellar tracking: assessment and analysis of the literature. *Clinical orthopaedics and related research, 412*, 241-259.

74. Reider, B., Marshall, J. L., & Ring, B. (1981). Patellar tracking. *Clin Orthop Relat Res*(157), 143-148.

75. Stein, L. A., Endicott, A. N., Sampalis, J. S., Kaplow, M. A., Patel, M. D., & Mitchell, N. S. (1993). Motion of the patella during walking: a video digital-fluoroscopic study in healthy volunteers. *AJR Am J Roentgenol, 161*(3), 617-620. doi: 10.2214/ajr.161.3.8352119

76. Ahmed, A., Shi, S., Hyder, A., & Chan, K. (1988). The effect of quadriceps tension characteristics on the patellar tracking pattern. *Trans Orthop Res Soc, 13*, 280.

77. Fujikawa, K., Seedhom, B. B., & Wright, V. (1983). Biomechanics of the patello-femoral joint. Part I: A study of the contact and the congruity of the patello-femoral compartment and movement of the patella. *Eng Med, 12*(1), 3-11.

78. Kwak, S. D., Ahmad, C. S., Gardner, T. R., Grelsamer, R. P., Henry, J. H., Blankevoort, L., . . . Mow, V. C. (2000). Hamstrings and iliotibial band forces affect knee kinematics and contact pattern. *Journal of Orthopaedic Research, 18*(1), 101-108. doi: 10.1002/jor.1100180115

79. Sakai, N., Luo, Z. P., Rand, J. A., & An, K. N. (2000). The influence of weakness in the vastus medialis oblique muscle on the patellofemoral joint: an in vitro biomechanical study. *Clin Biomech (Bristol, Avon), 15*(5), 335-339.

80. Hefzy, M., Hsieh, Y., & Raftopoulos, D. (1991). The effects of tibial rotations on patellofemoral contact areas. *Trans Orthop Res Soc, 16*, 573.

81. Lafortune, M., Cavanagh, P., Sommer, H., & Kalenak, A. (1992). Three-dimensional kinematics of the human knee during walking. *J Biomech, 25*(4), 347-357.

82. Grood, E. S., & Suntay, W. J. (1983). A joint coordinate system for the clinical description of three-dimensional motions: application to the knee. *J Biomech Eng, 105*(2), 136-144.

83. Heegaard, J. H., Leyvraz, P. F., & Hovey, C. B. (2001). A computer model to simulate patellar biomechanics following total knee replacement: the effects of femoral component alignment. *Clin Biomech (Bristol, Avon), 16*(5), 415-423. doi: 10.1016/S0268-0033(01)00020-1

84. Lee, T. Q., Yang, B. Y., Sandusky, M. D., & McMahon, P. J. (2001). The effects of tibial rotation on the patellofemoral joint: assessment of the changes in in situ strain in the peripatellar retinaculum and the patellofemoral contact pressures and areas. *J Rehabil Res Dev, 38*(5), 463-469.

85. Hehne, H. J. (1990). Biomechanics of the patellofemoral joint and its clinical relevance. *Clin Orthop Relat Res*(258), 73-85.

86. Agneskirchner, J. D., Hurschler, C., Wrann, C. D., & Lobenhoffer, P. (2007). The effects of valgus medial opening wedge high tibial osteotomy on articular cartilage pressure of the knee: a biomechanical study. *Arthroscopy, 23*(8), 852-861. doi: 10.1016/j.arthro.2007.05.018

87. Huberti, H. H., & Hayes, W. C. (1984). Patellofemoral contact pressures. The influence of q-angle and tendofemoral contact. *J Bone Joint Surg Am, 66*(5), 715-724.

88. Mizuno, Y., Kumagai, M., Mattessich, S. M., Elias, J. J., Ramrattan, N., Cosgarea, A. J., & Chao, E. Y. (2001). Q-angle influences tibiofemoral and patellofemoral kinematics. *J Orthop Res, 19*(5), 834-840. doi: 10.1016/S0736-0266(01)00008-0

89. Elahi, S., Cahue, S., Felson, D. T., Engelman, L., & Sharma, L. (2000). The association between varus-valgus alignment and patellofemoral osteoarthritis. *Arthritis Rheum, 43*(8), 1874-1880. doi: 10.1002/1529-0131(200008)43:8<1874::AID-ANR25>3.0.CO;2-2

90. Farahmand, F., Senavongse, W., & Amis, A. A. (1998). Quantitative study of the quadriceps muscles and trochlear groove geometry related to instability of the patellofemoral joint. *J Orthop Res, 16*(1), 136-143. doi: 10.1002/jor.1100160123

91. Lieb, F. J., & Perry, J. (1968). Quadriceps function. An anatomical and mechanical study using amputated limbs. *J Bone Joint Surg Am, 50*(8), 1535-1548.

92. Baker, K. R., Xu, L., Zhang, Y., Nevitt, M., Niu, J., Aliabadi, P., . . . Felson, D. (2004). Quadriceps weakness and its relationship to tibiofemoral and patellofemoral knee osteoarthritis in Chinese: the Beijing osteoarthritis study. *Arthritis Rheum, 50*(6), 1815-1821. doi: 10.1002/art.20261

93. Farrokhi, S., Piva, S. R., Gil, A. B., Oddis, C. V., Brooks, M. M., & Fitzgerald, G. K. (2013). Association of severity of coexisting patellofemoral disease with increased impairments and functional limitations in patients with knee osteoarthritis. *Arthritis Care Res (Hoboken), 65*(4), 544-551. doi: 10.1002/acr.21866

94. Terry, G. C., Hughston, J. C., & Norwood, L. A. (1986). The anatomy of the iliopatellar band and iliotibial tract. *Am J Sports Med, 14*(1), 39-45. doi: 10.1177/036354658601400108

95. Farahmand, F., Tahmasbi, M. N., & Amis, A. A. (1998). Lateral force-displacement behaviour of the human patella and its variation with knee flexion--a biomechanical study in vitro. *J Biomech, 31*(12), 1147-1152.

96. Zaffagnini, S., Colle, F., Lopomo, N., Sharma, B., Bignozzi, S., Dejour, D., & Marcacci, M. (2013). The influence of medial patellofemoral ligament on patellofemoral joint kinematics and patellar stability. *Knee Surg Sports Traumatol Arthrosc, 21*(9), 2164-2171. doi: 10.1007/s00167-012-2307-9

97. Philippot, R., Boyer, B., Testa, R., Farizon, F., & Moyen, B. (2012). The role of the medial ligamentous structures on patellar tracking during knee flexion. *Knee Surg Sports Traumatol Arthrosc, 20*(2), 331-336. doi: 10.1007/s00167-011-1598-6

98. Philippot, R., Chouteau, J., Testa, R., & Moyen, B. (2010). In vitro analysis of patellar kinematics: validation of an opto-electronic cinematic analysis protocol. *Knee Surgery, Sports Traumatology, Arthroscopy, 18*(2), 161-166.

99. Shih, Y. F., Bull, A. M., & Amis, A. A. (2004). The cartilaginous and osseous geometry of the femoral trochlear groove. *Knee Surg Sports Traumatol Arthrosc, 12*(4), 300-306. doi: 10.1007/s00167-003-0414-3

100. Kujala, U. M., Osterman, K., Kormano, M., Komu, M., & Schlenzka, D. (1989). Patellar motion analyzed by magnetic resonance imaging. *Acta Orthop Scand, 60*(1), 13-16.

101. Ahmed, A. M., Burke, D. L., & Hyder, A. (1987). Force analysis of the patellar mechanism. *J Orthop Res, 5*(1), 69-85. doi: 10.1002/jor.1100050110

102. Anderst, W. J., Les, C., & Tashman, S. (2005). In vivo serial joint space measurements during dynamic loading in a canine model of osteoarthritis. *Osteoarthritis Cartilage, 13*(9), 808-816. doi: 10.1016/j.joca.2005.04.019

103. Tashman, S., Anderst, W., Kolowich, P., Havstad, S., & Arnoczky, S. (2004). Kinematics of the ACL-deficient canine knee during gait: serial changes over two years. *J Orthop Res, 22*(5), 931-941. doi: 10.1016/j.orthres.2004.01.008

104. Herzog, W., Diet, S., Suter, E., Mayzus, P., Leonard, T. R., Muller, C., . . . Epstein, M. (1998). Material and functional properties of articular cartilage and patellofemoral contact mechanics in an experimental model of osteoarthritis. *J Biomech, 31*(12), 1137-1145.

105. Andriacchi, T. P., Briant, P. L., Bevill, S. L., & Koo, S. (2006). Rotational changes at the knee after ACL injury cause cartilage thinning. *Clinical orthopaedics and related research, 442*, 39-44.

106. Andriacchi, T. P., & Dyrby, C. O. (2005). Interactions between kinematics and loading during walking for the normal and ACL deficient knee. *J Biomech, 38*(2), 293-298.

107. Andriacchi, T. P., & Mündermann, A. (2006). The role of ambulatory mechanics in the initiation and progression of knee osteoarthritis. *Current opinion in rheumatology, 18*(5), 514-518.

108. Tashman, S., Collon, D., Anderson, K., Kolowich, P., & Anderst, W. (2004). Abnormal rotational knee motion during running after anterior cruciate ligament reconstruction. *Am J Sports Med, 32*(4), 975-983.

109. Deneweth, J. M., Bey, M. J., McLean, S. G., Lock, T. R., Kolowich, P. A., & Tashman, S. (2010). Tibiofemoral joint kinematics of the anterior cruciate ligament-reconstructed knee during a single-legged hop landing. *Am J Sports Med, 38*(9), 1820-1828. doi: 10.1177/0363546510365531

110. Hoshino, Y., Fu, F. H., Irrgang, J. J., & Tashman, S. (2013). Can joint contact dynamics be restored by anterior cruciate ligament reconstruction? *Clin Orthop Relat Res, 471*(9), 2924-2931. doi: 10.1007/s11999-012-2761-1

111. Lohmander, L. S., Englund, P. M., Dahl, L. L., & Roos, E. M. (2007). The long-term consequence of anterior cruciate ligament and meniscus injuries osteoarthritis. *Am J Sports Med, 35*(10), 1756-1769.

112. Lohmander, L. S., Ostenberg, A., Englund, M., & Roos, H. (2004). High prevalence of knee osteoarthritis, pain, and functional limitations in female soccer players twelve years after anterior cruciate ligament injury. *Arthritis Rheum, 50*(10), 3145-3152. doi: 10.1002/art.20589

113. Oiestad, B. E., Engebretsen, L., Storheim, K., & Risberg, M. A. (2009). Knee osteoarthritis after anterior cruciate ligament injury: a systematic review. *Am J Sports Med, 37*(7), 1434-1443. doi: 10.1177/0363546509338827

114. Griffin, T. M., & Guilak, F. (2005). The role of mechanical loading in the onset and progression of osteoarthritis. *Exercise and sport sciences reviews, 33*(4), 195-200.

115. Koo, S., Alexander, E., Gold, G., Giori, N., & Andriacchi, T. (2003). *Morphological thickness in tibial and femoral cartilage are influenced by gait characteristics in healthy and osteoarthritic knees.* Paper presented at the Proceedings of the 2003 ASME Summer Conference, Miami, FL.

116. Fujisawa, T., Hattori, T., Takahashi, K., Kuboki, T., Yamashita, A., & Takigawa, M. (1999). Cyclic mechanical stress induces extracellular matrix degradation in cultured chondrocytes via gene expression of matrix metalloproteinases and interleukin-1. *J Biochem, 125*(5), 966-975.

117. Powers, C. M. (2003). The influence of altered lower-extremity kinematics on patellofemoral joint dysfunction: a theoretical perspective. *J Orthop Sports Phys Ther, 33*(11), 639-646. doi: 10.2519/jospt.2003.33.11.639

118. Powers, C. M., Lilley, J. C., & Lee, T. Q. (1998). The effects of axial and multi-plane loading of the extensor mechanism on the patellofemoral joint. *Clin Biomech (Bristol, Avon), 13*(8), 616-624.

119. Csintalan, R. P., Schulz, M. M., Woo, J., McMahon, P. J., & Lee, T. Q. (2002). Gender differences in patellofemoral joint biomechanics. *Clin Orthop Relat Res*(402), 260-269.

120. Lee, T. Q., Anzel, S. H., Bennett, K. A., Pang, D., & Kim, W. C. (1994). The influence of fixed rotational deformities of the femur on the patellofemoral contact pressures in human cadaver knees. *Clin Orthop Relat Res*(302), 69-74.

121. Li, G., DeFrate, L. E., Zayontz, S., Park, S. E., & Gill, T. J. (2004). The effect of tibiofemoral joint kinematics on patellofemoral contact pressures under simulated muscle loads. *J Orthop Res, 22*(4), 801-806. doi: 10.1016/j.orthres.2003.11.011

122. Li, G., Sakamoto, M., & Chao, E. Y. (1997). A comparison of different methods in predicting static pressure distribution in articulating joints. *J Biomech, 30*(6), 635-638.

123. Brechter, J. H., & Powers, C. M. (2002). Patellofemoral joint stress during stair ascent and descent in persons with and without patellofemoral pain. *Gait Posture, 16*(2), 115-123.

124. Nakagawa, S., Kadoya, Y., Kobayashi, A., Tatsumi, I., Nishida, N., & Yamano, Y. (2003). Kinematics of the patella in deep flexion. Analysis with magnetic resonance imaging. *J Bone Joint Surg Am, 85-A*(7), 1238-1242.

125. Draper, C. E., Besier, T. F., Santos, J. M., Jennings, F., Fredericson, M., Gold, G. E., . . . Delp, S. L. (2009). Using real-time MRI to quantify altered joint kinematics in subjects with patellofemoral pain and to evaluate the effects of a patellar brace or sleeve on joint motion. *J Orthop Res, 27*(5), 571-577. doi: 10.1002/jor.20790

126. Hinman, R. S., & Crossley, K. M. (2007). Patellofemoral joint osteoarthritis: an important subgroup of knee osteoarthritis. *Rheumatology (Oxford), 46*(7), 1057-1062. doi: 10.1093/rheumatology/kem114

127. Hinman, R. S., Crossley, K. M., McConnell, J., & Bennell, K. L. (2003). Efficacy of knee tape in the management of osteoarthritis of the knee: blinded randomised controlled trial. *BMJ, 327*(7407), 135. doi: 10.1136/bmj.327.7407.135

128. Cushnaghan, J., McCarthy, C., & Dieppe, P. (1994). Taping the patella medially: a new treatment for osteoarthritis of the knee joint? *BMJ, 308*(6931), 753-755.

129. Pollo, F. E., Otis, J. C., Backus, S. I., Warren, R. F., & Wickiewicz, T. L. (2002). Reduction of medial compartment loads with valgus bracing of the osteoarthritic knee. *Am J Sports Med, 30*(3), 414-421. doi: 10.1177/03635465020300031801

130. Powers, C. M., Ward, S. R., Chan, L. D., Chen, Y. J., & Terk, M. R. (2004). The effect of bracing on patella alignment and patellofemoral joint contact area. *Med Sci Sports Exerc, 36*(7), 1226-1232.

131. Kerrigan, D. C., Lelas, J. L., Goggins, J., Merriman, G. J., Kaplan, R. J., & Felson, D. T. (2002). Effectiveness of a lateral-wedge insole on knee varus torque in patients with knee osteoarthritis. *Arch Phys Med Rehabil, 83*(7), 889-893.

132. Quilty, B., Tucker, M., Campbell, R., & Dieppe, P. (2003). Physiotherapy, including quadriceps exercises and patellar taping, for knee osteoarthritis with predominant patello-femoral joint involvement: randomized controlled trial. *J Rheumatol, 30*(6), 1311-1317.

133. Fitzgerald, G. K. (2005). Therapeutic exercise for knee osteoarthritis: considering factors that may influence outcome. *Eura Medicophys, 41*(2), 163-171.

134. Fitzgerald, G. K., Piva, S. R., & Irrgang, J. J. (2003). A modified neuromuscular electrical stimulation protocol for quadriceps strength training following anterior cruciate ligament reconstruction. *J Orthop Sports Phys Ther, 33*(9), 492-501. doi: 10.2519/jospt.2003.33.9.492

135. Besier, T. F., Gold, G. E., Beaupré, G. S., & Delp, S. L. (2005). A modeling framework to estimate patellofemoral joint cartilage stress in vivo. *Medicine and science in sports and exercise, 37*(11), 1924.

136. Huiskes, R., & Chao, E. Y. (1983). A survey of finite element analysis in orthopedic biomechanics: the first decade. *J Biomech, 16*(6), 385-409.

137. Li, W., Li, Q., Steven, G. P., & Xie, Y. M. (2003). An evolutionary approach to elastic contact optimization of frame structures. *Finite Elements in Analysis & Design, 40*(1), 61-81. doi: 10.1016/S0168-874X(02)00179-8

138. Brown, T. D. (2004). Finite element modeling in musculoskeletal biomechanics. *Journal of applied biomechanics, 20*(4), 336-366.

139. Spyrakos, C. C. (1996). *Finite element modeling in engineering practice : includes examples with ALGOR*. Pittsburgh, PA: Distributed by Algor Pub. Div.

140. Fernandez, J. W., & Hunter, P. J. (2005). An anatomically based patient-specific finite element model of patella articulation: towards a diagnostic tool. *Biomech Model Mechanobiol, 4*(1), 20-38. doi: 10.1007/s10237-005-0072-0

141. Heegaard, J., Leyvraz, P. F., Curnier, A., Rakotomanana, L., & Huiskes, R. (1995). The biomechanics of the human patella during passive knee flexion. *J Biomech, 28*(11), 1265-1279.

142. Besier, T. F., Gold, G. E., Delp, S. L., Fredericson, M., & Beaupré, G. S. (2008). The influence of femoral internal and external rotation on cartilage stresses within the patellofemoral joint. *Journal of Orthopaedic Research, 26*(12), 1627-1635.

143. An, K. N., Himeno, S., Tsumura, H., Kawai, T., & Chao, E. Y. (1990). Pressure distribution on articular surfaces: application to joint stability evaluation. *J Biomech, 23*(10), 1013-1020.

144. Blankevoort, L., Kuiper, J. H., Huiskes, R., & Grootenboer, H. J. (1991). Articular contact in a three-dimensional model of the knee. *J Biomech, 24*(11), 1019-1031.

145. Kwak, S., Blankevoort, L., & Ateshian, G. (2000). A mathematical formulation for 3D quasi-static multibody models of diarthrodial joints. *Computer methods in biomechanics and biomedical engineering, 3*(1), 41-64.

146. Bei, Y., & Fregly, B. J. (2004). Multibody dynamic simulation of knee contact mechanics. *Med Eng Phys, 26*(9), 777-789. doi: 10.1016/j.medengphy.2004.07.004

147. Yoshida, H., Faust, A., Wilckens, J., Kitagawa, M., Fetto, J., & Chao, E. Y. (2006). Three-dimensional dynamic hip contact area and pressure distribution during activities of daily living. *J Biomech, 39*(11), 1996-2004. doi: 10.1016/j.jbiomech.2005.06.026

148. Genda, E., Iwasaki, N., Li, G., MacWilliams, B. A., Barrance, P. J., & Chao, E. Y. (2001). Normal hip joint contact pressure distribution in single-leg standing--effect of gender and anatomic parameters. *J Biomech, 34*(7), 895-905.

149. Abraham, C. L., Maas, S. A., Weiss, J. A., Ellis, B. J., Peters, C. L., & Anderson, A. E. (2013). A new discrete element analysis method for predicting hip joint contact stresses. *J Biomech, 46*(6), 1121-1127. doi: 10.1016/j.jbiomech.2013.01.012

150. Kern, A. M., & Anderson, D. D. (2015). Expedited patient-specific assessment of contact stress exposure in the ankle joint following definitive articular fracture reduction. *J Biomech, 48*(12), 3427-3432. doi: 10.1016/j.jbiomech.2015.05.030

151. Anderson, D. D., Iyer, K. S., Segal, N. A., Lynch, J. A., & Brown, T. D. (2010). Implementation of discrete element analysis for subject-specific, population-wide investigations of habitual contact stress exposure. *J Appl Biomech, 26*(2), 215-223.

152. Segal, N. A., Anderson, D. D., Iyer, K. S., Baker, J., Torner, J. C., Lynch, J. A., . . . Brown, T. D. (2009). Baseline articular contact stress levels predict incident symptomatic knee osteoarthritis development in the MOST cohort. *J Orthop Res, 27*(12), 1562-1568. doi: 10.1002/jor.20936

153. Halloran, J. P., Easley, S. K., Petrella, A. J., & Rullkoetter, P. J. (2005). Comparison of deformable and elastic foundation finite element simulations for predicting knee replacement mechanics. *J Biomech Eng, 127*(5), 813-818.

154. Elias, J. J., & Saranathan, A. (2013). Discrete element analysis for characterizing the patellofemoral pressure distribution: model evaluation. *J Biomech Eng, 135*(8), 81011. doi: 10.1115/1.4024287

155. Elias, J. J., Wilson, D. R., Adamson, R., & Cosgarea, A. J. (2004). Evaluation of a computational model used to predict the patellofemoral contact pressure distribution. *J Biomech, 37*(3), 295-302.

156. Smith, C. R., Won Choi, K., Negrut, D., & Thelen, D. G. (2016). Efficient computation of cartilage contact pressures within dynamic simulations of movement. *Computer Methods in Biomechanics and Biomedical Engineering: Imaging & Visualization*, 1-8. doi: 10.1080/21681163.2016.1172346

157. Elias, J. J., Cech, J. A., Weinstein, D. M., & Cosgrea, A. J. (2004). Reducing the lateral force acting on the patella does not consistently decrease patellofemoral pressures. *Am J Sports Med, 32*(5), 1202-1208. doi: 10.1177/0363546503262167

158. Elias, J. J., & Cosgarea, A. J. (2007). Computational modeling: an alternative approach for investigating patellofemoral mechanics. *Sports Med Arthrosc, 15*(2), 89-94. doi: 10.1097/JSA.0b013e31804bbe4d

159. Elias, J. J., & Cosgarea, A. J. (2006). Technical errors during medial patellofemoral ligament reconstruction could overload medial patellofemoral cartilage: a computational analysis. *Am J Sports Med, 34*(9), 1478-1485. doi: 10.1177/0363546506287486

160. Elias, J. J., Kilambi, S., & Cosgarea, A. J. (2010). Computational assessment of the influence of vastus medialis obliquus function on patellofemoral pressures: model evaluation. *J Biomech, 43*(4), 612-617. doi: 10.1016/j.jbiomech.2009.10.039

161. Elias, J. J., Kirkpatrick, M. S., Saranathan, A., Mani, S., Smith, L. G., & Tanaka, M. J. (2011). Hamstrings loading contributes to lateral patellofemoral malalignment and elevated cartilage pressures: an in vitro study. *Clin Biomech (Bristol, Avon), 26*(8), 841-846. doi: 10.1016/j.clinbiomech.2011.03.016

162. Elias, J. J., Kelly, M. J., Smith, K. E., Gall, K. A., & Farr, J. (2016). Dynamic Simulation of the Effects of Graft Fixation Errors During Medial Patellofemoral Ligament Reconstruction. *Orthop J Sports Med, 4*(9), 2325967116665080. doi: 10.1177/2325967116665080

163. Fregly, B. J., Besier, T. F., Lloyd, D. G., Delp, S. L., Banks, S. A., Pandy, M. G., & D'Lima, D. D. (2012). Grand challenge competition to predict in vivo knee loads. *Journal of Orthopaedic Research, 30*(4), 503-513.

164. Baldwin, M. A., Clary, C., Maletsky, L. P., & Rullkoetter, P. J. (2009). Verification of predicted specimen-specific natural and implanted patellofemoral kinematics during simulated deep knee bend. *J Biomech, 42*(14), 2341-2348. doi: 10.1016/j.jbiomech.2009.06.028

165. Henninger, H. B., Reese, S. P., Anderson, A. E., & Weiss, J. A. (2010). Validation of computational models in biomechanics. *Proc Inst Mech Eng H, 224*(7), 801-812. doi: 10.1243/09544119JEIM649

166. Martin, J. A., Brown, T. D., Heiner, A. D., & Buckwalter, J. A. (2004). Chondrocyte senescence, joint loading and osteoarthritis. *Clin Orthop Relat Res*(427 Suppl), S96-103.

167. Duncan, R., Peat, G., Thomas, E., Wood, L., Hay, E., & Croft, P. (2009). Does isolated patellofemoral osteoarthritis matter? *Osteoarthritis Cartilage, 17*(9), 1151-1155. doi: 10.1016/j.joca.2009.03.016

168. Powers, C. M., Heino, J. G., Rao, S., & Perry, J. (1999). The influence of patellofemoral pain on lower limb loading during gait. *Clin Biomech (Bristol, Avon), 14*(10), 722-728.

169. Perry, J., Antonelli, D., & Ford, W. (1975). Analysis of knee-joint forces during flexed-knee stance. *J Bone Joint Surg Am, 57*(7), 961-967.

170. Reilly, D. T., & Martens, M. (1972). Experimental analysis of the quadriceps muscle force and patello-femoral joint reaction force for various activities. *Acta Orthop Scand, 43*(2), 126-137.

171. Goymann, V., Haasters, J., & Heller, W. (1974). [Proceedings: Current studies on the biomechanics of the patella]. *Z Orthop Ihre Grenzgeb, 112*(4), 623-625.

172. Huberti, H. H., Hayes, W. C., Stone, J. L., & Shybut, G. T. (1984). Force ratios in the quadriceps tendon and ligamentum patellae. *J Orthop Res, 2*(1), 49-54. doi: 10.1002/jor.1100020108

173. Eckstein, F., & Glaser, C. (2004). Measuring cartilage morphology with quantitative magnetic resonance imaging. *Semin Musculoskelet Radiol, 8*(4), 329-353. doi: 10.1055/s-2004-861579

174. Draper, C. E., Besier, T. F., Gold, G. E., Fredericson, M., Fiene, A., Beaupre, G. S., & Delp, S. L. (2006). Is cartilage thickness different in young subjects with and without patellofemoral pain? *Osteoarthritis Cartilage, 14*(9), 931-937. doi: 10.1016/j.joca.2006.03.006

175. Lee, T. Q., Morris, G., & Csintalan, R. P. (2003). The influence of tibial and femoral rotation on patellofemoral contact area and pressure. *J Orthop Sports Phys Ther, 33*(11), 686-693.

176. Perry, J. (1992). *Gait analysis : normal and pathological function*. Thorofare, N.J.: SLACK inc.

177. Hofer, J. K., Gejo, R., McGarry, M. H., & Lee, T. Q. (2012). Effects of kneeling on tibiofemoral contact pressure and area in posterior cruciate-retaining and posterior cruciate-sacrificing total knee arthroplasty. *J Arthroplasty, 27*(4), 620-624. doi: 10.1016/j.arth.2011.07.011

178. Ostermeier, S., Holst, M., Hurschler, C., Windhagen, H., & Stukenborg-Colsman, C. (2007). Dynamic measurement of patellofemoral kinematics and contact pressure after lateral retinacular release: an in vitro study. *Knee Surg Sports Traumatol Arthrosc, 15*(5), 547-554. doi: 10.1007/s00167-006-0261-0

179. Fischer, K. J., Manson, T. T., Pfaeffle, H. J., Tomaino, M. M., & Woo, S. L. (2001). A method for measuring joint kinematics designed for accurate registration of kinematic data to models constructed from CT data. *J Biomech, 34*(3), 377-383.

180. Kuster, M., Sakurai, S., & Wood, G. (1995). Kinematic and kinetic comparison of downhill and level walking. *Clin Biomech (Bristol, Avon), 10*(2), 79-84.

181. Pearle, A. D., Solomon, D. J., Wanich, T., Moreau-Gaudry, A., Granchi, C. C., Wickiewicz, T. L., & Warren, R. F. (2007). Reliability of navigated knee stability examination a cadaveric evaluation. *Am J Sports Med, 35*(8), 1315-1320.

182. Elias, J. J., Kilambi, S., Goerke, D. R., & Cosgarea, A. J. (2009). Improving vastus medialis obliquus function reduces pressure applied to lateral patellofemoral cartilage. *J Orthop Res, 27*(5), 578-583. doi: 10.1002/jor.20791

183. Otto, J., Brown, T., Heiner, A., Pedersen, D., & Callaghan, J. (1998). *Characterization of the dynamic response of a piezoresistive contact stress sensor.* Paper presented at the Transactions of the Annual Meeting-Orthopaedic Research Society 808.

184. . Standard Guide for Measurement Systems Analysis (MSA). (2017): ASTM International.

185. Nagamine, R., Otani, T., White, S. E., McCarthy, D. S., & Whiteside, L. A. (1995). Patellar tracking measurement in the normal knee. *J Orthop Res, 13*(1), 115-122. doi: 10.1002/jor.1100130117

186. Lenssen, A. F., van Dam, E. M., Crijns, Y. H., Verhey, M., Geesink, R. J., van den Brandt, P. A., & de Bie, R. A. (2007). Reproducibility of goniometric measurement of the knee in the in-hospital phase following total knee arthroplasty. *BMC Musculoskelet Disord, 8*, 83. doi: 10.1186/1471-2474-8-83

187. Wilson, D. R., Apreleva, M. V., Eichler, M. J., & Harrold, F. R. (2003). Accuracy and repeatability of a pressure measurement system in the patellofemoral joint. *J Biomech, 36*(12), 1909-1915.

188. Bachus, K. N., DeMarco, A. L., Judd, K. T., Horwitz, D. S., & Brodke, D. S. (2006). Measuring contact area, force, and pressure for bioengineering applications: using Fuji Film and TekScan systems. *Med Eng Phys, 28*(5), 483-488. doi: 10.1016/j.medengphy.2005.07.022

189. Harris, M. L., Morberg, P., Bruce, W. J., & Walsh, W. R. (1999). An improved method for measuring tibiofemoral contact areas in total knee arthroplasty: a comparison of K-scan sensor and Fuji film. *J Biomech, 32*(9), 951-958.

190. Brimacombe, J. M., Wilson, D. R., Hodgson, A. J., Ho, K. C., & Anglin, C. (2009). Effect of calibration method on Tekscan sensor accuracy. *J Biomech Eng, 131*(3), 034503. doi: 10.1115/1.3005165

191. Almeida, S. A., Trone, D. W., Leone, D. M., Shaffer, R. A., Patheal, S. L., & Long, K. (1999). Gender differences in musculoskeletal injury rates: a function of symptom reporting? *Med Sci Sports Exerc, 31*(12), 1807-1812.

192. Devereaux, M. D., & Lachmann, S. M. (1984). Patello-femoral arthralgia in athletes attending a Sports Injury Clinic. *Br J Sports Med, 18*(1), 18-21.

193. Fairbank, J. C. T., Pynsent, P. B., Vanpoortvliet, J. A., & Phillips, H. (1984). Mechanical Factors in the Incidence of Knee Pain in Adolescents and Young-Adults. *Journal of Bone and Joint Surgery-British Volume, 66*(5), 685-693.

194. Levine, J. (1979). Chondromalacia Patellae. *Physican Sportsmed., 7*, 41-49.

195. Loud, K. J., & Micheli, L. J. (2001). Common athletic injuries in adolescent girls. *Current Opinion in Pediatrics, 13*(4), 317-322.

196. Davies, A. P., Vince, A. S., Shepstone, L., Donell, S. T., & Glasgow, M. M. (2002). The radiologic prevalence of patellofemoral osteoarthritis. *Clin Orthop Relat Res*(402), 206-212.

197. Oiestad, B. E., Holm, I., Engebretsen, L., Aune, A. K., Gunderson, R., & Risberg, M. A. (2013). The prevalence of patellofemoral osteoarthritis 12 years after anterior cruciate ligament reconstruction. *Knee Surg Sports Traumatol Arthrosc, 21*(4), 942-949. doi: 10.1007/s00167-012-2161-9

198. Heywood, W. B. (1961). Recurrent dislocation of the patella. *J Bone Joint Surg., 43-B*, 508-517.

199. Insall, J., Falvo, K. A., & Wise, D. W. (1976). Chondromalacia Patellae. A prospective study. *Journal of Bone & Joint Surgery - American Volume, 58*(1), 1-8.

200. Moller, B. N., Moller-Larsen, F., & Frich, L. H. (1989). Chondromalacia induced by patellar subluxation in the rabbit. *Acta Orthop Scand, 60*(2), 188-191.

201. Outerbridge, R. E. (1961). The etiology of chondromalacia patellae. *Journal of Bone and Joint Surgery-British Volume, 43-B*, 752-757.

202. Ahmed, A. M., Burke, D. L., & Yu, A. (1983). In-vitro measurement of static pressure distribution in synovial joints--Part II: Retropatellar surface. *J Biomech Eng, 105*(3), 226-236.

203. Haut, R. C. (1989). Contact pressures in the patellofemoral joint during impact loading on the human flexed knee. *J Orthop Res, 7*(2), 272-280.

204. Beillas, P., Papaioannou, G., Tashman, S., & Yang, K. H. (2004). A new method to investigate in vivo knee behavior using a finite element model of the lower limb. *J Biomech, 37*(7), 1019-1030. doi: 10.1016/j.jbiomech.2003.11.022

205. Drury, N. J. (2008). *Evaluating the anterior stability provided by the glenohumeral capsule: a finite element approach.* University of Pittsburgh.

206. Iwasaki, N., Genda, E., Barrance, P. J., Minami, A., Kaneda, K., & Chao, E. Y. (1998). Biomechanical analysis of limited intercarpal fusion for the treatment of Kienbock's disease: a three-dimensional theoretical study. *J Orthop Res, 16*(2), 256-263. doi: 10.1002/jor.1100160213

207. Fitzpatrick, C. K., Baldwin, M. A., & Rullkoetter, P. J. (2010). Computationally efficient finite element evaluation of natural patellofemoral mechanics. *J Biomech Eng, 132*(12), 121013. doi: 10.1115/1.4002854

208. Cohen, Z. A., Roglic, H., Grelsamer, R. P., Henry, J. H., Levine, W. N., Mow, V. C., & Ateshian, G. A. (2001). Patellofemoral stresses during open and closed kinetic chain exercises An analysis using computer simulation. *Am J Sports Med, 29*(4), 480-487.

209. Liao, T. C., Yang, N., Ho, K. Y., Farrokhi, S., & Powers, C. M. (2015). Femur Rotation Increases Patella Cartilage Stress in Females with Patellofemoral Pain. *Med Sci Sports Exerc, 47*(9), 1775-1780. doi: 10.1249/MSS.0000000000000617

210. Elias, J. J., Bratton, D. R., Weinstein, D. M., & Cosgarea, A. J. (2006). Comparing two estimations of the quadriceps force distribution for use during patellofemoral simulation. *J Biomech, 39*(5), 865-872. doi: 10.1016/j.jbiomech.2005.01.030

211. Schmitz, A., & Piovesan, D. (2016). Development of an Open-Source, Discrete Element Knee Model. *IEEE Trans Biomed Eng, 63*(10), 2056-2067. doi: 10.1109/TBME.2016.2585926

212. Adouni, M., Shirazi-Adl, A., & Shirazi, R. (2012). Computational biodynamics of human knee joint in gait: from muscle forces to cartilage stresses. *J Biomech, 45*(12), 2149-2156.

213. Fregly, B. J., Banks, S. A., D'Lima, D. D., & Colwell, C. W., Jr. (2008). Sensitivity of knee replacement contact calculations to kinematic measurement errors. *J Orthop Res, 26*(9), 1173-1179. doi: 10.1002/jor.20548

214. Altman, D. G., & Bland, J. M. (1983). Measurement in Medicine: The Analysis of Method Comparison Studies. *Journal of the Royal Statistical Society. Series D (The Statistician), 32*(3), 307-317. doi: 10.2307/2987937

215. Giavarina, D. (2015). Understanding Bland Altman analysis. *Biochem Med (Zagreb), 25*(2), 141-151. doi: 10.11613/BM.2015.015

216. Oberkampf, W. L., Trucano, T. G., & Hirsch, C. (2004). Verification, validation, and predictive capability in computational engineering and physics. *Applied Mechanics Reviews, 57*(5), 345. doi: 10.1115/1.1767847

217. Arya, S., Mount, D., Netanyahu, N., Silverman, R., & Wu, A. (1998). An optimal algorithm for approximate nearest neighbor searching fixed dimensions. *Journal of the ACM (JACM), 45*(6), 891-923. doi: 10.1145/293347.293348

218. Kern, A. M. (2011). Large population evaluation of contact stress exposure in articular joints for prediction of osteoarthritis onset and progression. *University of Iowa*.

219. Froimson, M. I., Ratcliffe, A., Gardner, T. R., & Mow, V. C. (1997). Differences in patellofemoral joint cartilage material properties and their significance to the etiology of cartilage surface fibrillation. *Osteoarthritis Cartilage, 5*(6), 377-386.

220. Higginson, G. R., & Snaith, J. E. (1979). The Mechanical Stiffness of Articular Cartilage in Confined Oscillating Compression. *Eng Med, 8*(1), 11-14. doi: 10.1243/EMED_JOUR_1979_008_005_02

221. Farrokhi, S., Tashman, S., Gil, A. B., Klatt, B. A., & Fitzgerald, G. K. (2012). Are the kinematics of the knee joint altered during the loading response phase of gait in individuals with concurrent knee osteoarthritis and complaints of joint instability? A dynamic stereo X-ray study. *Clin Biomech (Bristol, Avon), 27*(4), 384-389. doi: 10.1016/j.clinbiomech.2011.10.009

222. Lenhart, R. L., Kaiser, J., Smith, C. R., & Thelen, D. G. (2015). Prediction and Validation of Load-Dependent Behavior of the Tibiofemoral and Patellofemoral Joints During Movement. *Ann Biomed Eng, 43*(11), 2675-2685. doi: 10.1007/s10439-015-1326-3

223. Fernandez, J. W., Akbarshahi, M., Crossley, K. M., Shelburne, K. B., & Pandy, M. G. (2011). Model predictions of increased knee joint loading in regions of thinner articular cartilage after patellar tendon adhesion. *J Orthop Res, 29*(8), 1168-1177. doi: 10.1002/jor.21345

224. Henak, C. R., Kapron, A. L., Anderson, A. E., Ellis, B. J., Maas, S. A., & Weiss, J. A. (2014). Specimen-specific predictions of contact stress under physiological loading in the human hip: validation and sensitivity studies. *Biomech Model Mechanobiol, 13*(2), 387-400. doi: 10.1007/s10237-013-0504-1

225. Hale, J. E., & Brown, T. D. (1992). Contact stress gradient detection limits of Pressensor film. *J Biomech Eng, 114*(3), 352-357.

226. Wu, J. Z., Herzog, W., & Epstein, M. (1998). Effects of inserting a pressensor film into articular joints on the actual contact mechanics. *J Biomech Eng, 120*(5), 655-659.

227. Cicuttini, F. M., Baker, J., Hart, D. J., & Spector, T. D. (1996). Association of pain with radiological changes in different compartments and views of the knee joint. *Osteoarthritis Cartilage, 4*(2), 143-147.

228. Englund, M., & Lohmander, L. S. (2005). Patellofemoral osteoarthritis coexistent with tibiofemoral osteoarthritis in a meniscectomy population. *Ann Rheum Dis, 64*(12), 1721-1726. doi: 10.1136/ard.2005.035568

229. Boegard, T., Rudling, O., Petersson, I. F., & Jonsson, K. (1998). Correlation between radiographically diagnosed osteophytes and magnetic resonance detected cartilage defects in the patellofemoral joint. *Ann Rheum Dis, 57*(7), 395-400.

230. Duncan, R., Peat, G., Thomas, E., Wood, L., Hay, E., & Croft, P. (2008). How do pain and function vary with compartmental distribution and severity of radiographic knee osteoarthritis? *Rheumatology (Oxford), 47*(11), 1704-1707. doi: 10.1093/rheumatology/ken339

231. McWalter, E. J., Cibere, J., MacIntyre, N. J., Nicolaou, S., Schulzer, M., & Wilson, D. R. (2007). Relationship between varus-valgus alignment and patellar kinematics in individuals with knee osteoarthritis. *J Bone Joint Surg Am, 89*(12), 2723-2731. doi: 10.2106/JBJS.F.01016

232. Borotikar, B. S., & Sheehan, F. T. (2013). In vivo patellofemoral contact mechanics during active extension using a novel dynamic MRI-based methodology. *Osteoarthritis Cartilage, 21*(12), 1886-1894. doi: 10.1016/j.joca.2013.08.023

233. Altman, R., Asch, E., Bloch, D., Bole, G., Borenstein, D., Brandt, K., . . . et al. (1986). Development of criteria for the classification and reporting of osteoarthritis. Classification of osteoarthritis of the knee. Diagnostic and Therapeutic Criteria Committee of the American Rheumatism Association. *Arthritis Rheum, 29*(8), 1039-1049.

234. Kellgren, J. H., & Lawrence, J. S. (1957). Radiological assessment of osteo-arthrosis. *Ann Rheum Dis, 16*(4), 494-502.

235. Bellamy, N. (2005). The WOMAC Knee and Hip Osteoarthritis Indices: development, validation, globalization and influence on the development of the AUSCAN Hand Osteoarthritis Indices. *Clin Exp Rheumatol, 23*(5 Suppl 39), S148-153.

236. Bellamy, N., Buchanan, W. W., Goldsmith, C. H., Campbell, J., & Stitt, L. W. (1988). Validation study of WOMAC: a health status instrument for measuring clinically important patient relevant outcomes to antirheumatic drug therapy in patients with osteoarthritis of the hip or knee. *The Journal of rheumatology, 15*(12), 1833-1840.

237. Bellamy, N., Campbell, J., Stevens, J., Pilch, L., Stewart, C., & Mahmood, Z. (1997). Validation study of a computerized version of the Western Ontario and McMaster Universities VA3.0 Osteoarthritis Index. *J Rheumatol, 24*(12), 2413-2415.

238. Irrgang, J. J., Snyder-Mackler, L., Wainner, R. S., Fu, F. H., & Harner, C. D. (1998). Development of a patient-reported measure of function of the knee. *J Bone Joint Surg Am, 80*(8), 1132-1145.

239. Williams, V. J., Piva, S. R., Irrgang, J. J., Crossley, C., & Fitzgerald, G. K. (2012). Comparison of reliability and responsiveness of patient-reported clinical outcome measures in knee osteoarthritis rehabilitation. *J Orthop Sports Phys Ther, 42*(8), 716-723. doi: 10.2519/jospt.2012.4038

240. Gnat, R., Kuszewski, M., Koczar, R., & Dziewonska, A. (2010). Reliability of the passive knee flexion and extension tests in healthy subjects. *J Manipulative Physiol Ther, 33*(9), 659-665. doi: 10.1016/j.jmpt.2010.09.001

241. McIntosh, A. S., Beatty, K. T., Dwan, L. N., & Vickers, D. R. (2006). Gait dynamics on an inclined walkway. *J Biomech, 39*(13), 2491-2502. doi: 10.1016/j.jbiomech.2005.07.025

242. Lay, A. N., Hass, C. J., & Gregor, R. J. (2006). The effects of sloped surfaces on locomotion: a kinematic and kinetic analysis. *J Biomech, 39*(9), 1621-1628. doi: 10.1016/j.jbiomech.2005.05.005

243. Astephen, J., & Deluzio, K. (2005). Changes in frontal plane dynamics and the loading response phase of the gait cycle are characteristic of severe knee osteoarthritis application of a multidimensional analysis technique. *Clin Biomech (Bristol, Avon), 20*(2), 209-217.

244. Schipplein, O., & Andriacchi, T. (1991). Interaction between active and passive knee stabilizers during level walking. *Journal of Orthopaedic Research, 9*(1), 113-119.

245. Anderst, W., Zauel, R., Bishop, J., Demps, E., & Tashman, S. (2009). Validation of three-dimensional model-based tibio-femoral tracking during running. *Med Eng Phys, 31*(1), 10-16. doi: 10.1016/j.medengphy.2008.03.003

246. Bland, J. M., & Altman, D. G. (1996). Transforming data. *BMJ, 312*(7033), 770.

247. Fitzgerald, G. K., Piva, S. R., Irrgang, J. J., Bouzubar, F., & Starz, T. W. (2004). Quadriceps activation failure as a moderator of the relationship between quadriceps strength and physical function in individuals with knee osteoarthritis. *Arthritis Rheum, 51*(1), 40-48. doi: 10.1002/art.20084

248. Saranathan, A., Kirkpatrick, M. S., Mani, S., Smith, L. G., Cosgarea, A. J., Tan, J. S., & Elias, J. J. (2012). The effect of tibial tuberosity realignment procedures on the patellofemoral pressure distribution. *Knee Surg Sports Traumatol Arthrosc, 20*(10), 2054-2061. doi: 10.1007/s00167-011-1802-8

249. Thoma, L. M., McNally, M. P., Chaudhari, A. M., Best, T. M., Flanigan, D. C., Siston, R. A., & Schmitt, L. C. (2017). Differential knee joint loading patterns during gait for individuals with tibiofemoral and patellofemoral articular cartilage defects in the knee. *Osteoarthritis Cartilage*. doi: 10.1016/j.joca.2017.02.794

250. Powers, C. M., Chen, Y. J., Scher, I., & Lee, T. Q. (2006). The influence of patellofemoral joint contact geometry on the modeling of three dimensional patellofemoral joint forces. *J Biomech, 39*(15), 2783-2791. doi: 10.1016/j.jbiomech.2005.10.008

251. Halonen, K. S., Mononen, M. E., Jurvelin, J. S., Toyras, J., Klodowski, A., Kulmala, J. P., & Korhonen, R. K. (2016). Importance of Patella, Quadriceps Forces, and Depthwise Cartilage Structure on Knee Joint Motion and Cartilage Response During Gait. *J Biomech Eng, 138*(7). doi: 10.1115/1.4033516

252. Chen, Y. J., Scher, I., & Powers, C. M. (2010). Quantification of patellofemoral joint reaction forces during functional activities using a subject-specific three-dimensional model. *J Appl Biomech, 26*(4), 415-423.

253. Cohen, Z. A., Henry, J. H., McCarthy, D. M., Mow, V. C., & Ateshian, G. A. (2003). Computer simulations of patellofemoral joint surgery. Patient-specific models for tuberosity transfer. *Am J Sports Med, 31*(1), 87-98. doi: 10.1177/03635465030310012701

254. Wilson, W., van Burken, C., van Donkelaar, C., Buma, P., van Rietbergen, B., & Huiskes, R. (2006). Causes of mechanically induced collagen damage in articular cartilage. *J Orthop Res, 24*(2), 220-228. doi: 10.1002/jor.20027